KATHMANDU UNIVERSITY

SCHOOL OF ENGINEERING

DEPARTMENT OF MECHANICAL ENGINEERING

DISSERTATION ON

PERFORMANCE EVALUATION OF CENTRIFUGAL PUMP WITH APPLICATION IN TURBINE MODE

In Partial Fulfillment of the Requirements for the

Master by Research Degree in Mechanical Engineering

Nischal Pokharel [013075-11]

October 2022

DECLARATION

I hereby declare that I am the sole author of the dissertation.

I authorize Kathmandu University to lend this thesis to other institutions or individuals for the purpose of scholarly research. I further authorize the Kathmandu University to reproduce the thesis by photocopying or by other means, in total or in part, at the request of other institutions or individuals for the purpose of scholarly research.

_____

Nischal Pokharel [013075-11]

October 2022

DISSERTATION EVALUATION

Performance evaluation of centrifugal pump with application in turbine mode

By

Nischal Pokharel

This is to certify that I have examined the above Dissertation and have found that it is complete and satisfactory in all respects and that any revisions required by the report examination committee have been made.

_____

Supervisor
Prof. Bhola Thapa, PhD
Department of Mechanical Engineering
Kathmandu University

_____

Supervisor
Associate Prof. Biraj Singh Thapa, PhD
Department of Mechanical Engineering,
Kathmandu University

_____

Prof. Daniel Tuladhar, PhD
Head of Department
Department of Mechanical Engineering,
Kathmandu University

_____

External Examiner
Associate Prof. Bjørn Winther Solemslie, PhD
Department of Energy and Process Engineering
Norwegian University of Science and Technology

_____

Prof. Manish Pokharel, PhD
Dean
School of Engineering , Kathmandu University

October 2022

PREFACE

This study was conducted at the Turbine Testing Laboratory (TTL) of Kathmandu University's Department of Mechanical Engineering. The work was partly supported by EnergizeNepal Project at TTL, which aims to improve the capacity of research and education as well as develop human resources and technology required for the development of the renewable energy sector in Nepal and the region. While, experiment work was partly funded by the project entitled, “Capacity and Competence Development for Introducing Francis Turbine in Nepalese Micro-Hydro Project” along with the Department of Mechanical Engineering with a motive to provide a testing facility and experiment in pumps at Kathmandu University. The focus of this research was to develop competence in designing, manufacturing, installing, and operating of pumps in Nepal and self-sustainability in it.

ACKNOWLEDGEMENT

I want to sincerely thank Prof. Bhola Thapa and Associate Prof. Biraj Singh Thapa as my supervisors for their valuable suggestions, encouragement and continuous guidance and support. I would like to express my immense appreciation to Prof. Hari Prasad Neopane for his valuable ideas. His experience in the field of hydraulic machinery provides a milestone for this study. I am very grateful for the contribution made by Dr. Sailesh Chitrakar for CFD analysis.

I would like to thank Eldar Onsoyen family members for creating Eldar Onsoyen Endowment Fund at Kathmandu University through which I received my fellowship during this study.

Importantly, the contribution made by all TTL people is remarkable in my study. I would like to thank Mr. Amul Ghimire for sharing his knowledge on the Francis turbine to do a similar type of research on the pump. I cannot forget the contribution of Mr. Aatmaram Kyastha to CFD and experimental works. I would like to thank Mr. Prajwal Sapkota for always being by my side during the experiment for data logging and acquisition. I am very grateful to Mr. Bhuwan Pd. Bhattarai and Aman Kapali for rig setup and experimentation. I also want to thank Mr. Dadiram Dahal for sharing his academic experience with me. I could not forget the contribution of Dr. Ram Lama in providing his valuable suggestion at each time of my presentation.

I am also thankful to Prof. Bim Prasad Shrestha for providing me student fellowship exchange opportunity at Wuhan University. I also thank Prof. Qian Zhongdong and Asst. Prof Guo Zhiwei from Wuhan University in sharing their knowledge at Wuhan University.

I would like also like to thank the Narayani Lift irrigation Project staff for facilitating a field visit to their pump house to explore there. Similarly, I appreciate Mr. Dhurva Pokharel from the MK Paper Mill providing his insight with the pumping system used

in the process of processing papers and also for donating various pump impellers for research purposes to Kathmandu University.

I would like to thank CFturbo sales for providing an academic license in the course of my study which was very helpful in the design of the impeller and its modeling.

Furthermore, I am also thankful to my students for their support and help to finish this research work.

Finally, I appreciate my family and friends for their constant love and support. I want to dedicate my dissertation to my parents: Khadendra Prasad Pokharel and Indira Pokharel. I also want to express my gratitude to my lovely wife Nisha Niraula for her consistent support and patience while I was working on my study.

TABLE OF CONTENTS

LIST OF FIGURES

LIST OF TABLES

ABSTRACT

Pumps are mechanical devices to lift the fluid from one energy level to another. Generally, they are used to transport fluids from lower levels to a higher level or from one place to another. Pumps are widely used technology in different types of industries where fluids are involved. Applications like water distribution systems, sewage management, irrigation, hydropower, and various other application areas cannot function without the use of pumps. In the context of Nepal, pumps are being used in different industrial as well as household applications. The majority of the pumps being used in Nepal are imported from either India or China. As of today, Nepalese industries have not been able to comprehend the prospect of manufacturing pumps in Nepal. Although Nepal has a long history of using pumps on an industrial scale, research in this area cannot be found.

Francis turbines are supposedly the appropriate turbine of choice in Nepalese hydropower, including those that have already been developed and those that will be developed in the future. However, designing and manufacturing Francis turbines is a time-consuming task, and local manufacturers who specialize in Cross-flow turbines lack the technology and expertise to produce modern Francis turbines. Sediment in Himalayan Rivers, is a major operational challenge because it reduces turbine lifetime by a large factor, increasing hydropower maintenance costs. The operational region of the Francis turbine and the Pump as Turbine (PAT) overlaps significantly, indicating that PAT can be used in many of Nepal's hydropower projects. Pump manufacturers in China and India are already well-known for developing a wide range of pumps and supplying them to Nepal. Despite the tremendous opportunity, the use of pumps for turbine mode applications in Nepalese hydropower could not be found. Furthermore, no research on the effects of sediment on pumps operating as pumps or turbines can be found in Nepal.

In this study, the status of pump technology used in Nepal is discussed starting with the history of pumps used in Nepal along with the existing application areas of pumps in the country for various types, sizes, and capacity are described. Similarly, problems associated with existing pumps are highlighted. The maintenance process of pumps and their reliability are discussed. The data for the existing market of pumps is presented where centrifugal pumps have been identified as a suitable pump for implementation as a turbine in hydropower as an alternative to the Francis turbine which is supposedly the suitable turbine of choice in the context of Nepal but a very difficult job for manufacturers.

With the identification of a centrifugal pump that can be used as a turbine, a suitable size of the centrifugal pump was brought for its performance testing. Design of experiments was done for it and tested in pump mode and turbine mode and the performance curve was done for the same. For the design modification, the original impeller was closely measured, and reversed engineering with close and frequent measurements was applied for obtaining its basic dimensions. Then the blade profile was provided with the design methodology available from the literature. This was the first modification of the impeller. The second modification was done on the impeller of the same original impeller diameter but with the design methodology of the Francis turbine. Similarly, the third modification was done on the leading and trailing edges making the profile like that of the turbine. The original impeller, first modification, and second modification were tested experimentally first and second modifications were tested numerically as well as experimentally and the third modification was tested numerically.

Since sediment in the Himalayan rivers is the major obstacles in operation for hydro turbines, it was identified that PAT can also not escape from this problem. For this, the study was done on the effect of sediment erosion in pumps and turbines using numerical and experimental methods. The locally available impeller was modeled in CF turbo with reverse engineering and numerical analysis was done in ANSYSCFX. For the experimental analysis test setup was developed with a painted impeller and the results

on erosion were compared with the experiment. Despite the fact that the experiment was carried out in a relatively simple arrangement, areas prone to erosion were revealed. In order to implement the PAT in Nepalese hydropower, the experiment in PAT was performed in order to investigate how a locally available pump can be used in reverse mode for micro hydropower. The performance curves for various operating scenarios were plotted for PAT. It was revealed the performance of an existing pump in turbine mode can compete with other conventional turbines in terms of cost and operation in the context of Nepal. However, the head and discharge requirements at BEP for turbine mode are slightly higher than those for pump mode. So the proper selection of PAT is necessary for its implementation in hydropower.

LIST OF ABBREVIATIONS

3D	3-Dimension
ANSYS	Analysis Systems
BEP	Best Efficiency Point
CAD	Computer-Aided Design
CFD	Computational Fluid Dynamics
CFX	Central Florida Expressway Authority
FEA	Finite Element Analysis
HPP	Hydro Power Plant
KE	Kinetic Energy
KU	Kathmandu University
kW	Kilowatts
LABVIEW	Laboratory Virtual Instrument Engineering Workbench
MATLAB	Matrix Laboratory
MHP	Micro Hydro Power
MW	Mega Watts
NEA	Nepal Electricity Authority
NPSH	Net Positive Suction Head
PAT	Pump as Turbine
RANS	Reynolds-averaged Navier-Stokes
RPM	Revolution per minute
TTL	Turbine Testing Lab
VFD	Variable Frequency Drive

LIST OF SYMBOLS

Symbol	Description	Unit
π	Constant	[-]
ρ	Density of water	[kg/m^3]
g	Acceleration due to gravity	[m/s^2]
Q	Discharge	[l/s]
Q_t	Discharge for Turbine mode	[l/s]
Q_p	Discharge for pump mode	[l/s]
Q_{site}	Discharge available at the site	[l/s]
Q_{BEPt}	Discharge at BEP for turbine mode	[l/s]
Q_{BEPp}	Discharge at BEP for pump mode	[l/s]
H	Head	[m]
H_e	Euler's Head	[m]
H_{site}	Head available at the site	[m]
H_{BEPt}	Head at BEP for turbine mode	[m]
H_{BEPp}	Head at BEP for pump mode	[m]
H_{net}	Difference of delivery head and suction head	[m]
n_q	Specific speed of pump in SI system	[-]
n_s	Specific speed of pump in US system	[-]
ψ	Specific head constant	[-]
n	Revolution per minute	[RPM]
ω	Angular revolution	[rad/s]
D_1	Inlet diameter of impeller	[mm]
D_2	Outlet diameter of impeller	[mm]
d_s	Suction pipe diameter	[mm]

d_d	Delivery pipe diameter	[mm]
D_s	Suction diameter of impeller	[mm]
B_2	Outlet width of the impeller	[mm]
u_1	Peripheral velocity of impeller at inlet	[m/s]
u_2	Peripheral velocity of impeller at outlet	[m/s]
w_1	Relative velocity of impeller at inlet	[m/s]
w_2	Relative velocity of impeller at outlet	[m/s]
c_1	Absolute velocity of impeller at inlet	[m/s]
c_2	Absolute velocity of impeller at outlet	[m/s]
α_1	Flow angle at inlet	[^{0}]
α_2	Flow angle at outlet	[^{0}]
β_1	Inlet blade angle	[^{0}]
β_2	Outlet blade angle	[^{0}]
c_{u1}	Tangential component of absolute velocity at inlet	[m/s]
c_{u2}	Tangential component of absolute velocity at outlet	[m/s]
c_{m1}	Flow component of absolute velocity at inlet	[m/s]
c_{m2}	Flow component of absolute velocity at outlet	[m/s]
h	Head conversion factor for turbine mode	[-]
q	Discharge conversion factor for turbine mode	[-]
η	Efficiency	[-]
$\eta_{(p)}$	Efficiency in pump mode	[-]
$\eta_{(t)}$	Efficiency in turbine mode	[-]
$P_{out(p)}$	Hydraulic power output for pump mode	[W]
$P_{in(p)}$	Shaft power input for pump mode	[W]

$P_{out(t)}$	Shaft power output for turbine mode	[W]
$P_{in(t)}$	Hydraulic power input for turbine mode	[W]
P_d	Pressure head at delivery side of impeller	[m]
P_s	Pressure head at suction side of impeller	[m]
E	Mass of eroded wall by mass of particle	[Kg]
V_p	Particle impact velocity	[m/s]
V_1	Velocity constant of Tabakoff model	[m/s]
V_2	Velocity constant of Tabakoff model	[m/s]
V_3	Velocity constant of Tabakoff model	[m/s]
γ	Impact angle between approaching particle and wall	[^{0}]
k_2	Design constant of Tabakoff model	[-]
k_{12}	Design constant of Tabakoff model	[-]
γ_0	Maximum impingement angle	[^{0}]

Dedicated to my parents

CHAPTER 1 INTRODUCTION

1.1 Introduction

Among the various source of renewable energy, hydropower is one of the most choices of renewable energy due to its abundance. In the context of Nepal, it is often said that it has a theoretical potential of 83,000 MW of which 43,442 MW is technically feasible [1]. With the first hydropower establishment in Nepal in 1911 as Pharping hydropower, Nepal has a very long history of hydropower with more than 110 years from now [2]. However, it has not made significant progress to date. As per the latest NEA annual report 2021, the annual generation of electricity in Nepal in the fiscal year is only about 1451 MW [3]. But the recent plan and policies and regulation in Nepal has shown that sooner the future of hydroelectricity is bright as various hydropower is under construction and in the pipeline. Turbines are one of the crucial components of hydropower in transmitting mechanical power from hydraulic energy through the shaft which in turn generates electricity through a generator. There are various types of turbines used in hydropower, among them Francis turbine is the most common type. Considering the scenario in Nepal, a study performed showed that 75% of future hydropower in Nepal will use Francis turbine [4].

Another study conducted by scholars on 61 micro hydro power schemes in Nepal found that 52% of them were in the range of Francis turbines. However, all of those micro hydropower systems used Cross-Flow and Pelton turbines which were less efficient in comparison [5]. The same study found that if micro hydro had used Francis turbines in those locations, its power and efficiency would have been higher. Due to a lack of competences in manufacturing Francis turbines, Nepalese micro hydro developers and turbine manufacturers are installing Cross flow turbines, which operate at a low efficiency. This is also true in other developing countries where the potential of micro hydro is not being fully realized due to a lack of manufacturers developing turbines with higher efficiency. [6]. Apart from the technical challenges related to the manufacture of the Francis turbine, there are also operational challenges in Nepalese hydropower due

to the sediment-laden river. Many hydropower developers complain about decreased efficiency after just a short period of operation, resulting in significant monetary losses. The regularity of maintenance and repair of underwater parts in Francis turbines operating in sediment-laden rivers is relatively high, increasing the machine's outage time. One of the primary causes of machine outage may be due to the turbine's improper assembly design [7].

Some of the issues associated with the Francis turbine could be mitigated if an alternative existed. Aside from the Pelton and Francis turbines, the pump as turbine (PAT) has been distinguished as an alternative to the Francis turbine with regard to efficiency and full-load operation [8]. Furthermore, the head and flow range of PAT overlaps at some regions to that of Francis turbines as shown in Figure 1.1.

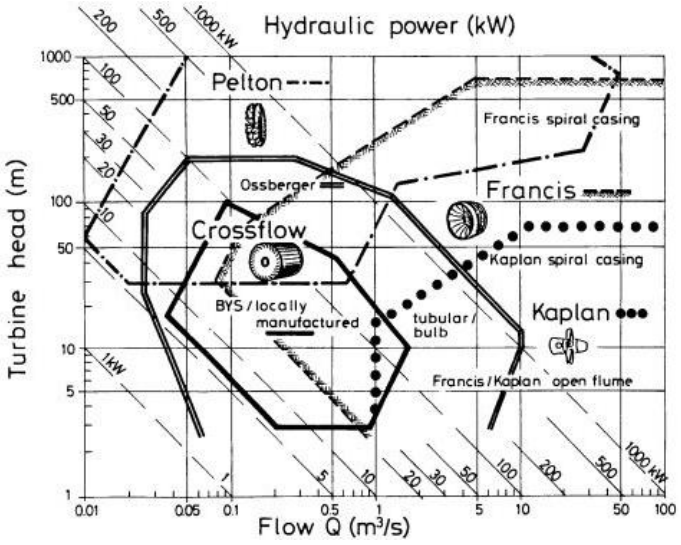

Figure 1.1 Operating range of various turbines with PAT [9]

A lot of research has been done worldwide on PAT and proven its effectiveness. However, in the context of Nepal, this concept of PAT has not been realized to date. In addition to this, the policy of government over large hydropower has suppressed small hydropower. As reported by various micro hydropower manufacturers in Nepal, their

machine is idle conditions, since the market of large hydropower is dominated by internal manufacturers. Despite the fact that there are over fifty eight manufacturing companies which have competences for developing micro hydro turbines, nobody has produced a turbine for even small hydropower. Most of such companies specialize in specific types of turbines. Manufacturing Francis has been big dream for them, despite having capacity for maintenance of turbines in the country. But some of these manufacturers have the capabilities and encouragement to produce turbines with capacities of up to 5 MW [10].

On one hand, those micro hydro manufacturers are not able to jump in their capacity and grab the market of large hydropower, and on the other hand, they are not getting a proper market for their production. In these circumstances, the existence of those industries has been important. Knowing the fact that the manufacturing parts of centrifugal pump and turbine are quite similar in terms of components, the long experience of local manufacturers in Nepal can be utilized in pumps as the pumps available in Nepal are all imported from Foreign country which has large market [11].

Instead of frequently designing and manufacturing site-specific turbines, selecting a pump from the market with certain calculations of head and discharge value for any site can be much more efficient. This is even more appealing financially because their payback periods, at two years, are much shorter than those of other turbines [8]. Since there is no such adequate research on the sediment erosion for PAT, it is still unrealistic to compare the two in this regard. Although much research has been done worldwide in the domain of the pump as turbines and successfully installed, this remains a challenge for a country like Nepal where sediment is predominant.

So, it has been very necessary to develop competence in pump manufacturing in Nepal to grab the existing market and also the alternative to other turbines if the pump is used in reversed mode. The current research focuses on the status of pump technology used in Nepal. The data for the existing market of pumps with problems associated in terms

of operation are described. Moreover, the focus is given to the centrifugal pumps which are the most common types found in Nepal and can be used as turbine mode too. Both numerical and experimental investigation has been performed to investigate the implementation pump in turbine mode considering the local sediment scenario. The possible design tool to design the pump has been identified. Finally, a different methodology to use a pump in turbine mode has been purposed.

1.2 Objectives

The main objective of this research is:

- Investigate the performance of the centrifugal pump and its application in turbine mode to identify the operational characteristics and optimization possibilities.

Following specific objectives are determined to achieve the main objective:

- Study the status of pump technology in Nepal and identify a suitable centrifugal pump for laboratory testing
- Numerical and experimental analysis of centrifugal pump in pump and turbine mode at various operating conditions
- Design modifications of existing impeller for better efficiency in turbine mode

1.3 Scope and Limitations

In this study, numerical as well as experimental technique is utilized for studying the performance of the pump in both pump mode and turbine mode. This study mainly focuses on testing centrifugal pumps in both pump and turbine mode. The study is done in two phases of experiments one for a performance test and the other for an erosion test. Numerical studies are performed using ANSYS CFX. For the numerical model, the impeller profile has been generated from the manufacturing drawing along with CF turbo for generating a meridional view. The meshing of the domain is carried out using a turbo grid and workbench. Fluid Solid Intersection analysis is not carried out for

mechanical design instead analytical procedures are followed. The study mainly focuses on an experiment of an existing pump in both modes as a reference case and various modifications of the impeller. Also, for numerical modeling, the actual impeller has not been modeled due to limitation of limited information from the supplier, limitations in reverse engineering, and limitations in CFturbo software.

1.4 Study Methodology

The methodology of this research is divided into four main parts: Literature review, Modelling, Numerical study, and Experimental analysis.

In the first part, various types of pumps are described. The design methods for hydraulic design of centrifugal pumps described by various researchers are discussed. Then the study is mainly focused on the context of Nepal. The status of pump technology used in Nepal is presented. Starting with the history of pumps in Nepal, the past 10 years' data on the pump market is presented. The areas where pumps are used in Nepal are discussed along with the problems encountered in pump operation. In the modeling part, the existing local pump available in the market is used. The information provided by the supplier is used to draw a hydraulic profile of the impeller and spiral casing. With a closed measurement of the impeller and spiral casing and additional information from the supplier drawing, the information is put in CFturbo software and the model of the impeller and spiral casing is generated. The obtained hydraulic model is used for the numerical study.

Numerical simulations are carried out using CFD with commercially available ANSYS CFX 18.1. The study is done for various design modifications of the existing impeller. Also, for the erosion test, the erosion pattern around the impeller is studied numerically.

For the experimental analysis, two phases of the experiment have been carried out. One for the performance test and another for the erosion test. The performance test was are carried out in a dedicated test rig established at the Turbine Testing lab, KU, which

required flow, which is controlled by the VFD and bypass valve, and after pressuring the flow at the high-pressure tank the water flows through the turbine. Electronic pressure and flow sensors are used for flow and pressure measurement while a torque transducer measures torque and rpm. LabVIEW is used for data logging and processing.

For the erosion test, a separate rig has been constructed in which two pumps were used one for pump mode and another for turbine mode. The impeller was painted which was operated in a sediment environment and erosion patter were noted after the experiment. Finally, validation of the CFD result is carried out by comparing it with the experimental results.

1.5 Organization of Thesis

This thesis is organized into seven chapters. In chapter one, a brief introduction and background explaining the problems and research gaps along with the objectives, scope, and limitations of this research study are discussed. While chapter two is dedicated to, all the literature related to the study. In this chapter, the theory of centrifugal pumps is discussed. The chapter also gives an overview of the pump as a turbine including its history, design methodology, and current trend. Chapter three is related to a literature review with research on the status of pump technology in Nepal that covers its market, operational areas, and associated problems and maintenance strategy in their operations. In chapter four the overall performance of centrifugal pumps is discussed including the design methodology of centrifugal pumps from reverse engineering and numerical and experimental methodology. Chapter five gives an overview of centrifugal pump performance in an erosion environment. The conclusion of the study is presented in chapter six. In chapter seven the related future works and recommendations are given. The summary of published papers and introduction to CFturbo are given in the appendix section.

CHAPTER 2 LITERATURE REVIEW

2.1 Introduction to pumps

A pump is a device that converts mechanical energy into kinetic and pressure energy by moving fluids [12]. Pumps can be classified according to the application areas, materials, working fluids, position and installation in space. All of these classifications, may be limited in their scope and frequently overlap. A more fundamental classification system first defines the principle mentioning the type of energy is added to the fluid. Secondly it identifies how this principle is implemented and finally it distinguishes the specific geometries that are commonly used. This system is thus related to the pump itself and is unrelated to any external consideration or even the materials from which it may be constructed [13].

So broadly in this scenerio, all pumps can be classified into two types. The first one is dynamic pumps, wherein the energy is continuously added to increase the fluid velocities in the system to the greater value than the values at the discharge. Due to this reduction in velocity within or beyond the pump system, it produces a pressure increase. The second type of pumps is displacement pump, where the energy is added periodically by applying force to one or more movable boundaries for any desired number of enclosing elements [13].

During the pumping action of a dynamic pressure pump, tangential force is transmitted, which generally accelerates the fluid via rotation of the impeller. As illustrated in Figure 2.1, they are further categorized as centrifugal pumps and other special effect pumps. A centrifugal pump employs a revolving impeller that increases the pressure energy of a fluid. A propeller pump is categorized as high flow, low lift impeller type that draws water up an outer casing and out of a discharge outlet with the help of a propeller blade impeller head. Turbine pumps are centrifugal pumps that employ pressure and flow in conjunction with a rotational motion to transport fluid.

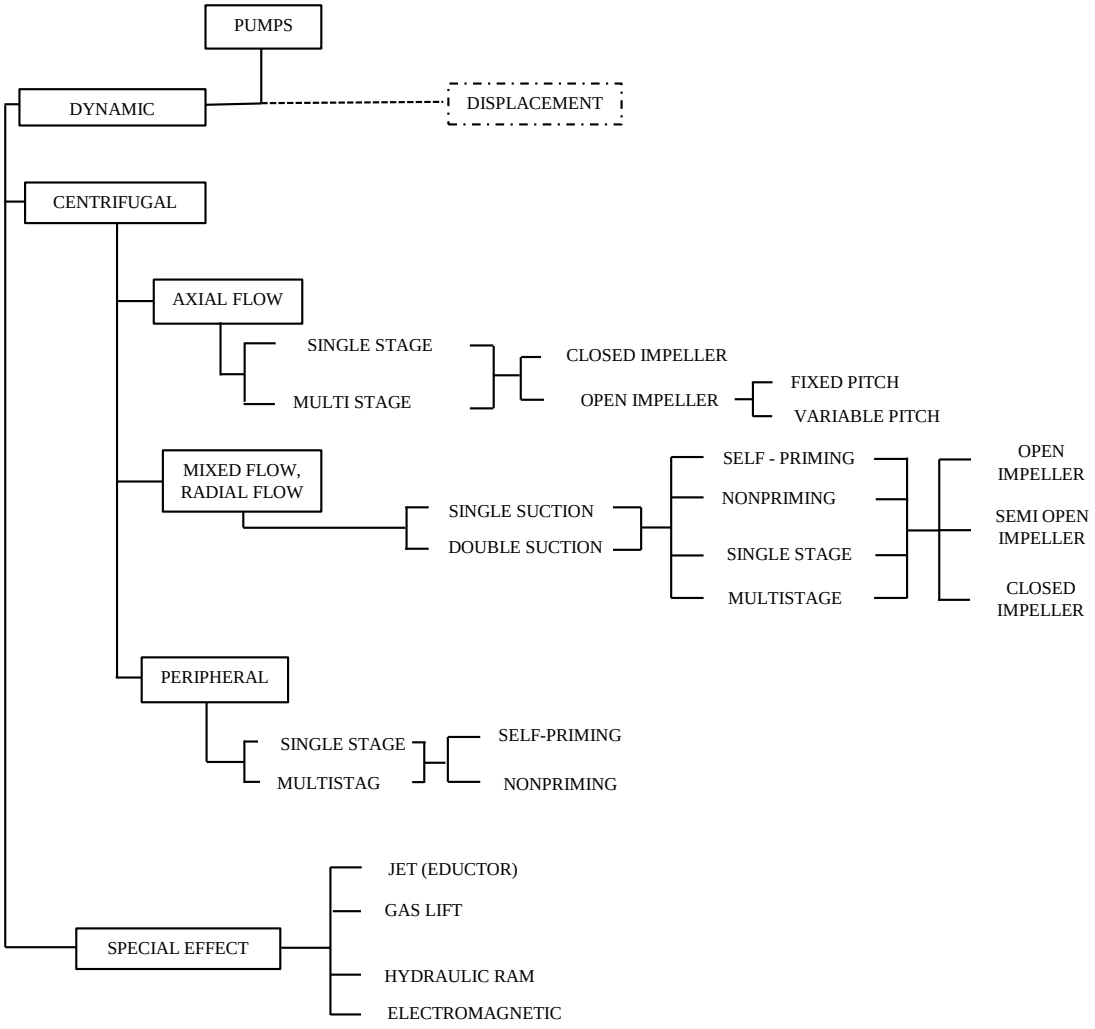

Figure 2.1 Classifications of dynamic pumps [14]

Displacement pumps are intended to move a fixed volume of fluid throughout each cycle of operation. Their volumetric flow rate is calculated by multiplying the displacement per cycle of the moving part that is either spinning or reciprocating by the cycle rate. As indicated on the right side of Figure 2.2, they are further classified as reciprocating pumps and rotary pumps. Pumping in reciprocating pumps is accomplished by the to and fro motion of the piston or diaphragm inside the cylinder. In rotary pumps, the relative movement of the spinning parts and the pump's stationary element causes the pumping action. Reciprocating pumps include piston or diaphragm pumps, whereas rotary pumps include gear, lobe, screw, and vane.

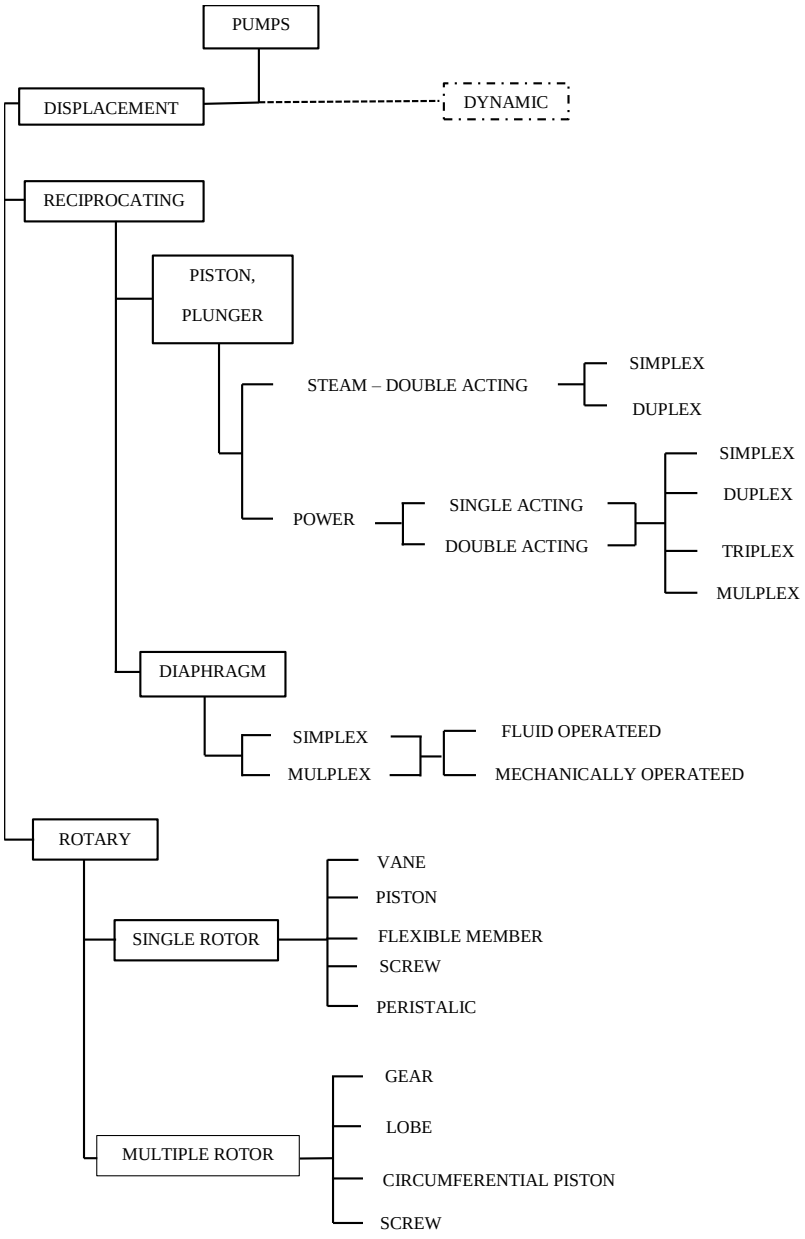

Figure 2.2 Classification of displacement pumps [14]

Among all the types of pumps discussed, centrifugal pumps are the most popular type of pump accessible in most applications due to its simple working principle and low production cost [14]. They have quite long history of usage with a proven technology. Another factor is that they resemble reaction turbines in sight and performance. A

centrifugal pump receives usable energy, transforms it to kinetic energy, and then transfers it to a fluid stream, whereas a reaction turbine does the inverse, absorbing energy from a fluid stream and converting it to work [15]. The components of centrifugal pumps and reaction turbines are quite similar, despite their different modes of operation. The essential components for both are the runner volute, pressure pipe, and draft tube, which are common to pumps and turbines despite their different names. As a result, researchers began to recognize that the centrifugal pump may also work in turbine mode. In reverse mode, any centrifugal pumps, from low to high specific speed, single or multistage, radially or axially split, horizontal or vertical installations, can be employed [16]. Due to this fact, in this study mainly centrifugal pumps are discussed for their operation in turbine mode.

2.2 Theory of Centrifugal pumps

2.2.1 Fundamental equations

The rotational motion of the impeller determines the fluid motion in any turbo machinery. The absolute velocity may be thought of as the velocity with respect to a stationary part, such as the housing or the diffuser. This velocity is the sum of two velocities that is defined as the impeller's peripheral velocity and the fluid velocity relative to the impellers.

To obtain the theoretical head of centrifugal pump the principle of angular momentum is applied for the mass of the liquid passing through the impeller. The time rate of change of angular momentum of a body with respect to the axis of its rotation is equal to the torque of the resultant force on the body for the same axis [17].

The theoretical head of a centrifugal pump is given by the equation:

$$H_i = \frac{u_2.c_{u2} - u_1.c_{u1}}{g} \tag{2.1}$$

If we neglect the hydraulic losses between the locations for actual total dynamic head of a pump, the equation is then known as Euler's equation.

If the liquid enters the impeller without any tangential component which means that if $c_{u1} = 0$, Euler's turbine equation is then reduced to:

$$H_e = \frac{u_2 . c_{u2}}{g} \qquad 2.2$$

Also, from the concept of velocity triangle,

$$w_2^2 = c_2^2 + u_2^2 - 2u_2 . c_2 . \cos\alpha_2 \qquad (2.3)$$
$$w_1^2 = c_1^2 + u_1^2 - 2u_1 . c_1 . \cos\alpha_1$$

This makes the Euler equation as:

$$H_i = \frac{c_2^2 - c_1^2}{2.g} + \frac{u_2^2 - u_1^2}{2.g} + \frac{w_2^2 - w_1^2}{2.g} \qquad (2.4)$$

Applying the Euler's head equation in its simpler form, as shown in equation 2.2, it can be showed that the variation of Euler's head with capacity is represented by the equation of a straight line.

Substituting,

$$c_{u2} = u_2 - w_{u2} = u_2 - \frac{c_{m2}}{\tan\beta_2} \qquad (2.5)$$

into equation 2.2 it is obtained,

$$H_e = \frac{u_2^2}{g} - \frac{u_2.c_{m2}}{g.\tan\beta_2} \tag{2.6}$$

Since c_{m2} is the flow component of velocity defined by,

$$Q = \pi.D_2.B_2.c_{m2} \tag{2.7}$$

$$H_e = \frac{u_2^2}{g} - \frac{u_2}{\pi.D_2.B_2.g.\tan\beta_2}.Q \tag{2.8}$$

The above equation represents the equation of a straight line with Y axis as H_e and X-axis as Q. The line meets X-axis at $\frac{u_2^2}{g}$ and has a slope of $\frac{u_2}{\pi.D_2.B_2.g.\tan\beta_2}$.

Simply, it can be written as:

$$H_e = A - B.Q$$

Where,

$$A = \frac{u_2^2}{g}, B = \frac{u_2.c_{m2}}{g.\tan\beta_2}$$

Different cases of β_2 exists for centrifugal pumps which are shown in Figure 2.3-2.6. When $\beta_2 > 90^0$ Tan β_2 will be negative and hence head increase with discharge as per Equation 2.8. Also, the high velocity at exist c_2 required a more efficient conversion of kinetic energy into pressure energy and the losses are more due to the formation of eddies. Such action can be realized only by an impulse action. Due to this, they have low efficiency and are not used.

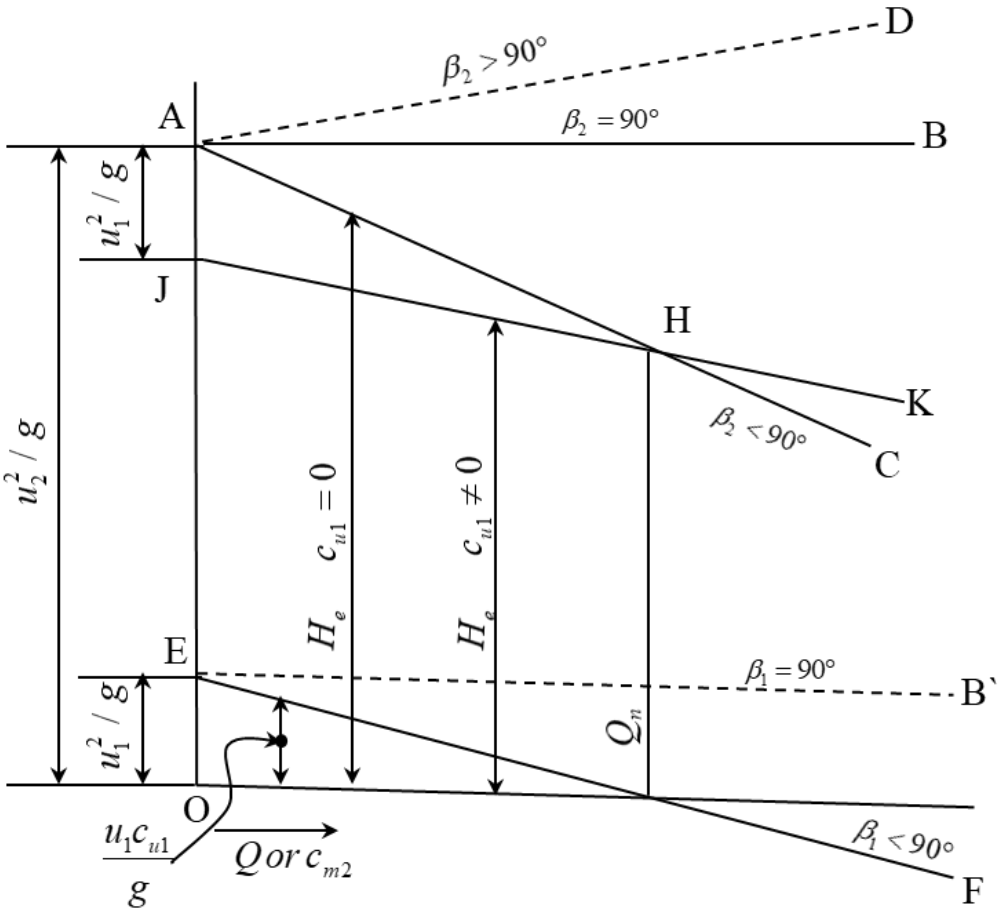

Figure 2.3 Euler's head-capacity characteristics [17]

When $\beta_2 = 90^0$, the head remains constant with outlet velocity. Such blades are easy for manufacturing. There is equal energy conservation in the impeller and casing which gives a high-pressure ratio with good efficiency.

When $\beta_2 < 90^0$, Tan β_2 will be positive and hence head decrease with discharge as per Equation 2.8. In this case, c_{m2} is minimum and so is c_2 as much reduced which produces a low head. From an efficiency point of view backward curved vanes are mostly used.

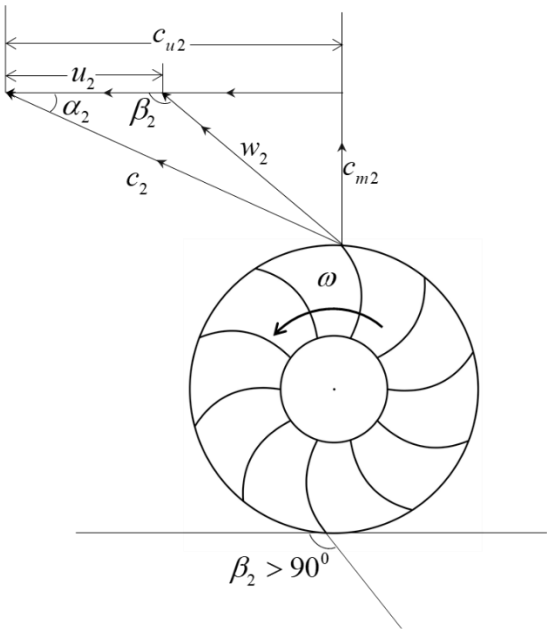

Figure 2.4 Velocity Triangle when $\beta_2 > 90^0$

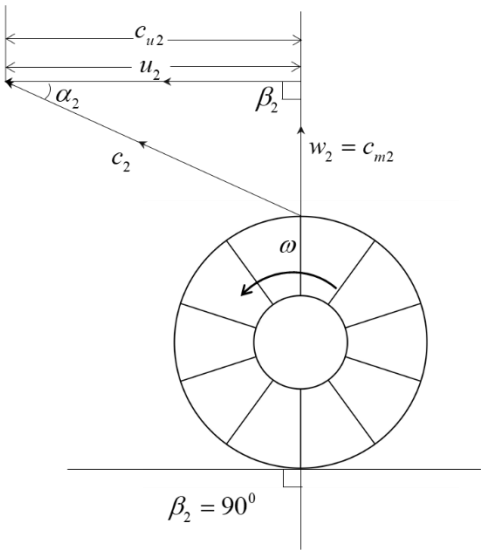

Figure 2.5 Velocity Triangle when $\beta_2 = 90^0$

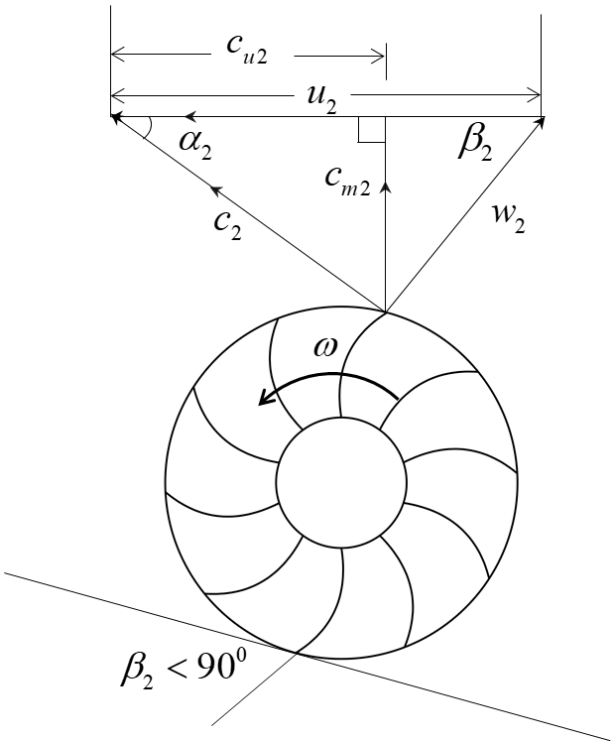

Figure 2.6 Velocity Triangle when $\beta_2 < 90^0$

Again, if we look for power requirements for different conditions for the above mentioned head,

We have,

$$P = \rho.g.Q.H_e = \rho.g(A.Q - B.Q^2) \tag{2.9}$$

The above equation is quadratic. It has different forms for different values of β_2.

When $\beta_2 = 90^0$ the equation represents a straight line passing through the origin.

When $\beta_2 < 90^0$ the equation represents a parabola tangent to a straight line representing $\beta_2 = 90^0$.

When $\beta_2 > 90^0$ equation also represents a parabola tangent to the straight line representing $\beta_2 = 90^0$, but lies above it.

From Figure 2.7, we can see that for the same power input we can obtain the highest discharge for $\beta_2 < 90^0$. In addition, to achieve a higher head high power is required. So in terms of pump efficiency also, maximum efficiency is obtained when the curves are backward. This is the reason why centrifugal pumps always have backward curved vanes.

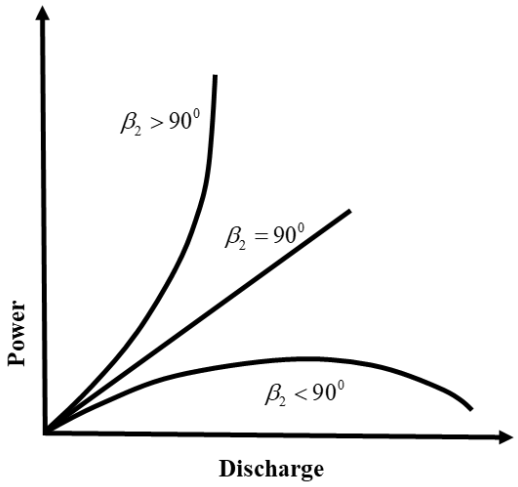

Figure 2.7 Power versus discharge at various β_2 [17]

2.2.2 Specific speed

Specific speed can be defined as a characteristic index or distinguishing feature of a pump when various impellers can be used for the same head and capacity. Pumps with the same specified speed will have the same performance and physical proportions, even if their outer diameters and actual operating speeds differ.

Specific speed is defined as the speed of a geometrically identical pump when delivering one m3/sec discharge against a head of one meter

Mathematically,

$$n_q = \frac{N.\sqrt{Q}}{H^{3/4}} \tag{2.10}$$

Where,

$n_s =$ The actual speed of the pump in rpm,

Q = Quantity flowing in m^3/s

H = Delivery head (total/manometric) in m.

The units of specific speed may be different as per standard. Forms found in US and other standards are relatable by [13]:

$n_q(m^3/s, m = n_s(USgpm, ft)/51.64$

The specific speed for different types of the centrifugal pump is shown in Table 2.1 [12]:

Table 2.1 Types of impellers with specific speed

S.N.	Types of Impellers	Specific Speed
1.	Slow speed radial flow runner	10-30
2.	Normal speed radial flow runner	30-50
3.	High speed radial flow runner	50-80
4.	Mixed flow runner	80-160
5.	Axial flow runner	110-500

2.2.3 Specific Head Coefficient

The head coefficient describes the head produced by a pump under specific operating condition. It is a dimensionless coefficient that is considered to be constant for pumps operating under identical flow conditions. It describes the pump's working behavior in terms of the head in greater detail [17].

Mathematically,

$$\psi = 2.g.\frac{H}{u_2^2} \tag{2.11}$$

Where,

u_2 = The circumferential speed of the impeller at the outlet

$H =$ Total head of the centrifugal pump

$g =$ Gravitational constant

If there is a variation in head at constant rotational speed of pump, then $\psi \sim$ H. Hence the head coefficient (ψ) is an indicative of the ordinate that is analogous to H on H/Q curves which plotted by a non-dimensional representation.

In terms of representation in specific energy (Y), the above equation becomes

$$\psi = \frac{Y}{u_2^2 / 2}$$

Where, Y= g.H is defined as useful mechanical energy developed by the centrifugal pump to the fluid circulated per unit mass of fluid circulated.

The specific energy helps to determine the basic size of the centrifugal pump.

2.3 Wear in centrifugal pumps

2.3.1 Overview

Pump performance degraded after specific periods of operation, despite their widespread usage and demand. These pumps have problems with cavitation, corrosion, erosion, and fracture failure [11]. Many researchers have investigated the causes of such problems, and only a few have proposed solutions. However, the most common types of wear encountered in centrifugal pumps are cavitation, corrosion, erosion, and fatigue [18], [13],[19],[20].

Cavitation can be defined as the formation and subsequent collapse of vapor bubbles at any flow situation which occurs in an environment with an ambient pressure that is equal to or less than the vapor pressure of the liquid in the medium. Cavitation can be minimized by running at a net positive suction head (NPSH) which is larger than NPSH as recommended by the manufacturers in their rating curve, however it is difficult to remove [21]. A typical example of cavitation is shown in Figure 2.8.

Figure 2.8 Cavitation effect in centrifugal pump impeller [22]

Corrosion is defined as a change in the physical, chemical, and mechanical properties of a substance caused by chemical and electrochemical interactions. Corrosion metals and alloys are frequently destroyed by their surroundings as well as chemical and electrochemical interactions. The production of iron oxide weakens centrifugal pumps on the surface. This weak surface is imparted when the pump is turned on, causing the pumps to operate poorly. Corrosion degrades the material and causes it to lose function, resulting in permanent damage [20]. An example of corrosion is shown in Figure 2.9

Figure 2.9 Corrosion in centrifugal pump impeller [23]

Erosive wear is created by impact of solid or liquid particles against a solid surface. Pumps work in a wide range of environments and with a wide range of abrasive liquid

and solid slurries. The rotating speed of the pump, the shape of the impeller all along casing, the velocity of flow, and the material employed all influence the erosion of various pump components [24].

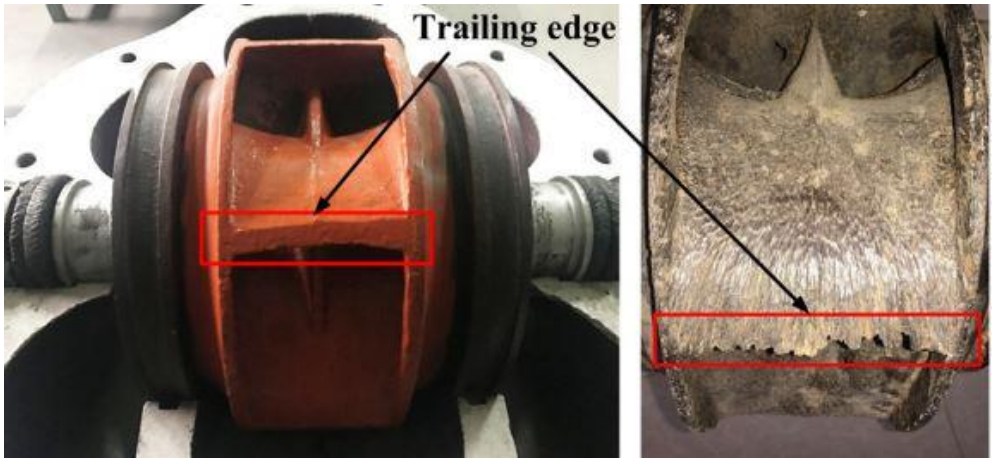

Figure 2.10 Erosion on pump impeller before and after experiment [25]

There are three forms of fatigue: cyclical loading, material fatigue, and environmentally assisted fatigue. Pumps are devices that transport fluid, creating a cyclic demand on their components. Despite the fact that centrifugal pumps are essentially steady-state spinning machines, they do undergo pulsations or varying applied loads. These cyclic stresses might be created by fluid contact between impeller exit vanes and diffuser vanes, or between impeller vanes and the casing at the cutwater for a volute pump. Bending moments happening on the pump shaft or rotor assembly component provide mechanically generated forces [26]. The shaft of the rotor faces both cyclic flexural and torsional load during the pumping action. Variable stresses having a high mean stress level may also emerge from the start-and-stop cycles. In this regard, traditional high-cycle fatigue analysis is typically applied in the shaft's safe design [27]. Typical fatigue damage to the shaft is shown in Figure 2.11.

Figure 2.11 Fracture rotor shaft of centrifugal pump [27]

2.3.2 Recent development for wear minimization

Cavitation, erosion, corrosion, and fatigue are the most common wear processes seen in centrifugal pumps. Cavitation is connected to pump installation, operation, and system curves. Similarly, the erosion phenomena is connected to the working environment, which is mostly dependent on working fluid. The corrosion mechanism is linked to the chemical characteristics of the substance. The fatigue process is related to the endurance limit.

The most important method for minimizing such issues is to select a pump that is appropriate for its operating environment and the type of fluid being handled. Furthermore, the manufacturer's performance curve should be properly followed. Material selection and optimization is one method for reducing such issues, but it adds more expense, which means the expenditures must be balanced against the function of the pump utilized. Most researchers employ design optimization in conjunction with numerical models and CFD to enhance the wear performance of centrifugal pumps. However, experimental validation is not extensively researched and implemented in such applications. As a result, further research should be conducted to validate improved designs in actual field circumstances.

2.4 Introduction to Pump as turbine

Pump as turbine (PAT) is a reverse operation of a commercially available pump to fulfill the power requirement of hydropower. Pump as turbines (PATs) may be utilized efficiently to use small hydro resources, with the significant benefit of being less expensive than standard hydraulic turbines [9].

Pumps can be used in turbine mode in small hydropower because of various advantages associated with it such as ease of availability, proven technology, long life span, availability for a wide range of heads and flows, low initial and maintenance cost, availability of spare parts such as seals, and so on [8] [28].

Pump as turbine (PAT) efficiency is often lower than that of traditional hydro turbines. However, efficiency is not the major criteria for such machines, and it is preferred that such machines be operated around the maximum efficiency point.

2.4.1 Historical development of PAT

In 1930, the first pump turbine was installed on a remote farm in North England's Yorkshire Dales. This plan has been tested for five years and its reliability has been verified before being exported to other nations [29]. Since then, the pump-turbine has been a popular issue among researchers and field engineers, and it has been utilized at several sites, mostly for energy provision in remote mountainous regions far from central grid reach.

2.4.2 Selection of PAT

The suitable type of pump is determined by the head and discharge available at the location, the initial and maintenance costs, the ease of availability of the pump, and other factors. In reverse mode, centrifugal pumps with low to high specific speed, single or multistage, radially or axially split, and horizontal or vertical installations can be employed [16]. As indicated in Figure 2.12, the pump to be utilized as a turbine can be chosen based on head and discharge.

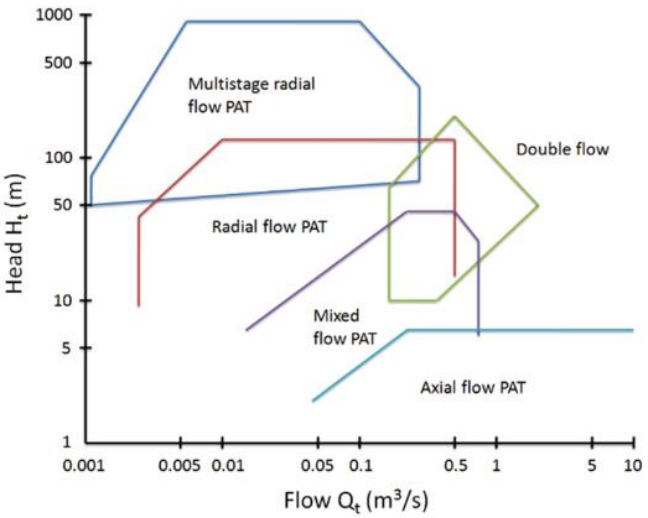

Figure 2.12 Different pumps suitable as turbines [8]

The performance of Multistage, single impeller centrifugal, and axial flow pumps can be compared to Pelton, Francis, and Kaplan turbines in the field conditions respectively. The pump performs best as a turbine in the head range of 13-75 m. Furthermore, when the head grows, it also increases the cost per kW [30]. The operating range of PAT can competitively replace conventional turbines as shown in Figures 2.13 and Figure 2.14.

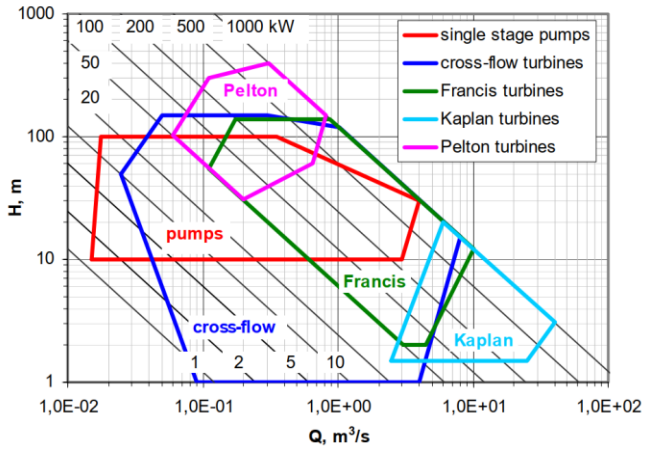

Figure 2.13 Operational range of PAT versus other turbines [31]

Pumps in turbine mode of operation may be applied in a wide range of parameters, replacing a major portion of the small hydro operating range with heads between 2 and almost 1000 m and capacities up to almost 2 MW [32].

In typical hydro turbines, the rotational speed is kept constant against varied power demand by altering the guide vane locations. Because PAT lacks guide vanes, it may be thought of as a turbine with a complete guide vane opening, and hence its speed changes with the varied power output. This may result in PAT instabilities at part load and lowers the part load efficiency, which is one of the primary difficulties hindering PAT technology. It can be shown that traditional turbines have a large working range between 20% and 90% of discharge, but the PAT operates more efficiently in the discharge range of only 80% to 100%. As a result, their applications for fixed load applications are recommended at the highest attainable efficiency, near to full load operation [8].

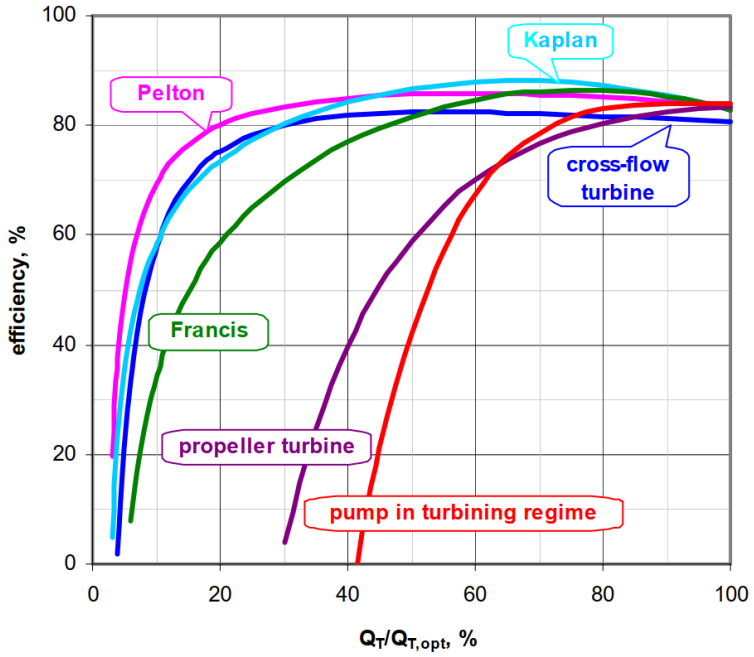

Figure 2.14 Operation range of PAT versus other turbines at various loads [31]

The primary drawbacks of basic PATs are their inability to regulate the flow because they do not have flow control mechanisms like of guide vanes due to which they have

poor performance in non-design operating situations, such as partflow and overflow conditions. As a result, they can only perform efficiently within a narrow range of discharges near to full load of 80-100% [28]. Not only has the efficiency, but in a high range of head for lower specific head there results in flow instability generally defined as S-shaped characteristics [33].

The instabilities caused by the S-shape results in the changes in flow rate, torque, speed, and head, which have a deleterious impact on the startup of pump turbine, synchronization in grid and also in load rejection processes. At region of S shape, same speeds correspond to three different flow conditions with a positive slope along the operating line for pump turbines. As a result it will develop both positive and negative torques subsequently which can easily damage the pump-turbine components, as shown in Figure 2.15.

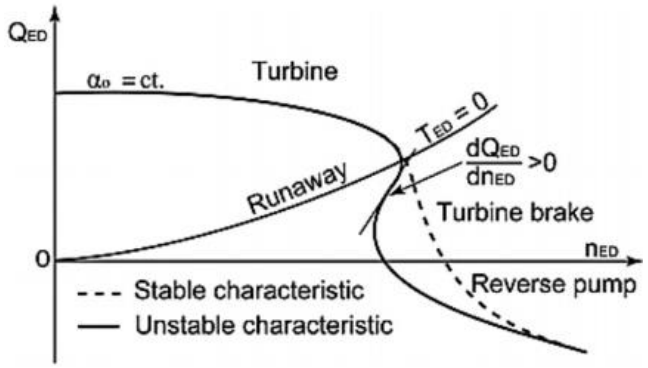

Figure 2.15 S-shaped characteristics of PAT [31]

2.4.3 PAT performance prediction

The performance of the pump when operating as a turbine differs from the performance when operating as a pump. However, the characteristics of operation in turbine mode are not provided by the pump manufacturers. As a result, PAT performance prediction is essential as it decides whether the chosen pump can run at peak efficiency. One of the primary goals of all PAT researchers throughout the world has been to develop a system for making reliable forecasts of pump turbine operation [34].

Many researchers have conducted numerous experimental and theoretical investigations. The researchers' initial goal was to determine the relationships of best efficiency point (BEP) characteristics between the pump mode and turbine mode of the same machine. A correct prediction in BEP will provide the investment with a suitable preliminary pump selection. Researchers have found that the performance of the pump in turbine mode is slightly different in pump mode. Several authors proposed various models that are suitable for a given site. The performance prediction method of the pump as turbine has been compiled by various reviewers [35],[8],[28],[36].

Though their purposed models were different, the most common finding is that At the best efficiency point (BEP), head and flow are greater than in pump mode, and power output is more than the pump input power at the optimum efficiency. These approaches are based on calculating two conversion factors:

$$h = \frac{H_{BEP(t)}}{H_{BEP(p)}}$$
$$q = \frac{Q_{BEP(t)}}{Q_{BEP(p)}} \qquad (2.12)$$

It is simple to see from the preceding equations that q is the ratio of the flow rate at BEP for turbine mode and pump mode and similarly h is the ratio of head at BEP for turbine mode and pump mode respectively.

These two conversion factors might be utilized to make an initial decision on which machine to install. After knowing the site flow rate $Q_{site} = Q_{BEP(t)}$ and site head $H_{site} = H_{BEP(t)}$ and calculating the conversion factors it can be calculated for Q_{BEPp} and H_{BEPp} of the pump, and the pump manufacturers' catalogs can be taken for the selection [37].

The prediction technique from the pump mode application is the simplest as it just requires the user to have access to fundamental pump performance characteristics such

as flow rate, head, and efficiency. This makes it straightforward to discover relevant performance parameters in turbine mode by doing simple calculations. As a result, theoretical study was primarily focused on pump mode performance characteristics, with head and flow correction factors playing an important part in PAT performance prediction [28].

Hossain et al. [38] conducted an experimental comparison analysis of two commonly used theoretical PAT performance prediction approaches, by Chapallaz et al[9] and Sharma [39] to determine which is preferable to the others. The study indicated that Sharma's [39] method could only forecast the PAT BEP and power, but Chapallaz et al. [9] method provided a wide range of operating points from minimal to maximum deviation with information on PAT operation at and away from BEP. Chapallaz et al. [9] method gave the more details of the PAT performance characteristic. Therefore, for the preliminary selection of PAT, Chapllaz's [9] method can be of good choice due to its wide range of data.

CHAPTER 3 STATUS OF PUMP TECHNOLOGY IN NEPAL

3.1 History of pumps used in Nepal

The documented history of the earliest usage of pumps in Nepal is difficult to establish. However, it is conceivable that diesel-powered centrifugal pumps were employed in Nepal, before electricity came. Although the specific date is uncertain, various projects developed in the twentieth century provide a proper picture of the history of pump use in Nepal. Table 3.1 shows some of the specifics of lift irrigation projects in Nepal that generally utilized centrifugal pumps of various sizes and capacities [40].

Table 3.1 Lift irrigation projects in Nepal

S.N.	**Project**	**Date**	**Head**	**Flow**
1	Narayani Lift Irrigation Project	2040	37 [m]	7.2-17.2 [m^3/s]
2	Marchwar Lift Irrigation System	2047	11.9 [m]	2.3-3.855 [m^3/s]
3	Battar Lift Irrigation System	2038		
4	Western Koshi Pump Canal		16 [m]	11.3m^3/s
5	Kiran Nala Irrigation System	2054		150 [l/s]
6	Dhaulagiri Lift Irrigation System		10.1 [m]	150 [l/s]
7	Lamachaur lift scheme		68 [m]	5 [l/s]

The Narayani Lift irrigation project, one of Nepal's major irrigation projects, began operations in 2040 B.S. The project used electric-driven axial pumps to irrigate 47000 Hectares of land in the Chitwan area [40]. The Bhairahawa Lumbini Ground Water Irrigation Project is another example of an irrigation project that uses multistage turbine pumps to irrigate around 7600 Hectares of land in Nepal's Rupandehi district via 63 tube well projects [41]. Pumps were discovered to be utilized in industries conveying fluids at some step of their operations, aside from irrigation and drinking water projects. Table 3.2 shows some of the early industries founded in Nepal.

Table 3.2 Industries established in Nepal using a centrifugal pump

S.N.	Industry	Date	Purpose
1.	Raghupati Jute Mill	2018 B.S.	Jute processing
2.	Lumbini Sugar Mill	2038 B.S.	Sugar processing
3.	Bhrikuti Paper Mill	2040 B.S.	Paper processing
4.	Indushanker Sugar Mill	2042 B.S.	Sugar processing
5.	MK Paper Mill	2050 B.S.	Old paper recycle

Pumps are used in several phases of industrial operations by industries such as Bhrikuti paper mill, which was founded in 2040 B.S., MK paper mills, Lumbini sugar mill, and Indusankar sugar mills. In these industries, centrifugal pumps with closed impellers and semi-open impellers are often utilized. Lighter fluid mixtures need closed impellers, whereas dense fluid mixtures require semi-open impellers, based on the characteristics of the fluids involved. In Nepal, industrialization and urbanization increased the usage of pumps and other advanced technology. Following the establishment of the Department of Water Supply and Sewerage (DWSS) in 1972 A.D., the responsibility of providing free water facilities and sanitation services to people living in rural areas was transferred to the Department of Water Supply and Sewerage, and pumps were utilized in boring systems and overhead tanks as well [42]. The DWSS was responsible with management and maintenance. Nepal Water Delivery Corporation should provide and maintain a drinking water supply system for the urban area at a low cost. Previously, the Panchayat Ministry was largely responsible for providing piped water facilities in rural areas. In addition to the drinking water supply system, sewage pumps have been used equally in these areas since the establishment of Nepal Water Supply and Sewerage Corporation in 1985, with two major water treatment plants constructed at Balkumari, presently known as Kodku, and Sundarighat, presently known as Dhobighat [43]. Various other water treatment plants in Nepal currently utilize sewage pumps of this type [44]. Pumps have now become an essential part of most Nepalese houses. Nepal Water Supply Corporation was also in responsible of municipal wastewater treatment, and they implemented a number of sewage pumps.

3.2 Current status of pump technology in Nepal

Pumps have a considerable market in Nepal. Pump imports have increased considerably over the last eight years, according to the government of Nepal's foreign trade import report record.

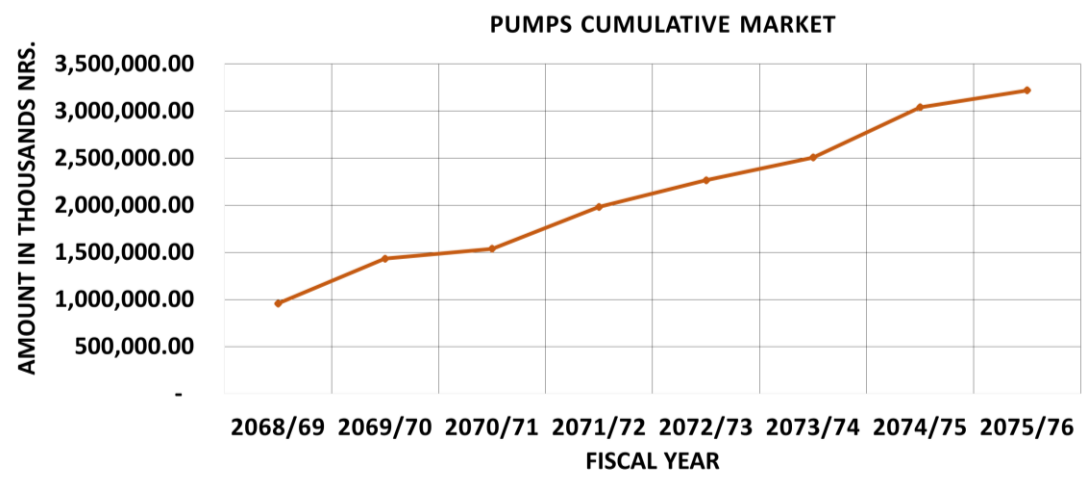

Figure 3.1 Pump cumulative market for different fiscal years.

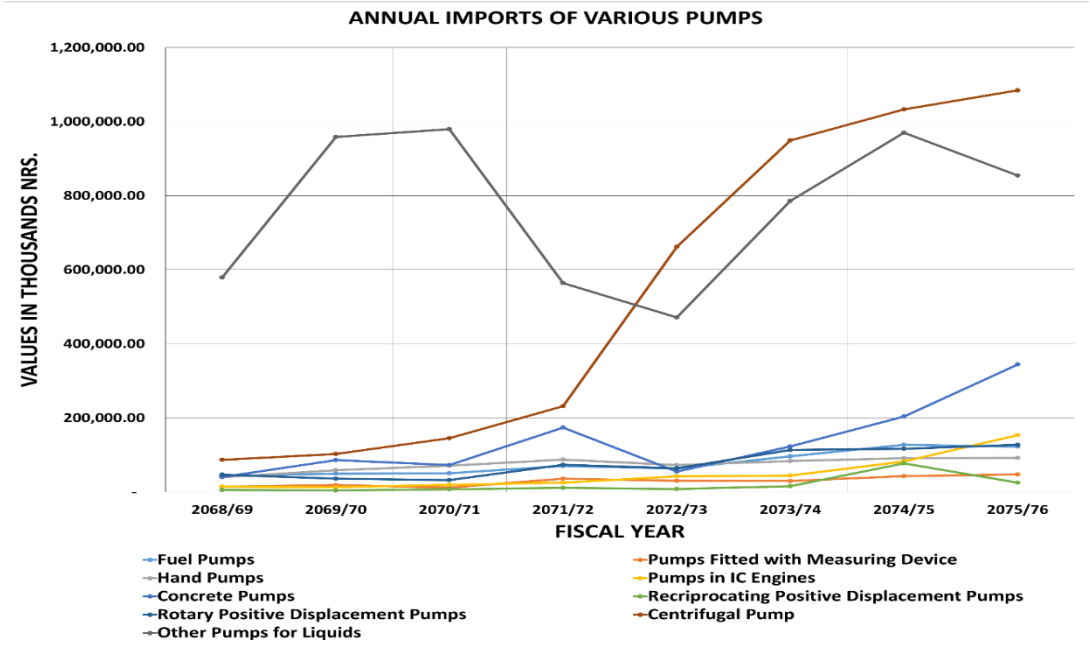

Figure 3.2 Annual imports of various pumps in different fiscal years of Nepal

According to the fiscal year reports of the last seven years, the import of pumps has risen from NRs. 950 million to well over NRs. 3 billion, as indicated in Figure 3.1 [45]. Various types of pumps were imported at this time. Figure 3.2 depicts the annual expenditure on the import of several types of pumps. Among the several types of pumps, centrifugal pumps are the most commonly utilized. The import of hand pumps has decreased significantly. In recent days, the import of concrete pumps has increased due to the construction of new projects utilizing advanced technology.

3.3 Problems faced by pumps and their maintenance in Nepal

In the context of Nepal, no research has been conducted to determine the state of pumps utilized in the country. We can be certain that pumps used in sectors with extremely corrosive fluids would require ongoing maintenance. Furthermore, the annual import of pumps for the same sectors would suggest that the pumps are constantly replaced. It might be due to a scarcity of pump manufacturing and repair businesses in Nepal. As a result, we can also say that pump maintenance is a possibility for investors. Figure 3.3 depicts the yearly market for pump spare parts in Nepal. According to the many field visits and experience given by the pump repairing industries, the pump's primary difficulties include erosion, corrosion as mechanical failure, and short circuit of the coil for the magnetic problem.

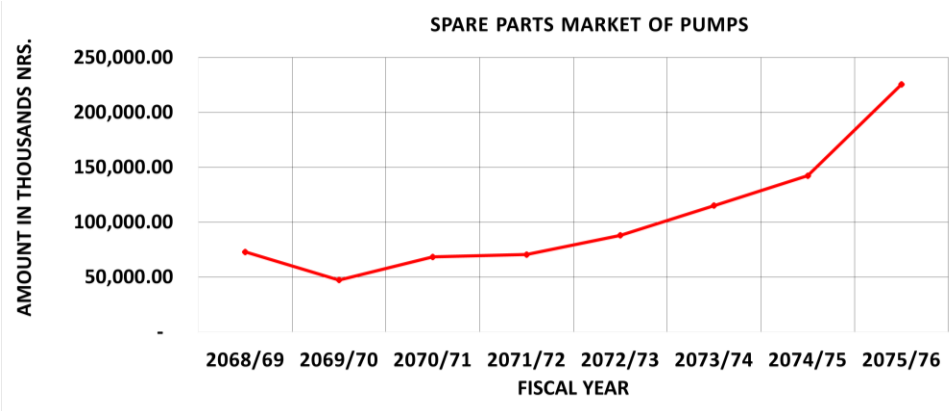

Figure 3.3 Annual maintenance market of pump

The axial pump utilized in the Narayani Lift irrigation system, one of Nepal's largest pumps, is experiencing serious slit erosion difficulties, as seen in Figure 3.4. The pumps' impellers are serviced on a regular basis. As of June 2019, just one of the four units remained operational due to the failure of the other three.

Figure 3.4 Erosion in the axial impeller of Narayani Lift Irrigation Project, Nepal

Pumps used in industry do not perform the same after a certain amount of time. Pumps are frequently observed damaged after specific cycles of operation, depending on the nature of the fluid conveyed. Pumps are used in paper mills to move the slurry of raw ingredients required to create paper.

Figure 3.5 Damaged casing and eroded impeller, MK paper mill, Nepal

The raw materials of a conventional recycling paper mill, where old papers are utilized to generate a slurry, are frequently affected by metal pins and other undesired

compounds. As seen in Figure 3.5, this contaminants and the paper itself have been degrading and corroding the impellers of pumps. Furthermore, because these pumps are utilized from a conventional market and are not built for the special qualities required by the operation, they suffer from cavitation. They frequently replace impellers rather than maintain them. Pumps are also employed in sugar mills to transfer sugarcane juice and heavier molasses. Sugarcanes have been shown to contain silica in some forms that are very erosive, as addressed in many research [46]. Thus, the pump impellers in these industries face the problem of erosion as well.

CHAPTER 4 PERFORMANCE TEST OF CENTRIFUGAL PUMP

4.1 Pump selection and specifications

With the literature review, it was identified that a centrifugal pump could operate in direct and reverse mode. Also in the context of Nepal, the local pump faces several wear problems including erosion. So, one of the suitable sizes of the centrifugal pump (D0) was identified for laboratory testing which description is given below in Table 4.1:

Table 4.1 Specification of Pump under study

S.N.	**Pump Parameter**	**Value**
1.	Specific Speed (Ns)	36
2.	Flow (Q)	10 [l/s]
3.	Head (H)	16 [m]
4.	Revolution (N)	2870 [rpm]
5.	Suction Diameter (d_s)	65 [mm]
6.	Delivery Diameter (d_d)	50 [mm]
7.	Impeller diameter (D)	116 [mm]
8.	Impeller Width (B)	19 [mm]
9.	Rated BEP head (H)	14.2 [m]
10.	Rated BEP flow (Q)	13 .81 [l/s]
11.	BEP efficiency (η)	72 %
12.	Hydraulic Output Power $P_{out(p)}$	1.57 kW
13.	Power Rated	2.33 kW
14.	Motor Input Power $P_{in(m)}$	3.7 kW

In this test, the original pump from the manufacturer was taken for the study for knowing its performance in pump mode and turbine mode. Both numerical and experimental studies were done in this study with various versions of designs. The design of the

existing impeller was modified from the various perspectives with available works of literature and testing was done.

4.2 Design modification methodology of the impeller

Four impellers were tested in this study in which three designs were tested in the experiment and three in CFD as described in Table 4.2 below and as shown in Figure 4.1.

Table 4.2 Impeller description taken for study

Symbol	Description	Experiment	CFD
D0	Original Impeller from manufacturer	☑	☒
D1	First Modification	☑	☑
D2	Francis Turbine	☑	☑
D3	Modification of D1 at leading and trailing edges	☒	☑

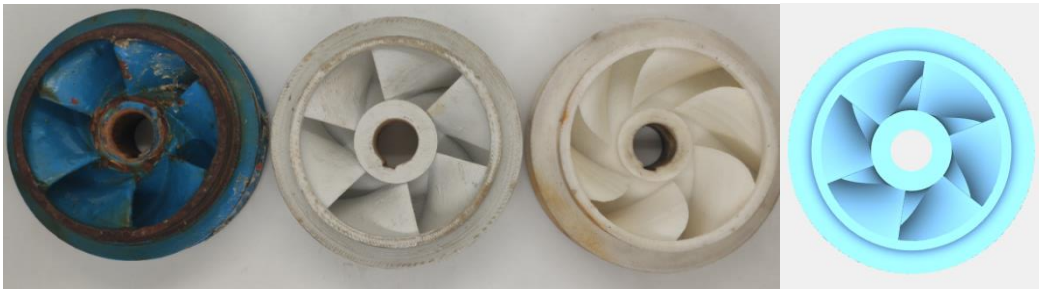

Figure 4.1 Different designs of D0, D1, D2, and D3 from left to right

In the first design (D1), the diameter of the impeller, suction diameter, inlet width hub, and shroud profile was kept constant of the original impeller. However, the blade angle was selected by self-study. The actual blade profile from the manufacturer could not be provided. So for the blade angle, the inlet and outlet blade angles were selected. The inlet blade angle was kept minimum and 10 degrees here so that the turbine mode performance could be increased. The outlet blade angle was kept at 21.4 degrees. The

distribution of the blade angle was taken as linear. The leading edge and trailing edge were taken from the original impeller. For the leading edge, the axis ratio of the ellipse was taken as 3 whereas the trailing edge was taken as the cutoff trailing edge. In design, all the geometric parameters were tried to be kept as close to the manufacturer's impeller. Only the blade angle was taken from that perspective which will be benefited in both pump mode and turbine mode.

In the second design modification (D2), only the diameter of the impeller and width was kept constant. The hub profile, shroud profile, and blade profile were constructed from the design methodology of Francis turbine using in-house software and methodology available in TTL [10]. The purpose of introducing the Francis turbine in PAT was for the improvement of its performance in turbine mode and also to know the reverse operation of the Francis turbine in pump mode without modifications.

In the third design modification (D3), the existing first design (D1) was modified on the leading edge and trailing edge. The axis ratio of the leading edge was reduced and the cutoff trailing edge was made an ellipse.

Out of the three modifications, the first and second design was 3D printed and experimental analysis was done and validated with CFD.

4.3 Numerical study methodology

The governing equations for an incompressible and isothermal flow are solved using a 3D-Averaged Reynold's Navier Stokes. For numerical simulations under steady-state settings, the commercial CFD solver ANSYS-CFX-18.1 was employed. In the turbulence equations, high-resolution discretization was employed in the advection scheme and first-order upwind in the turbulence equations. Root Mean Square (RMS) residuals less than 10E-5 were utilized as the convergence criterion. The following are some explanations of the governing equations, turbulence models, and other numerical model parameters:

$$\rho\left(\frac{\partial \vec{V}}{\partial t}+(\vec{V}.\nabla\vec{V})\right)=\rho.g-\nabla p+\mu.\nabla^2\vec{V} \tag{4.1}$$

Where,

$$\nabla^2=\frac{\partial^2}{\partial x^2}+\frac{\partial^2}{\partial y^2}+\frac{\partial^2}{\partial z^2} \tag{4.2}$$

There are four unknowns in this equation which are velocity components in all directions ($\vec{V}$) and pressure (p). Even though there are four equations to calculate four unknowns, such equations are highly nonlinear Partial Derivative Equations (PDE) which can be solved from computer computations. In this study, Reynolds average method has been followed where a variable, for example, u_i is divided into an average component $\overline{u_i}$ and a fluctuating term $\overline{u_i'}$. By addition of these extra elements to the original transport equation results in:

$$\frac{\partial \overline{u_i}}{\partial x_i}=0 \tag{4.3}$$

$$\frac{\partial \overline{u_i}}{\partial t}+\overline{u_j}\frac{\partial \overline{u_i}}{\partial x_j}=-\frac{1}{\rho}\frac{\partial \overline{p}}{\partial x_i}+\frac{\partial}{\partial x_j}\left(\nu\frac{\partial \overline{u_i}}{\partial x_j}-\overline{u_i'u_j'}\right) \tag{4.4}$$

Where,

$\overline{u_i}$ = Time-averaged velocity components

$\overline{p}$ = Time-averaged pressure

ν = Fluid kinematic viscosity

u_i' = Fluctuating velocity components

t = Time

Although Reynolds' averaging does not affect the continuity equation, it does result in an extra stress component operating on the mean flow owing to the variable velocity, which is known as Reynolds' stress $\tau_{ij} = \overline{u_i' u_j'}$. These terms derive from the un-averaged equations' non-linear convective term and describe the influence of turbulence on the mean flow. As a result, the governing equation has six unknowns that are solved using various turbulence models.

RANS turbulence models are classified as eddy-viscosity models or Reynolds stress models. The eddy viscosity model posits that the gradient diffusion hypothesis relates Reynolds stress to mean velocity gradients and eddy turbulent viscosity, such that:

$$\tau_{ij} = \overline{u_i' u_j'} = \nu_t \left(\frac{\partial \overline{u_i}}{\partial x_j} + \frac{\partial \overline{u_j}}{\partial x_i} \right) - \frac{2}{3} \left(k + \nu_t \frac{\partial \overline{u_k}}{\partial x_k} \right) \delta_{ij} \tag{4.5}$$

Where,

$k = \frac{1}{2} \overline{(u_i' u_j')} =$ Turbulent kinetic energy

$\delta_{ij} =$ Kronecker delta

$\nu_t =$ Turbulent or eddy viscosity

The velocity and turbulent length scale in two-equation eddy-viscosity turbulence models are solved by using two independent transport equations in which one is for kinetic energy k and other for turbulent dissipation rate ε or the specific dissipation rate ω. For $k - \varepsilon$ the model, the turbulence viscosity ν_t is related to the turbulence kinetic energy k and the dissipation rate ε by the relation:

$$\nu_t = C_\mu . \frac{k^2}{\varepsilon} \tag{4.6}$$

Where $C_\mu =$ Constant

Although the model was commonly utilized because of its resilience and quicker simulations when compared to other turbulence models, it has limits in steep pressure

gradients, flow including separations, rotation, and near-wall zones. For the near-wall boundary region, $k-\omega$ produce a more accurate result, but it is very sensitive outside of the boundary layer. For this, a blending between the $k-\omega$ model near the boundary and $k-\varepsilon$ the model in the free stream was developed by Menter [47]. In this model, BSL turbulence model was introduced as the first step by introducing a blending function F. In addition to this function, the SST model predicts eddy viscosity by accounting for the propagation of the primary turbulent shear stress. Alo, an earlier sensitivity investigation of turbulence models SST, BSL, and Omega RS with such applications revealed that the SST turbulence model is best suited for the CFD of this test rig [48].

For numerical study there consisted mainly runner, spiral casing, reducer, suction pipe, and delivery pipe as shown in Figure 4.2. The modeling of the impeller and spiral casing was done in CF turbo as described in Appendix II. Meshing is a very important step in numerical analysis as the structures, quality, and types of mesh have a vital role in the overall accuracy of the simulation as well as the time and convergence of the result. Hexahedral, tetrahedral, and hybrid mesh are generally used for CFD analysis. Tetrahedral take less time for meshing while hexahedral meshes are structured mesh which is more efficient in term of accuracy, CPU solving time, and memory allocation.

Figure 4.2 Numerical domain set up for analysis

For the meshing two strategies are used. For the spiral casing, reducer and draft tube tetra mesh were selected as shown in Figures 4.3 and Figure 4.4. The proximity and curvature functions were used for the wall refinement factor. Similarly, the inflation layer was put in the wall and the value of Y plus in post-processing was noted and changed until the required value is reached. For the meshing of the impeller, ANSYS TurboGrid was used as shown in Figure 4.5. The mesh was properly refined using the global size factor and trailing edge refinement factor for the targeted value of Y plus. The requirement of y+ is different from one turbulence model to another turbulence model. The y+ obtained from the analysis is compared with the recommended values for each turbulence model. If the y+ obtained from the result is not in the region, the factor is changed to a higher value to obtain the required result. The average value that could be obtained in the simulation is shown in Table 4.3. Similarly, the grid independence test has also been carried out under particular conditions and the same meshing has been performed in all the simulations. The efficiency value with a number of elements can be seen in Figure 4.6.

Figure 4.3 Tetra mesh of spiral casing and delivery pipe with wall refinement

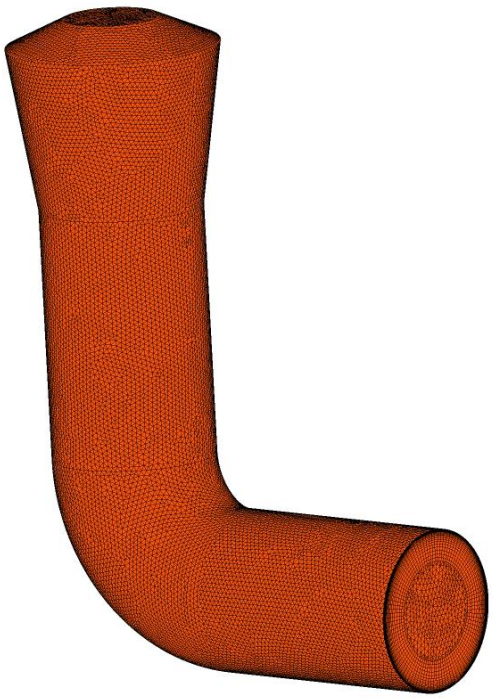

Figure 4.4 Tetra mesh of reducer and delivery pipe with wall refinement

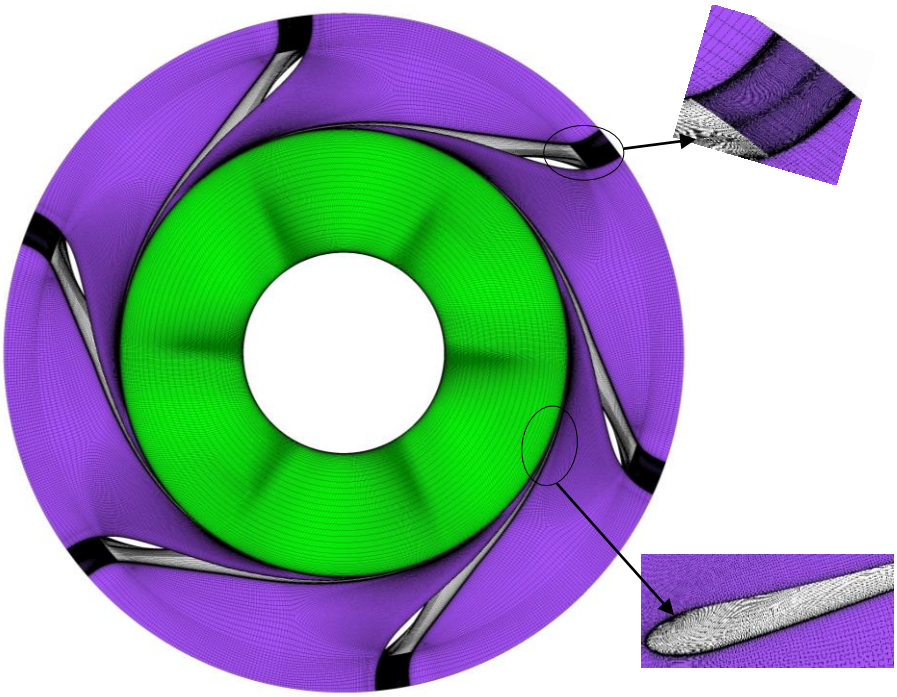

Figure 4.5 Hexahedral mesh of impeller in turbogrid

Table 4.3 Average value of Y plus at various regions.

S.N.	Location	The average value of Y plus
1.	Spiral Casing and delivery pipe	0.443062
2.	Runner Blade	11.2027
3.	Reducer and suction pipe	0.307139

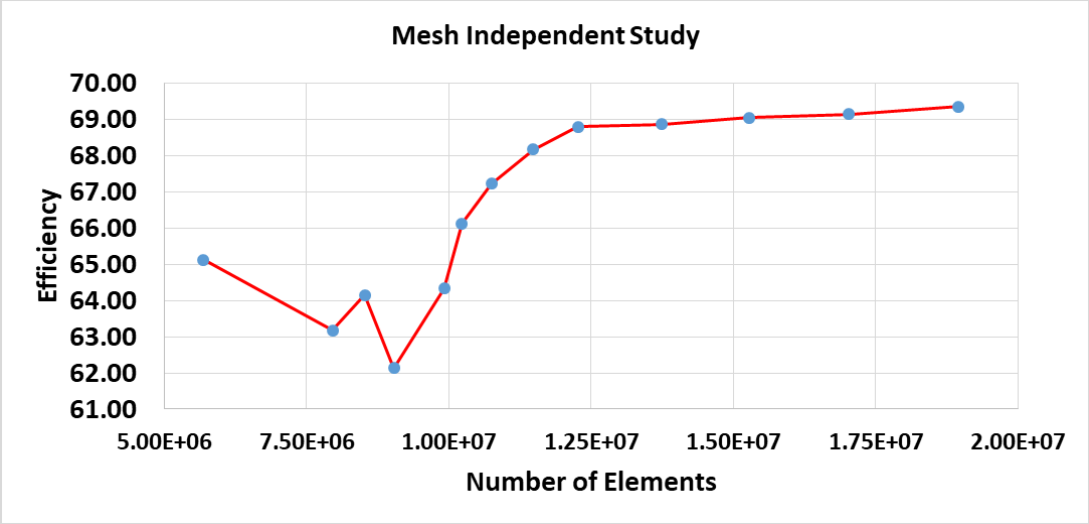

Figure 4.6 Grid independence study

The CFD is performed by setting the analysis to steady state type while no-slip vicious condition at a wall is applied. The spiral casing along with the delivery pipe and suction pipe along with the reducer was set as a stationery domain. The runner was set as a rotating domain in which the blade, hub, and shroud region were set as a wall. Two value of rpm was chosen for the study mainly 1500 rpm and 3000 rpm.

The reference pressure for all domains was set to 1 atm. For pump mode, the inlet condition was given as static pressure with relative pressure set to zero, and the outlet condition was given as mass flow rate. Similarly for turbine mode, the inlet condition was given as mass flow rate and the outlet condition was given as average static pressure with relative pressure of zero. The summary of boundary conditions for pump mode and

turbine mode is shown below in Table 4.4 and the volume for CFD is shown in Table 4.5.

Table 4.4 Boundary Condition for CFD analysis

Domain Name	**Type**	**Surfaces**	**Boundary Condition**	**Details**
Pump mode				
Spiral Casing with Delivery Pipe	Stationery	Casing inlet	Mass flow rate	2-30 [l/s]
		Casing wall	Smooth wall	No slip
Impeller	Rotating	Impeller Hub	Wall	1500 and 3000 [rpm]
		Impeller Shroud	Wall	
		Impeller Blade	Wall	
Reducer with Suction Pipe	Stationery	Delivery Outlet	Static Pressure	0 [atm]
		Pipe wall	Wall	No slip
Turbine mode				
Spiral Casing with Delivery Pipe	Stationery	Casing inlet	Mass flow rate	2-30 [l/s]
		Casing wall	Smooth wall	No slip
Impeller	Rotating	Impeller Hub	Wall	1500 & 3000 [rpm]
		Impeller Shroud	Wall	No slip
		Impeller Blade	Wall	No slip
Reducer with Suction Pipe	Stationery	Delivery Outlet	Static Pressure	0 [atm]
		Pipe wall	Wall	No slip

Table 4.5 Number of elements for CFD analysis

S.N	Description	Nodes	Elements
1.	Spiral Casing with Delivery Pipe	795,133.00	1,780,438.00
2.	Impeller	8,525,328.00	8,086,980.00
3.	Reducer with suction pipe	1,031,832.00	2,397,702.00
4.	Total	10,352,293.00	12,265,120.00

4.4 Experimental study methodology

The experiment was carried out in a closed loop system at Turbine Testing Laboratory, Kathmandu University. The lab has a maximum flow capacity of 500L/s with a head of 150m when operated in a closed loop system and 30m when operated in a natural head. The maximum capacity of a turbine that can be tested in the lab is 300kW. With the existing test facility of the turbine testing lab, the experimental setup is designed in such a way that a centrifugal pump can be tested in both pump and turbine mode. The setup for the experiment is shown in Figure 4.7.

Figure 4.7 Experimental set up of pump for both modes with water only

The experimental setup is designed in such a way that the pump can be tested in both pump and turbine mode at the same time. The schematic details of the rig are shown in Figure 4.8 along with the component description. The setup consisted of a large reservoir of TTL, large piping, a high-pressure tank, bends, reducers of different sizes, a T joint, etc. The experiment involved five measurements. Two pressure sensors are fitted just on the suction and delivery side of the pump for differential head measurement. Similar to the flow measurement the rig consists of a DN 100 Electromagnetic flow meter. For the torque and rpm measurement, the rig consisted of a torque transducer fitted in between the motor and pump shaft.

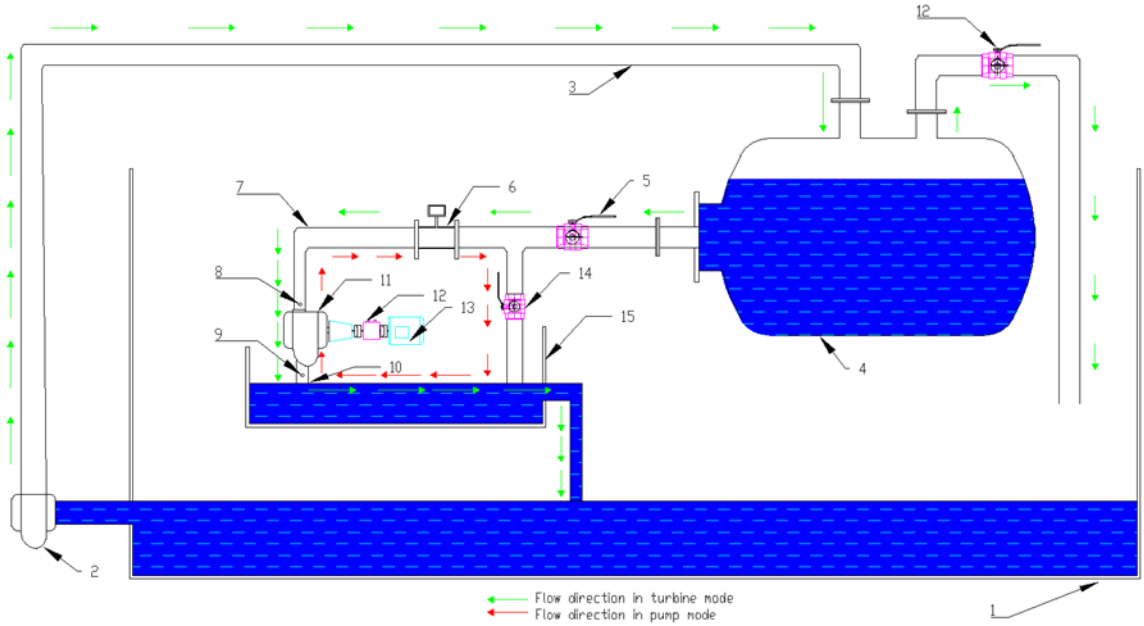

Figure 4.8 Schematic rig of the experiment

1. Large reservoir, 2.Large Pump, 3. Inlet pipe, 4. High-pressure tank, 5.Butterfly valve, 6.Flowmeter, 7.Delivery pipe, 8. Delivery side pressure Tapping, 9. Suction side pressure tapping, 10. Suction pipe, 11. Pump/PAT, 12.Torque transducer, 13. Induction motor, 14.Spherical valve, 15. Small reservoir.

The speed of the PAT was controlled by the VFD system. The impeller was tested in both pump mode and turbine mode. The rated rpm was kept a bit high in turbine mode. It is because for an induction motor to operate as a generator, it starts to generate power only when the synchronous speed is reached [49].

4.4.1 Pump mode operation

During pump mode operation as shown in the schematic set up in Figure 4.8. The water from the small reservoir goes to the suction pipe and then to the pump impeller. After that, it goes to the flow meter through the delivery pipe. In between the flow meter and high-pressure tank, there is one butterfly valve that remains closed during this operation. So, water goes back to the small reservoir through a supply pipe where a spherical valve remains open during this operation. Two pressure sensors are fitted on the suction side and delivery side of the pump for pressure measurements. In between the pump shaft and induction motor, a torque transducer has been fitted for torque and rpm measurement. The spherical valve fitted in the return pipe can be operated in varied positions manually through a lever for controlling the flow for different operating conditions.

4.4.2 Turbine mode operation

For turbine mode operation, the water from the larger reservoir of TTL goes into the high-pressure tank through an inlet pipe. In high pressure, there are two outlets on which one way goes into the PAT system and another way is used as a bypass system. Through one outlet the water goes to the butterfly valve from the high-pressure tank. The spherical valve remains closed in this operation. After the butterfly valve, the water is directed towards the pump which is being operated at turbine mode. After that, the water goes into the small reservoir and then back to the larger reservoir. The flow and head in this condition are controlled by the supply pump at TTL which is operated by the VFD system.

4.5 Observation methodology

Each of the signals was measured from mainly three sensors i.e. pressure transducer, flow meter, and torque transducer is received as voltage signals in the LabVIEW program. Those signals were converted into required output values through calibrated equations. For this, continuous data were recorded at a rate of 2000 data points per second, which were then processed, and an effective mean of the recorded data was utilized as output data from the data logger LabVIEW.

The efficiency of the pump in pump mode was calculated as:

$$\eta_p = \frac{P_{out(p)}}{P_{in(p)}} \tag{4.7}$$

Where

$P_{out(p)} = \rho.g.Q.H_{net} =$ Output power delivered by the pump

$\rho =$ The density of the fluid being handled

$g =$ Acceleration due to gravity

$Q =$ Discharge output delivered by the pump

$H_{net} = P_d - P_s =$ Net head delivered by the pump

$P_d =$ Pressure at the suction side of the pump impeller

$P_s =$ Pressure at the delivery side of the pump

$P_{in(p)} = \tau.\omega =$ Shaft power delivered to the pump

$\tau =$ Torque input to the shaft

$\omega = \frac{2\pi N}{60} =$ Angular rotation of the pump impeller

$N =$ Revolution per minute of the impeller.

With simplifications,

$$\eta_p = \frac{P_{out(p)}}{P_{in(p)}} = \frac{\rho.g.Q.H_{net}}{\tau.\omega}$$

$$\eta = \frac{60 \times \rho.g}{2.\pi} . \frac{Q(P_d - P_s)}{\tau.N} \tag{4.8}$$

From the above equations, it is seen that there are five variables to calculate the efficiency of the pump i.e., Q, P_d, P_s, τ, N . The value Q is measured by the flow meter. The value of P_d and P_s are measured by the two pressure sensors fitted each at the delivery and suction end of the pump. Similarly, the value of τ and N is measured by the torque transducer.

For the turbine mode operation, only the power output and power input will be interchanged which makes efficiency as:

$$\eta_{(t)} = \frac{P_{out(t)}}{P_{in(t)}} \tag{4.9}$$

Where,

$P_{out(t)} = \tau\omega$ Output shaft power is delivered by the pump impeller.

$\tau =$ Torque output from the shaft

$\omega = \frac{2\pi N}{60} =$ Angular rotation of the pump impeller

$N =$ Revolution per minute of the impeller.

$P_{in(t)} = \rho.g.Q.H_{net}$ =Input hydraulic power to the pump impeller

$\rho =$ The density of the fluid being supplied

$g =$ Acceleration due to gravity

$Q =$ Discharge input to the pump impeller

$H_{net} = P_d - P_s =$ Net head delivered to the pump

$P_d =$ Pressure at the suction side of the pump impeller

$P_s =$ Pressure at the delivery side of the pump

With simplifications,

$$\eta_{(t)} = \frac{P_{out(t)}}{P_{in(t)}} = \frac{\tau.\omega}{\rho.g.Q.H_{net}} \tag{4.10}$$

4.6 Result and discussions

4.6.1 Experimental performance of the original impeller

The performance of D0 is shown in Table 4.6 and the performance curve is shown in Figures 4.9-4.13.

Table 4.6 BEP performance of D0

Mode	**RPM**	**H [m]**	**Q [l/s]**	η **[%]**	**[P in [W]**	**P out [W]**
Pump	3000	14.50	10.28	63.45%	2298.12	1458.15
Turbine	3000	21.96	14.17	64.56%	3043.16	1964.72
		h=1.51	q=1.38			
Pump	1500	3.43	5.36	62.10%	289.8	179.9
Turbine	1500	10.90	11.13	57.94%	1186.49	687.49
		h=3.2	q=2.08			

From Table 4.6 it is seen that for a pump to operate in turbine mode, the head and discharge requirement at BEP is higher than in pump mode. Similarly, the efficiency in pump mode as a comparison to turbine mode is comparable with some differences noted.

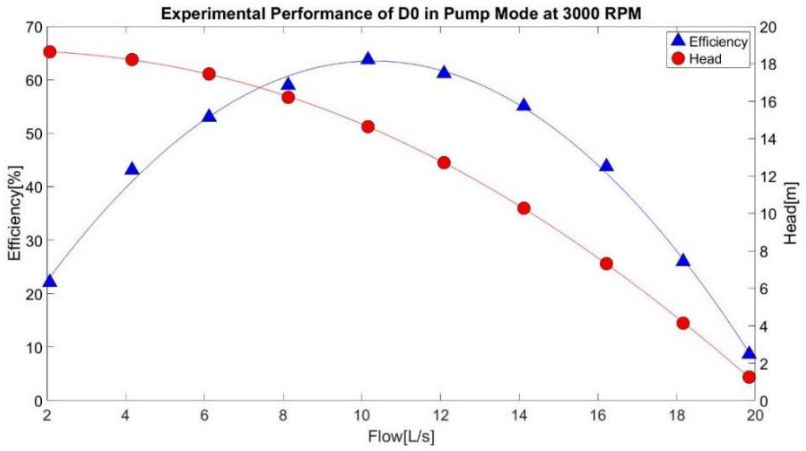

Figure 4.9 Experimental performance of D0 in pump mode at 3000 RPM

If the shaft power for both modes is compared, the shaft power requirement for turbine mode is higher but sometimes this may be because of the limitations for the same induction motor to operate at high power since the generator is designed for a specific speed and power. This can also be seen in Figure 4.10 that when the flow is reached beyond 14 l/s, the experiment has to be halted due to overheating of the motor and resistor.

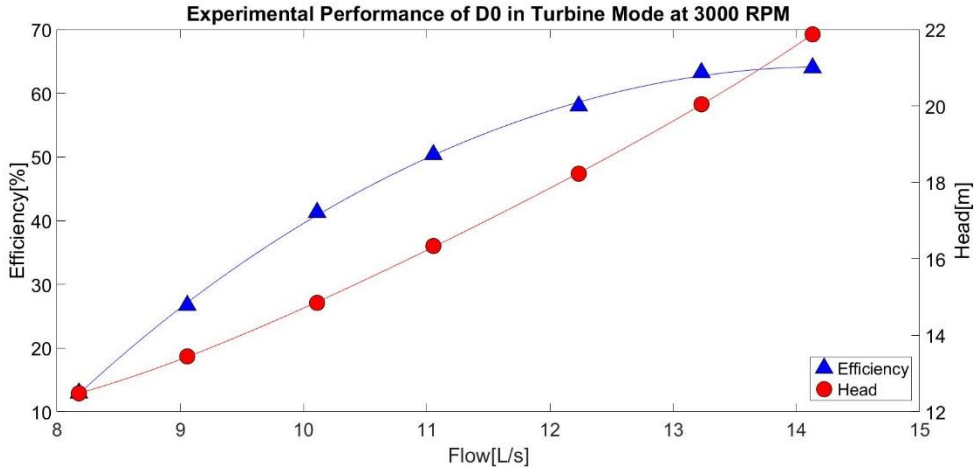

Figure 4.10 Experimental performance of D0 in Turbine mode at 3000 RPM

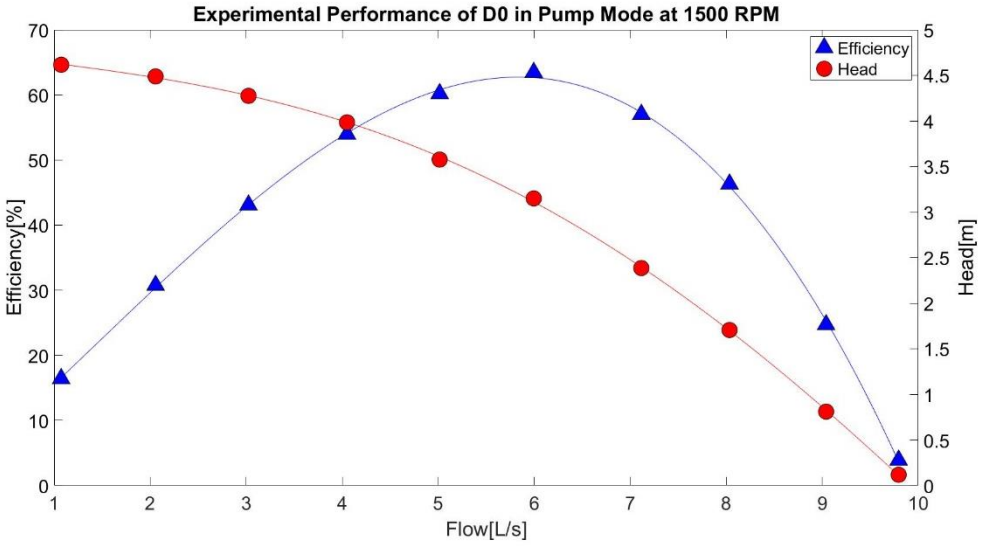

Figure 4.11 Experimental performance of D0 in pump mode at 1500 RPM

If we compare the result of the same machine in immediate lower synchronous speed i.e 1500 rpm, the pump could be operated in turbine mode at full capacity from full load part load conditions as shown in Figure 4.12. The efficiency of the device may be less at BEP, but the generated shaft power could be within the limit of induction motor requirements.

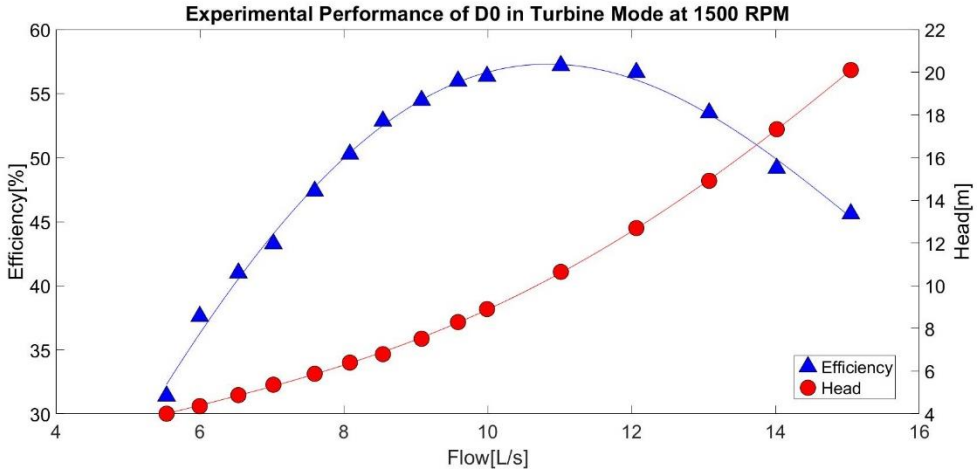

Figure 4.12 Experimental performance of D0 in turbine mode at 1500 RPM

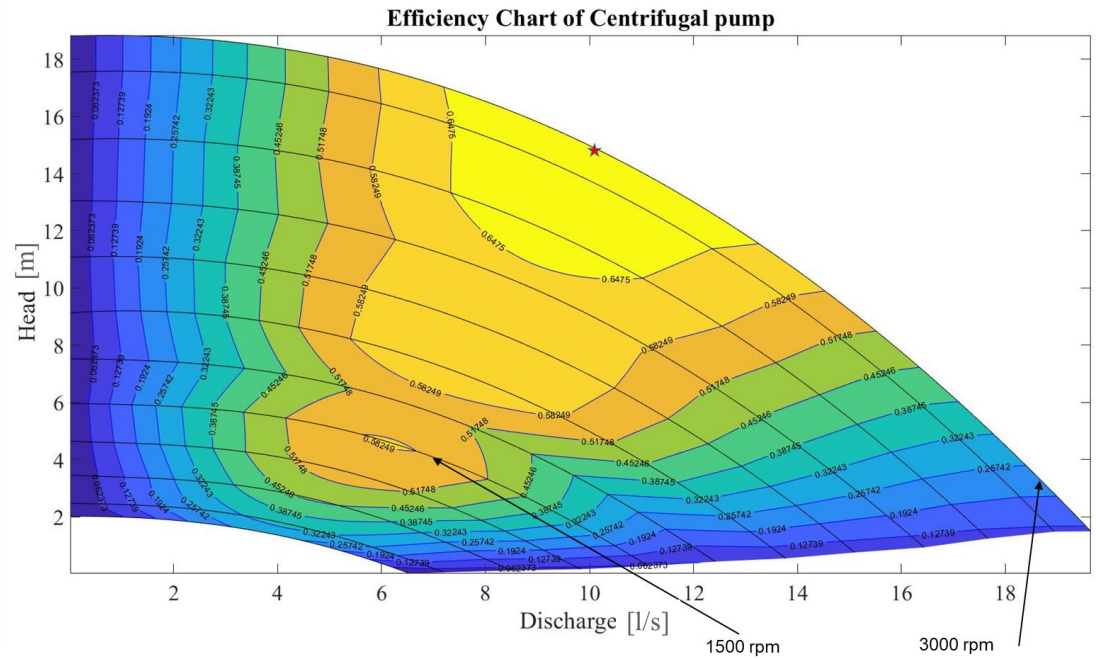

Figure 4.13 Hill chart diagram in pump mode for D0

In this study, the completer characteristics curve of the pump in different rpm has also been done. Since the pump manufacturers always provide the characteristics curve at a particular motor speed, the performance of the pump at various speeds may be quite unknown but may be required at the particular operation where variable frequency drives are used for particular industrial applications. The performance of D0 at various rpm from 1000 to 3000 is seen in Figure 4.13. It is seen that the peak efficiency was noted near the two synchronous speeds i.e. 1500 and 3000 rpm. This shows that for this pump to operate at variable speed, the speed should be near two synchronous speeds if the efficiency selection is the main criterion.

4.6.2 Experimental performance comparisons of various designs

For the experimental performance comparisons, mainly three designs i.e., D0, D1, and D2 were tested in the experiment in both mode at two synchronous speed, the BEP parameters for pump mode is shown in Table 4.7 and the performance curve for pump mode is shown in Figure 4.14-4.15.

Table 4.7 Experimental BEP comparision on pump mode

BEP Parameter for Pump Mode at 3000 rpm					
S.N.	H [m]	Q [l/s]	η	P in [W]	P out [W]
D0	14.50	10.28	63.45%	2298.12	1458.15
D1	15.48	10.85	65.83%	2494.52	1642.18
D2	15.78	11.17	53.09%	3245.70	1723.20
BEP Parameters for Pump Mode at 1500 rpm					
S.N.	H [m]	Q [l/s]	η	P in [W]	P out [W]
D0	3.43	5.36	62.10%	289.8	179.9
D1	3.74	5.28	64.76%	297.6	192.8
D2	3.88	5.56	54.88%	384.4	211.0

From Table 4.7 it is seen that at the actual synchronous speed of 3000 rpm the experimental result showed that the D1 had the highest efficiency in pump mode with values of efficiency for D1, D0, and D2 as 65.83 %, 63.45%, and 53.09%. The experimental results at 1500 rpm are also comparable to that of 3000 rpm. For the pump mode at 1500 rpm, D1 had the highest efficiency with the value of efficiency for D1, D0, and D2 as 64.76%, 62.10%, and 54.88%.

This shows that the efficiency in pump mode is highest for D1 and lowest for D2. Further, it reveals that by reverse engineering and changing the blade angle distribution the efficiency of the pump can be increased. Also, it is noteworthy that the performance of the Francis turbine in pump mode is weaker than that of the centrifugal pump

If the performance curve in pump mode is seen in Figure 4.14-4.15, another interesting fact can be deduced. Although the efficiency of the Francis turbine in pump mode at

BEP is less as it has a wide operating range in terms of head and discharge in comparison to the original centrifugal pump impeller.

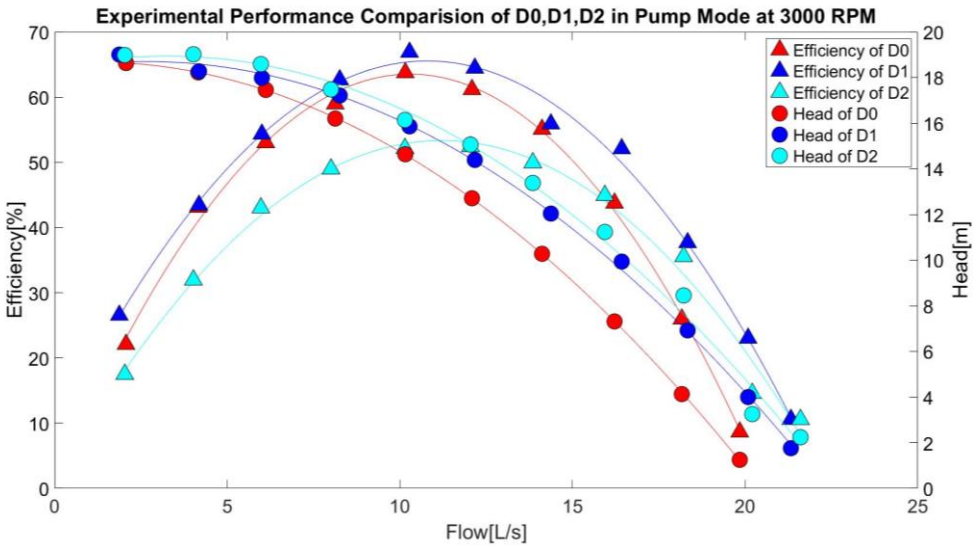

Figure 4.14 Experimental performance comparisons in pump mode at 3000 RPM

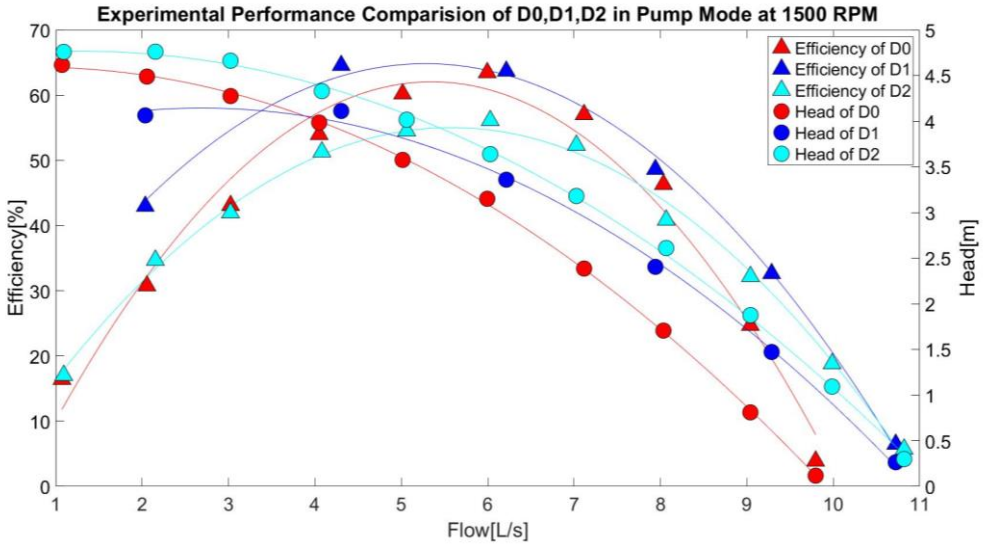

Figure 4.15 Experimental performance comparisons in pump mode at 1500 RPM

The BEP comparison of various designs in turbine mode is shown in Table 4.8. If we compare Table 4.7and Table 4.8, it can be seen that the turbine mode BEP is always in

higher condition than in pump mode. However, in turbine mode, D2 had the highest efficiency with the value of efficiency for D2, D1, and D0 as 72.13%, 69.17%, and 64.56%. This reveals that the Francis turbine can compete with PAT in turbine mode however its pump mode performance is weaker than the centrifugal pump. Similarly comparing the result of D0 and D1 it can be seen that by modifying the impeller from reverse engineering with changing outlet angle, the efficiency in turbine mode can be increased significantly with the advantage of the slight increase in efficiency in turbine mode.

The result in turbine mode at 1500 rpm is also comparable to 3000 rpm. In turbine mode at 1500 rpm, D2 has the highest efficiency with the value of efficiency for D2, D1, and D0 as 63.99 %, 59.66%, and 57.94 %.

Table 4.8 Experimental BEP Comparision for turbine mode

BEP Parameters for Turbine mode at 3000 rpm							
S.N.	H [m]	Q [l/s]	η	P in [W]	P out [W]	h	q
D0	21.96	14.17	64.56%	3043.16	1964.72	1.51	1.38
D1	23.93	14.53	69.17%	3400.30	2351.95	1.55	1.34
D2	37.02	21.34	72.13%	7728.23	5574.20	2.35	1.91
BEP parameters for Turbine mode at 1500 rpm							
S.N.	H [m]	Q [l/s]	η	P in [W]	P out [W]	h	q
D0	10.90	11.13	57.94%	1186.49	687.49	3.2	2.08
D1	9.91	10.47	59.66%	1014.91	605.48	2.7	1.99
D2	12.74	12.62	63.99%	1571.77	1005.79	3.3	2.27

The experimental performance comparison of various designs in turbine mode is shown in Figures 4.16-4.17. At 3000 rpm, due to the limitations in motor capacity, only part load and BEP conditions are reached. However, the result from Figure 4.16 could reveal that D2 has a well-off-design operation.

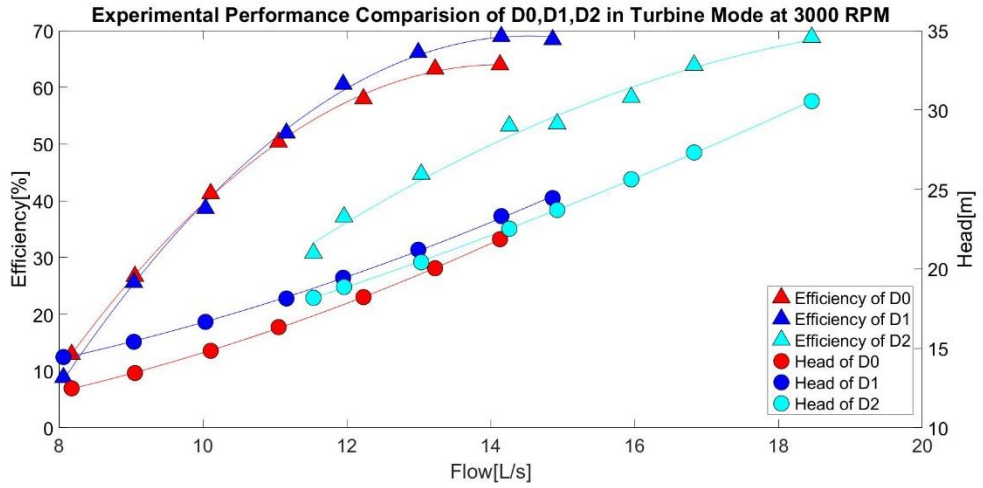

Figure 4.16 Experimental performance comparisons in turbine mode at 3000 RPM

The comparison is even clearer at the result of 1500 rpm as shown in Figure 4.17. It shows that D2 has the highest efficiency and its operation is even better at off BEP conditions in comparison to D1 and D0. Also if the result between D0 and D1 is compared, it shows that by modifying the original impeller the part load performance of D1 has increased however its performance at full load is similar to the original impeller.

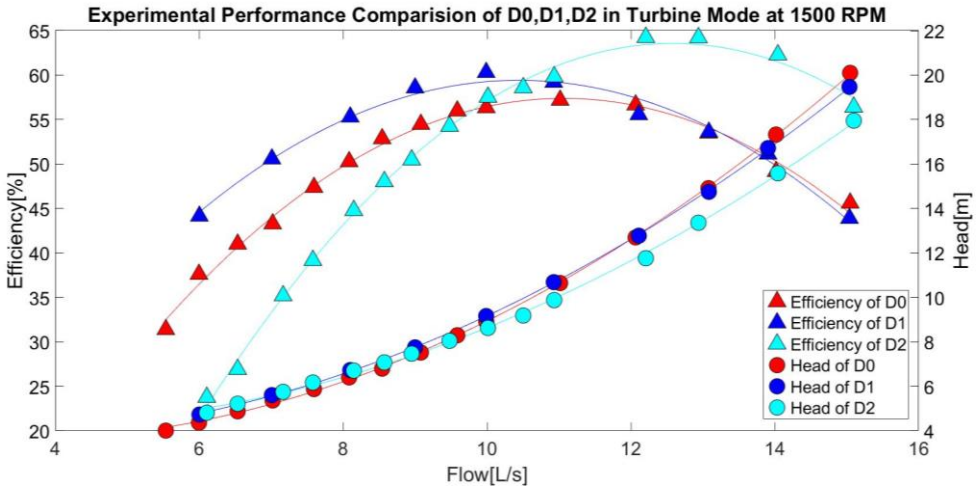

Figure 4.17 Experimental performance comparisons in turbine mode at 1500 RPM

4.6.3 Comparison of performance from the numerical and experimental study

In order to relate the CFD result with the experiment, the performance of two designs D1 and D2 were studied numerically as well as experimentally. If we compare the CFD predicted results with the experiment, results for D1 and D2 are comparable. The experimental result showed higher efficiency of D1 compared to D2 for pump mode. At 3000 rpm the efficiency at pump mode for D1 and D2 is 67.67% and 65.35%. Although the results could be compared in terms of efficiency in both designs for CFD and experiment, the deviation in various parameters was noted as shown in Table 4.9.

Table 4.9 CFD vs Experimental BEP comparision for pump mode

BEP Parameter for Pump Mode at 3000 rpm					
S.N.	**H [m]**	**Q [l/s]**	**η**	**P in [W]**	**P out [W]**
D1 CFD	14.17	12.84	67.70%	2628.41	1779.44
D1 EXP	15.48	10.85	65.83%	2494.52	1642.18
Deviation	9.26%	15.53%	2.76%	5.09%	7.71%
D2 CFD	13.36	13.41	60.35%	2903.89	1752.50
D2 EXP	15.78	11.17	53.09%	3245.70	1723.20
Deviation	18.12%	16.76%	12.03%	11.77%	1.67%
BEP Parameter for Pump Mode at 1500 rpm					
S.N.	**H [m]**	**Q [l/s]**	**η**	**P in [W]**	**P out [W]**
D1 CFD	3.67	6.35	69.51%	327.38	227.55
D1 EXP	3.74	5.28	64.76%	297.63	192.75
Deviation	1.91%	16.88%	6.83%	9.09%	15.30%
D2 CFD	3.61	7.61	63.57%	422.89	268.84
D2 EXP	3.88	5.56	54.88%	384.44	210.98
Deviation	7.35%	26.90%	13.67%	9.09%	21.52%

A clear picture of deviation is revealed in Figures 4.18-4.21. For pump mode operation at high flow conditions, more deviation in the head is noted. This means that the experimental data deviated from CFD at high flow and low head conditions which is in near BEP and full load conditions. This also signifies that our device is more uncertain in low head conditions.

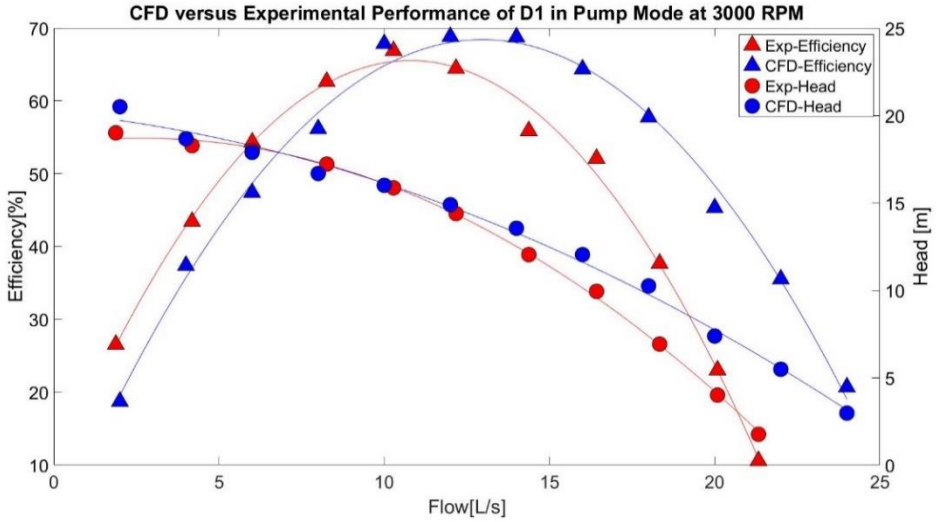

Figure 4.18 CFD Vs. Experimental performance of D1 in pump mode at 3000 RPM

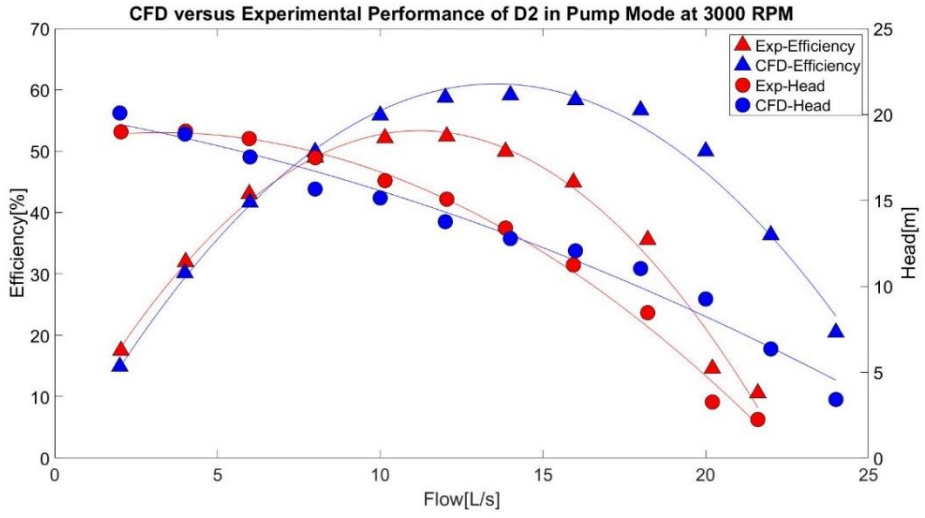

Figure 4.19 CFD Vs. Experimental performance of D2 in pump mode at 3000 RPM

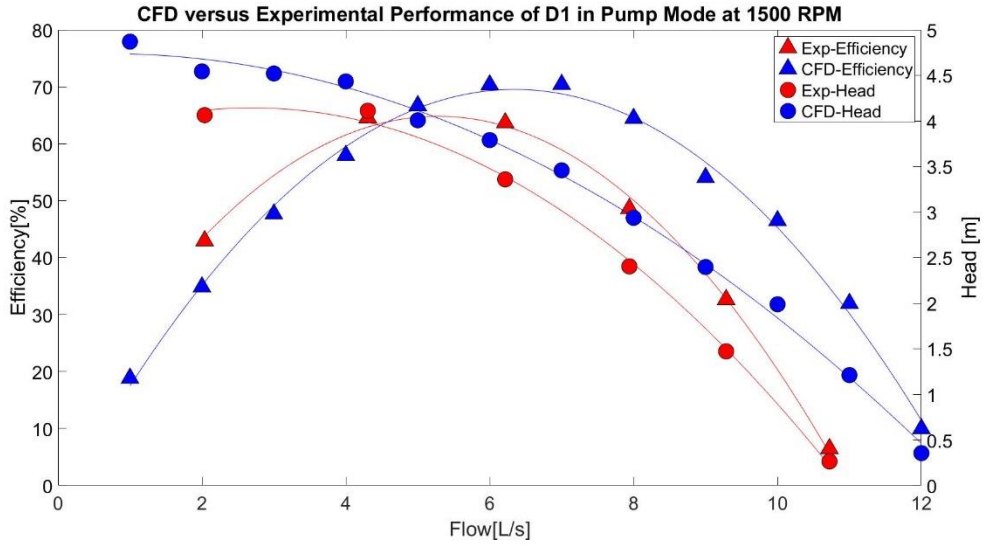

Figure 4.20 CFD Vs. Experimental performance of D1 in pump mode at 1500 RPM

Similarly, the performance of D2 in pump mode is also comparable to D1. The significant difference in results in CFD and experiment was seen at high flow and low head conditions. As seen in Figures 4.18-4.21, the efficiency curve of CFD and experiment is closer at part load conditions but farther in BEP and full load conditions.

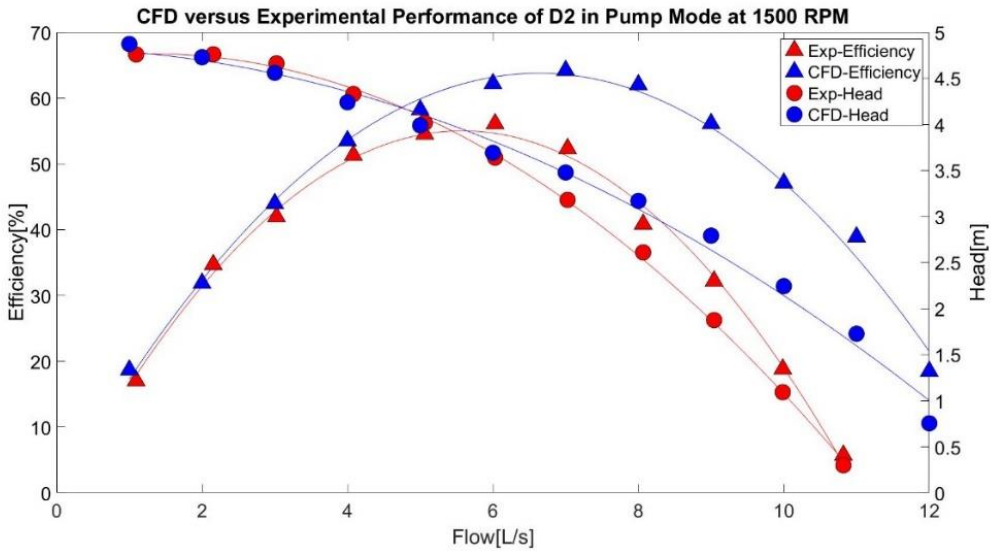

Figure 4.21 CFD Vs. Experimental performance of D2 in pump mode at 1500 RPM

The comparison of CFD results with the experiment in Turbine mode for D1 and D2 is shown in Table 4.10. If we compare Table 4.9 and Table 4.10 the efficiency deviation from CFD in the experiment is more in turbine mode than in pump mode.

Table 4.10 CFD vs Experimental BEP comparison for turbine mode

BEP Parameters for Turbine mode at 3000 rpm							
S.N.	H [m]	Q [l/s]	η	P in [W]	P out [W]	h	q
D1 CFD	32.37	25.92	0.91	8204.22	7497.12	2.28	2.02
D1 EXP	23.93	14.53	0.69	3400.30	2351.95	1.55	1.34
Deviation	26.08%	43.93%	24.31%	58.55%	68.63%	32.34%	33.62%
D2 CFD	33.91	31.79	0.95	10542.33	9995.86	2.54	2.37
D2 EXP	37.02	21.34	0.72	7728.23	5574.20	2.35	1.91
Deviation	9.18%	32.86%	23.93%	26.69%	44.23%	7.57%	19.34%
BEP Parameters for Turbine mode at 1500 rpm							
S.N.	H [m]	Q [l/s]	η	P in [W]	P out [W]	h	q
D1 CFD	6.62	11.23	0.89	727.04	650.16	1.80	1.77
D1 EXP	9.91	10.47	0.60	1014.91	605.48	2.65	1.99
Deviation	49.73%	6.77%	33.29%	39.59%	6.87%	46.93%	12.16%
D2 CFD	8.70	15.44	0.88	1014.91	605.48	2.41	2.03
D2 EXP	12.74	12.62	0.64	1571.77	1005.79	3.29	2.27
Deviation	46.31%	18.28%	27.13%	54.87%	66.12%	36.29%	11.79%

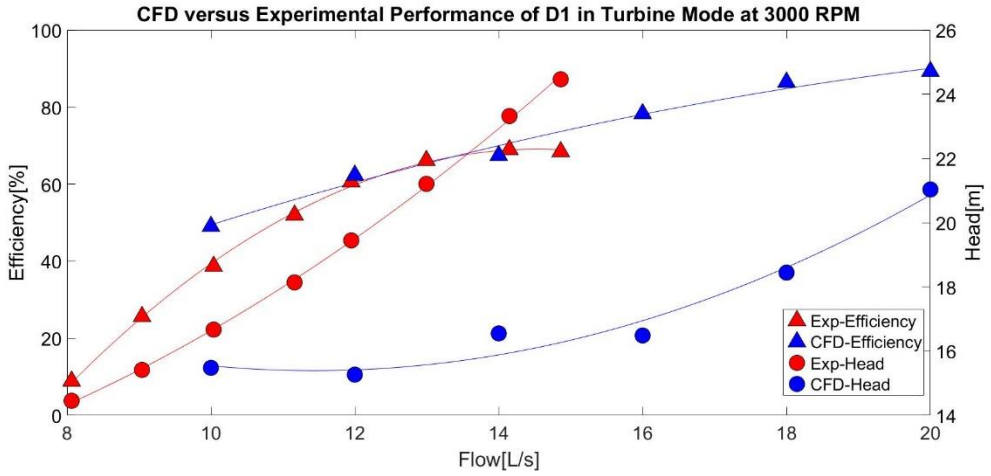

Figure 4.22 CFD Vs. Experimental performance of D1 in Turbine mode at 3000 RPM

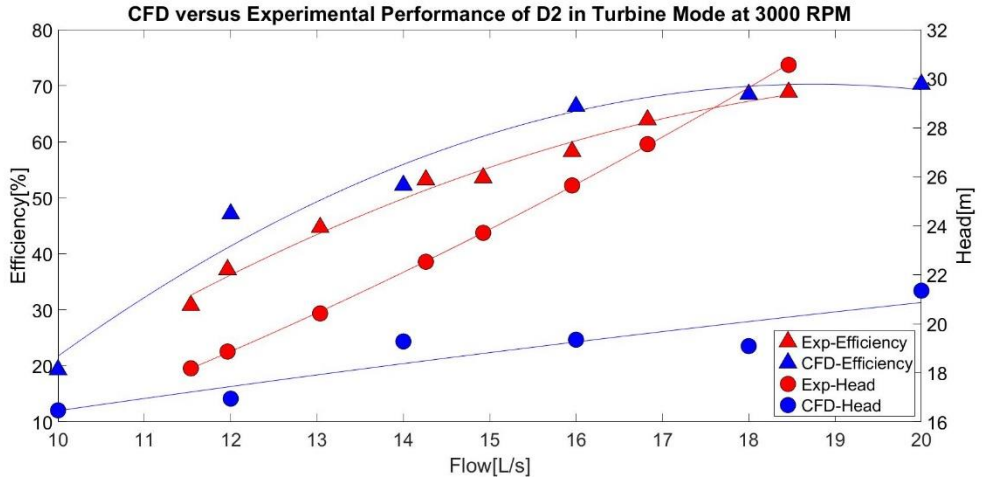

Figure 4.23 CFD Vs. Experimental performance of D2 in Turbine mode at 3000 RPM

Also looking at the performance curve in turbine mode, it can be seen that at the high head and high flow conditions the efficiency curve of the experiment is farther from CFD. But at low head and low flow condition head curve and flow curve are nearer as seen in Figures 4.24 and 4.25.

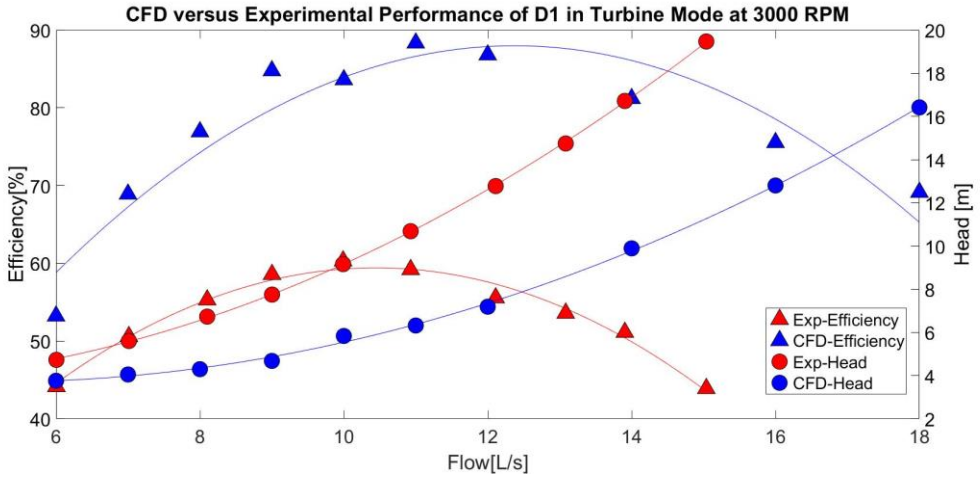

Figure 4.24 CFD Vs. Experimental performance of D1 in Turbine mode at 1500 RPM

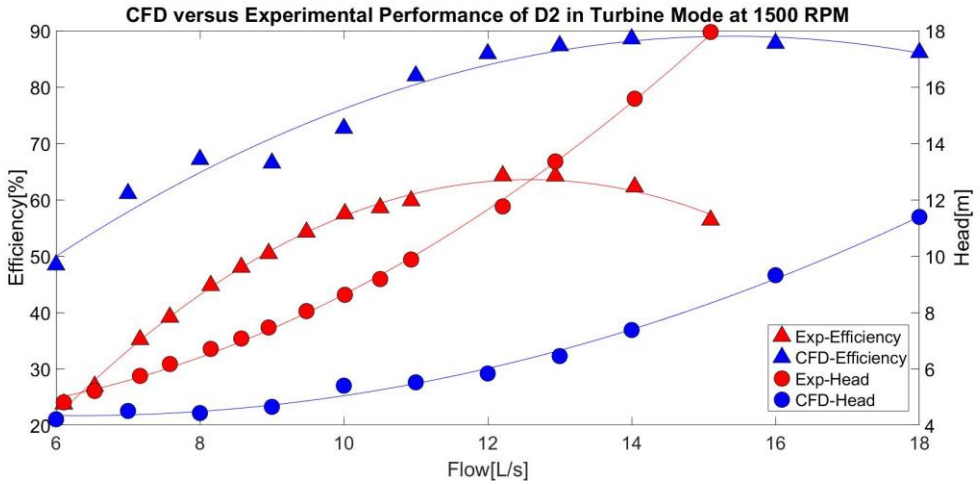

Figure 4.25 CFD Vs. Experimental performance of D2 in Turbine mode at 1500 RPM

With above all discussions, it can be said that the result from CFD and Experimental are comparable with some differences noted. The reasons for deviation could be different head losses in bends, reducers, and valves which are not included in CFD. Also at CFD, all the wall has been considered smooth which is not actually in the real case. Another reason is that the PLA material used in the impeller is not 100 % solid and has some porosity which may result in efficiency reduction in the experiment. The uncertainty of the device in the experiment could be another limitation for deviation.

4.6.4 CFD performance comparison of various designs

For the CFD comparisons, the performance of three designs was studied numerically for comparisons. The BEP parameters for pump mode is as shown in Table 4.11 which shows that among the three designs the efficiency for pump mode at 3000 rpm is highest for D1 with the efficiency of D1, D3, and D2 respectively 67.70 % , 66.90%, and 60.35%.

Similarly, the results at 1500 rpm are highest for D3 with the efficiency of D3, D1, and D2 respectively 70.50 %, 63.57%, and 69.51%.

Table 4.11 CFD BEP comparison for pump mode

BEP Parameter for Pump Mode at 3000 rpm					
S.N.	H [m]	Q [l/s]	η	P in [W]	P out [W]
D1	14.17	12.84	67.70%	2628.41	1779.44
D2	13.36	13.41	60.35%	2903.89	1752.50
D3	14.13	12.74	66.90%	2631.43	1760.40
BEP Parameters for Pump Mode at 1500 rpm					
S.N.	H [m]	Q [l/s]	η	P in [W]	P out [W]
D1	3.67	6.35	69.51%	327.38	227.55
D2	3.61	7.61	63.57%	422.89	268.84
D3	3.74	6.29	70.50%	326.01	229.85

The performance curve for various designs in pump mode is shown in Figures 4.26-4.27. The results show that for pump mode operation the efficiency of D1 and D3 are quite similar in BEP but D3 shows better performance at part load conditions. This reveals that by doing impeller trimming at trailing the part load operation in pump mode is improved. Also although the BEP efficiency of D2 is the least in comparison to D1 and D3 the operating range of head and flow is quite more.

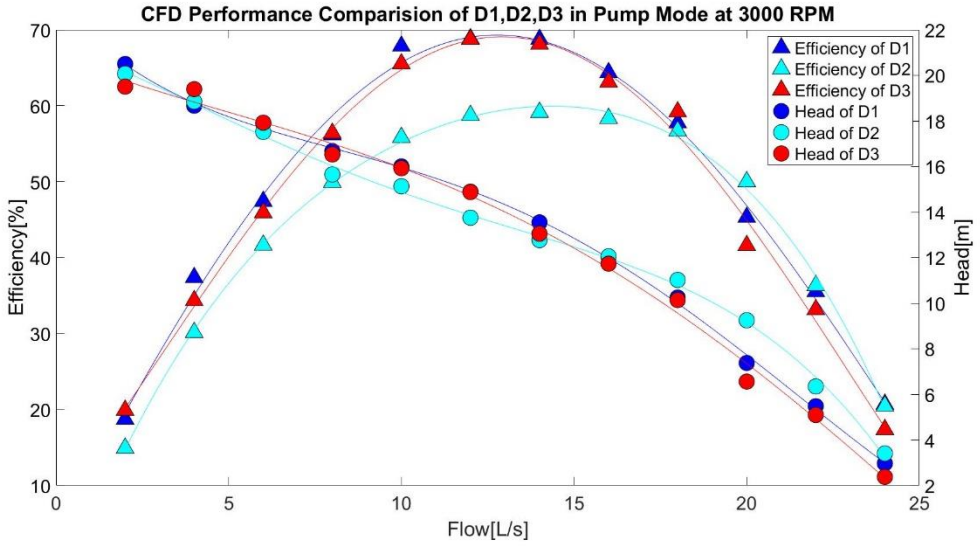

Figure 4.26 CFD performance comparison of D1, D2, and D3 in pump mode at 3000 rpm

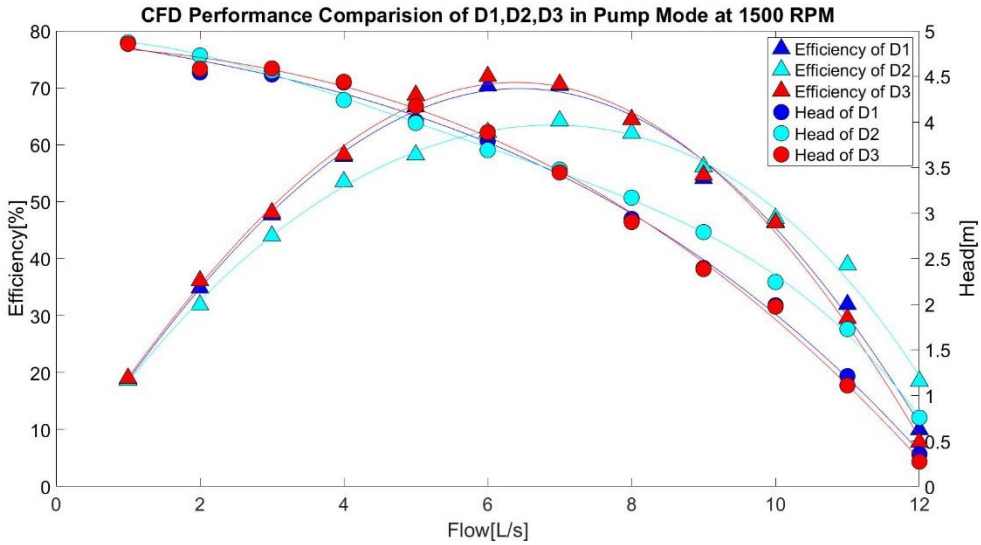

Figure 4.27 CFD performance comparison of D1,D2, D3 in pump mode at 1500 rpm

The BEP parameters of various designs in turbine mode are shown in Table 4.12. At BEP conditions for 3000 rpm, D2 had the highest efficiency with the efficiency of D2, D1, and D3 respectively as 94.82%, 94.57%, and 91.38%. This shows that the Francis turbine has the highest efficiency of any modifications of centrifugal pumps.

Table 4.12 CFD BEP comparison for turbine mode

BEP Parameters for Turbine mode at 3000 rpm							
S.N.	H [m]	Q [l/s]	η	P in [W]	P out [W]	h	q
D1	32.37	25.92	91.38%	8204.2	7497.12	2.28	2.02
D2	33.91	31.79	94.82%	10542.3	9995.86	2.54	2.37
D3	32.57	27.00	94.57%	8601.8	8134.70	2.31	2.12
BEP parameters for Turbine mode at 1500 rpm							
S.N.	H [m]	Q [l/s]	η	P in [W]	P out [W]	h	q
D1	6.62	11.23	89.42%	727.04	650.16	1.8	1.77
D2	8.70	15.44	87.82%	1014.91	605.48	2.4	2.03
D3	6.16	10.87	88.07%	1571.77	1005.79	1.6	1.73

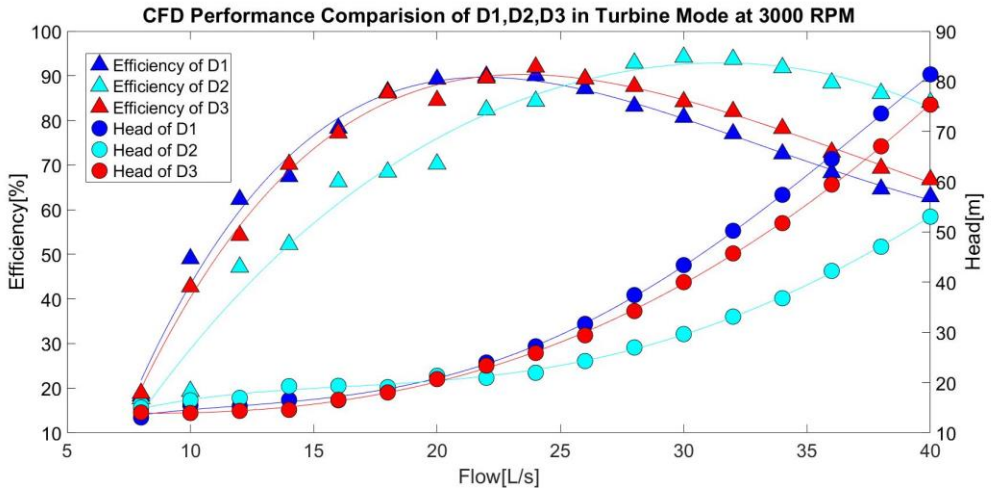

Figure 4.28 CFD performance comparison of D1, D2, and D3 in turbine mode at 3000 rpm

The performance curve in turbine mode is shown in Figures 4.28-4.29.

If the performance of D1 and D3 are compared, it shows that the efficiency curve of D1 and D3 are nearer at part load conditions and D3 is higher than D1 at BEP and full load conditions. This means by doing impeller trimming of the existing impeller both BEP efficiency and part load operation could be improved. Further, it is noted that D2 has

the highest efficiency and better off-design BEP performance in comparison to D1 and D3.

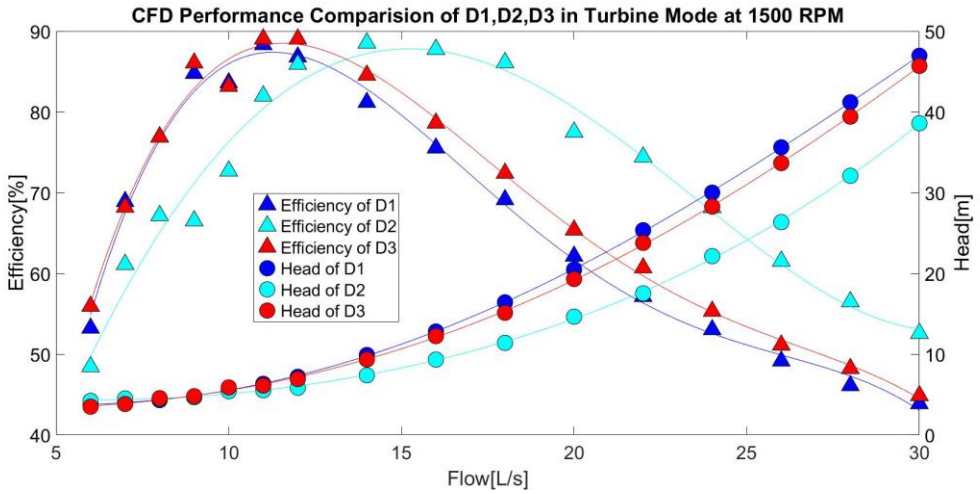

Figure 4.29 CFD performance comparison of D1, D2, and D3 in turbine mode at 1500 rpm

4.7 Calibration and Uncertainty Analysis

4.7.1 Calibration of devices

In this experiment mainly four devices were used for measurements. The two pressure sensors and flow meter the calibrated data provided by the supplier were used for the measurements. However, the torque transducer was calibrated in the lab. The torque transducer was calibrated to assure that the system's accuracy was determined. The torque transducer employed was a strain gauge-based YDRM-50 KM transducer capable of measuring up to 50 kgf-m. A static calibration method was utilized, which involved calibrated masses acting on a calibrated lever arm. The calibration system was made up of two identical lever arms that were attached to either end of the torque transducer's shaft. One lever arm was attached to the base, while the other arm was fixed at one end. The opposite end was fitted with fixed loads that generated a voltage signal, which was then transformed into torque.

Loading and unloading were performed to determine the corresponding torque for varied loads. The voltage readings throughout the loading and unloading cycles were examined to create a calibration equation, as illustrated in Figure 4.30. After analyzing the uncertainty in the torque transducer calibration, the average error is found to be 0.128 %, as shown in Figure 4.31.

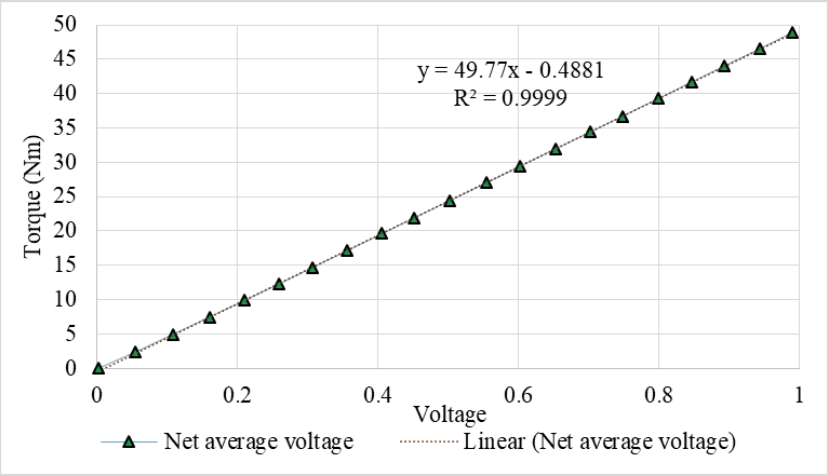

Figure 4.30 Torque transducer calibration curve in absolute value

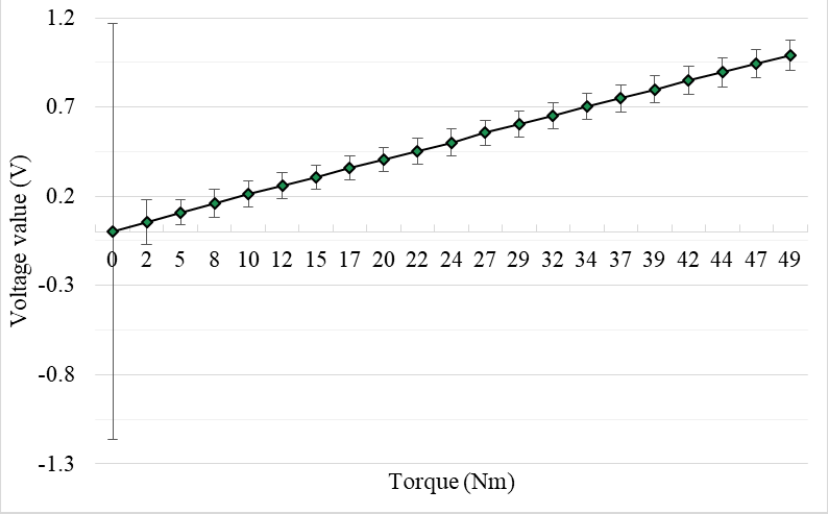

Figure 4.31 Errors bars in torque calibration in absolute value

4.7.2 Uncertainty Analysis

There are two types of uncertainties in an experiment. Type A uncertainty and Type B uncertainty. Type A uncertainty is an evaluation of measurement uncertainty by a statistical analysis of measured quantity obtained under defined measurement conditions [34]. This uncertainty can be minimized by increasing the number of measurements, Type B uncertainty is carried by means other than statistical analysis from a series of observations. Such uncertainty cannot be minimized by increasing the number of measurements.

4.7.2.1 Data preparation process

During the time of the experiment, the data acquisition rate was set to be 2000Hz with a sample size of 2000. It means 2000 samples were acquired in a second. The data had few outbound values which were removed using the median of 2000 samples within the confidence interval of 95% and recorded in a data file for about 30 seconds. Approximately, 60000 samples were recorded altogether.

$$Median = \frac{1}{N}\sum_{i=1}^{N}(x, y, t_i) \tag{4.11}$$

Now, data were converted into a corresponding unit (Nm) using a calibration equation, and the final value was obtained as the mean of all data for 30 seconds. The standard deviation of data was calculated from which the standard error of the mean was calculated.

$$\sigma = \sqrt{\frac{1}{N-1}.\sum_{i=1}^{N}(A(x, y) - A(x, y, t_i)} \tag{4.12}$$

$$\delta = \pm\left(\frac{\sigma}{N}\right) \tag{4.13}$$

From the above values %, Random Uncertainty of the mean was calculated.

$$\varepsilon = \pm \frac{\delta}{A(x,y)} \times 100 \tag{4.14}$$

Insertion of error bars with values from % Random uncertainty of means in calibration graph provided uncertainty graph. Endpoints of error bars were joined to develop a curve and its equation is found to obtain an uncertainty relation.

4.7.2.2 Uncertainty calculation

The data obtained after the removal of outbound values were then converted into their respective units (Nm) using the above-developed calibration equation. After that, similar steps were followed to calculate: the average, standard deviation, standard error of the mean, and finally, the percentage of random uncertainty of mean. This percentage random uncertainty of mean gives the Type A uncertainty. The uncertainty equation was used to calculate Type B uncertainty for the respective value of the calculated average. The Type A uncertainty ($u(\tau)_a$) and Type B uncertainty ($u(\tau)_b$) are combined using the root-sum-square method.

$$u(\tau)_c = \sqrt{\left[u(\tau)_a\right]^2 + \left[u(\tau)_a\right]^2} \tag{4.15}$$

A similar method was applied to calculate combined uncertainty for pressure, flow, and speed (rpm). For the flow meter and pressure sensors, the uncertainty provided by the manufacturer in calibration certificates was used. Certain assumptions were made to calculate the total uncertainty. For adding or subtracting the measurements, absolute uncertainty was added and for multiplying or dividing the measurements, percentage uncertainty was added.

Net Pressure = $(P_1 - P_2)$

Absolute Uncertainty of Net Pressure = SEM of P_1 + SEM of P_2

The absolute uncertainty of net pressure was converted into percentage form denoted as $u(P)_c$. The combined % uncertainty of flow and speed (rpm) is denoted as $u(Q)_c$ and $u(\omega)_c$ respectively.

The combined % uncertainty for efficiency is calculated as

$$u(\tau)_a = u(\tau)_c + u(P)_c + u(Q)_c + u(\omega)_c \tag{4.16}$$

Similar steps were followed for each rpm to calculate efficiency and uncertainty in respective efficiency. The efficiency vs rpm curve shows the BEP of the experiment whereas developing error bars in the curve shows the uncertainty for each rpm.

For 3000 rpm, type B uncertainty for torque and rpm was 1% while type B uncertainty for flow-meter and pressure sensor were 0.2% and 0.075% respectively which was provided by the manufacturer. Similarly, the random uncertainty of torque and rpm was 0.081% each and the random uncertainty for flow-meter and pressure sensor were 0.02% and 0.05% respectively. Figure 4.32 shows the error bar for the head and efficiency. The total uncertainty for efficiency was calculated to be 1.43% while for the head is 0.09 %. The error bar for the head is scaled by a factor of 100 for proper visualization.

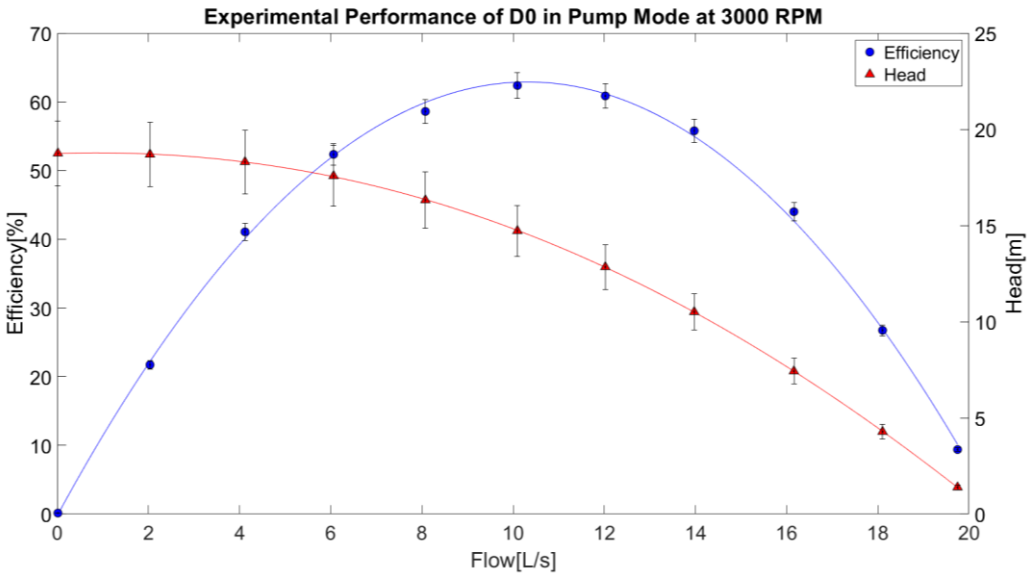

Figure 4.32 Uncertainty in head and efficiency in the experiment

CHAPTER 5 EROSION TEST OF CENTRIFUGAL PUMP

5.1 Experimental methodology

The main motivation of this research was to identify the erosion-prone areas when the pump is subjected to operation in an erosion environment. In order to accomplish these two pumps named Pump 1 and Pump 2 were used in this study. Pump 1 was designed to be operated in pump mode and pump 2 in turbine mode. Pump 1 is the same as D0 of the performance test experiment. Considering previous research indicated that the BEP of the impeller in turbine mode moves at high head and flow compared to the similar impeller in pump mode, the rated head and discharge of Pump 1 were chosen to be larger than those of Pump 2. Pump 2's head and discharge conversion coefficients are calculated to be 1.12 and 1.6, respectively. Table 5.1 shows the specs of each pump.

Table 5.1 Specifications of pumps for sediment erosion test rig

S.N	Specific Speed	Output Hydraulic Power (kW)	RPM	Head [m]	Discharge [l/s]	Operating mode
1.	42	2.82 kW	2870	18	16	Pump mode
2.	36	1.57 kW	2870	16	10	Turbine mode

The pump speed is kept as high as possible in turbine mode to make sure that the runaway speed does not exceed the pump's rated speed. In practice, the maximum allowable speed for pumps powered by 50Hz or 60Hz grid frequencies is frequently 3000 or 3600 rpm [9]. Furthermore, the connection of the generator load to the pump is taken into account when calculating the nominal speed of the turbine. One of the synchronous speeds is chosen to be the nominal speed of a turbine connected directly to a synchronous generator. Because they are smaller than generators with lower

synchronous speeds, generators with a synchronous speed of 1500 rpm are widely available on the market.

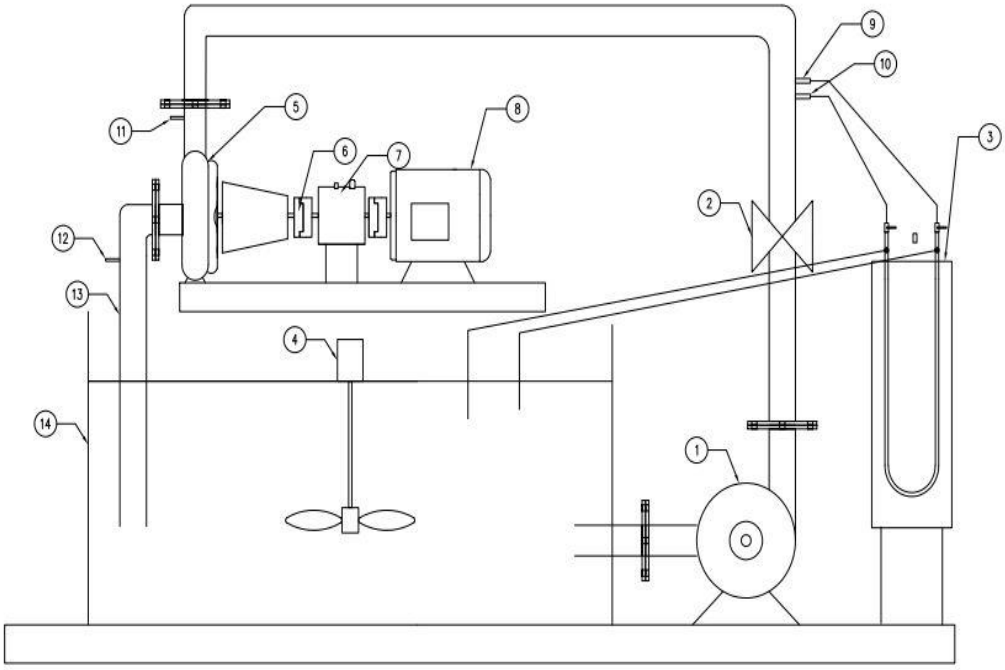

Figure 5.1 Schematic diagram of erosion test rig of PAT

1. Pump 1, 2. Butterfly valve 3. Mercury Manometer, 4. Stirrer, 5. Pump 2, 6. Coupling, 7. Torque Transducer, 8. Motor, 9. Pitot tube tapping point, 10. Wall velocity tapping point, 11. Inlet pressure sensor location, 12. Outlet pressure sensor location, 13. Delivery pipe, 14. Sump

Figure 5.2 Experimental setup for erosion test in pump and turbine mode

In this scenario, 1500 rpm is chosen as the nominal speed of the pump in turbine mode. Figure 5.1 depicts the schematic diagram. Figure 5.2 depicts the experimental setup.

Both pumps were controlled by variable frequency drives. Because a highly accurate electromagnetic flow meter was not available, the rate of discharge was determined using a pitot tube attached to the pipeline and an ultrasonic flow meter. Pressure sensors in the intake and outflow sections of Pump 2 were used to measure head.

The impellers of both pumps were colored in the following order: blue, green, yellow, orange, and red. Locally available acrylic-based aerosol spray paint was used. These colors provide rapid drying, high gloss, color retention, and good adhesion on both metal and wood surfaces. The color order was determined by the color mapping in the ANSYS CFD post-processor.

Painting in this order makes it easier to validate CFD results using experimental data. Pump 2 was operated in clean water by Pump 1 in turbine mode during the first experiment. Sediments were added to the sump in the second series of experiments to increase the sand concentration to 6000 ppm, which is the typical sand content in most Nepalese rivers [50].

Pump 1 ran at 2870 rpm at 50 Hz frequency, for which its motor was designed, whereas pump 2 ran at 1500 rpm using an induction motor and a Variable Frequency Drive controller. Pump 1 was set to discharge at 16 l/s at 14.85 meters head, powering pump 2. The experiment lasted three hours, with three one-hour intervals to keep the setup's temperature within safe ranges.

The sediment samples were taken during the monsoon season from a cooling tank at the Jhimruk power station in Nepal. The size range of the sediment used for the experiment, from 63 microns to 200 microns, corresponds to the range of sediment size passing

through the turbines in a genuine hydroelectric plant [51]. The sediment of the specified size was separated from the rest of the sand using sieve analysis. Previous research has determined that the silt in the Jhimruk power plant is typically between 100 and 200 microns in size, causing erosion in the hydro mechanical components. According to a recent research, about 59.4% of the sediment type consists of quartz material discovered downstream, which is a much harder substance than steel and causes erosion in hydraulic components [52].

5.2 Numerical methodology

In numerical analysis, the actual hydraulic CAD of the impeller and spiral casing was difficult to obtain, since the pump manufacturer do not provide a complete drawing. However, with the information available from the assembly drawings, closely measuring the dimensions and from reverse engineering, the CAD model of both the impeller was generated. For reverse engineering, impeller dimensions were closely measured from various locations and plotted in a dedicated pump design software i.e., CFturbo for getting a both meridional and axial view. The details of reverse engineering have been presented in Appendix II.

For spiral casing, a CAD model was generated from manufacturing drawing and closely measuring another internal dimension using CFturbo. Closely combining the numerical CAD model is generated as shown in Figure 5.3.

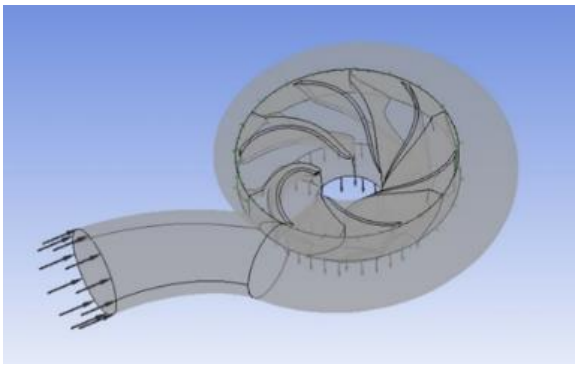

Figure 5.3 Numerical domain for sediment analysis

For numerical analysis, the hexahedral mesh elements were generated for the impeller in ANSYS Turbo grid 18.1. Similarly, the tetrahedral mesh were generated for the spiral casing in ANSYS workbench. The erosion pattern around the pump impeller was numerically investigated using ANSYS CFX. For erosion analysis, ANSYS CFX enables users to employ two erosion models provided i.e., Finnie and Tabakoff erosion models [53]. The latter model was adopted for this analysis, as from the recent study it has been revealed that the The Tabakoff model can depict the actual situation of sediment erosion in hydraulic machines because it considers more factors than the Finnie model and also integrates all angle of attack of sediment particle for erosion [54].

Rate of erosion E in the Tabakoff erosion model can be determined from the following equation.

$$E = f(\gamma)(V_p / V_1)^2 \cos^2\gamma[1 - R_T{}^2] + f(V_{PN}) \tag{5.1}$$

Where,

$$f(\gamma) = [1 + k_2.k_{12}.\sin(\gamma \Big/ \frac{\pi}{2\gamma})]^2$$

$$R_T = 1 - \frac{V_p}{V_3}\sin\gamma$$

$$f(V_{PN}) = (\frac{V_p}{V_2}\sin\gamma)^4$$

$k_2 = 1.0$ if $\gamma \le 2\gamma_0$ or 0.0 $\gamma > 2\gamma_0$

In this case, E is the dimensionless mass defined as mass of eroded wall material divided by the mass of particle. V_p is the impact velocity of the particle , γ is the impact angle in radians between the approaching particle track and the wall, γ_0 is the angle of maximum erosion. Similarly, k_2 and k_{12} are model constants that depend on the particle or wall material combination. The boundary conditions and values of constants used for the combination of quartz and steel are shown in Table 5.2 and Table 5.3.

Table 5.2 Boundary conditions for erosion test

Boundary Parameters	**Boundary Conditions**
Analysis Type	Steady State
Inlet	Mass Flow: 16 l/s
Outlet	Average Static Pressure: 0 Pa
Walls	No Slip
Turbulence Model	SST
Working Fluid	Water at 25^{o}C and quartz
Convergence Criteria	1E^{-4}

Table 5.3 Particles parameters for Tabakoff model

Variables	**Coefficient**	**Value**
k_{12}	k_{12}	0.585
Velocity	V_1	159.11 m/s
	V_2	194.75 m/s
	V_3	190.5 m/s
Angle of maximum erosion	γ_o	25^0

5.3 Result and discussions

From the results of the numerical analysis, the sediment erosion rate density is concentrated near the leading edge of the impeller in pump mode. The observed results are consistent with the findings of Dong et al [55]. This is due to the fact that the rate of erosion is heavily influenced by the velocity of the quartz impacting it, and the velocity of the fluid is typically greatest near the inlet side of the pump.

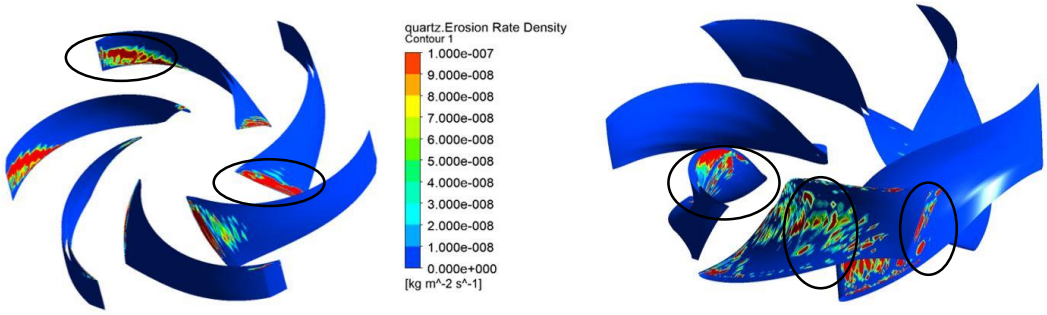

Figure 5.4 Erosion rate density on pump 1 and pump 2

The CFD study revealed that the erosion for Pump 1 occurred mostly at the leading edge on the pressure side and toward the trailing edge on the suction side, as shown in Figure 5.4 left side. Similarly, the experimental results demonstrated erosion at the leading edge shown by Figure 5.9 and along the trailing edge on the suction side shown by Figure 5.5. In addition, as illustrated in Figure 5.7, certain erosive phenomena were detected near the outlet on the pressure side. CFD studies revealed no evidence of erosion at this site. This might be due to the fact that this experiment only demonstrates the weak points in the hydraulic profile and not the real erosion of metal caused by sediment. The figure shows that just one to two layers of paint have been eroded at that place, indicating that it is a region with a lower risk of erosion than other areas where degradation has been observed, which could not be quantified on metals.

Similarly, the erosion pattern on the impeller of Pump 2, which was used as a turbine, was investigated. According to the numerical analysis of the runner, the erosion was largely focused in three areas: at the hub region on the suction side of the blade, along the pressure side, and at the trailing edge on the pressure side, as shown in Figure 5.4 right side. These erosion patterns were also seen in the experimental results. Figure 5.6 depicts the erosion at the hub region on the suction side, whereas Figure 5.10 depicts the erosion near the hub on the pressure side. However, the erosion on the pressure side is considerably less significant in the experimental results compared to the numerical analysis results.

Figure 5.5 Erosion at outlet suction side for Pump 1

Figure 5.6 Erosion near hub at suction side for Pump 2

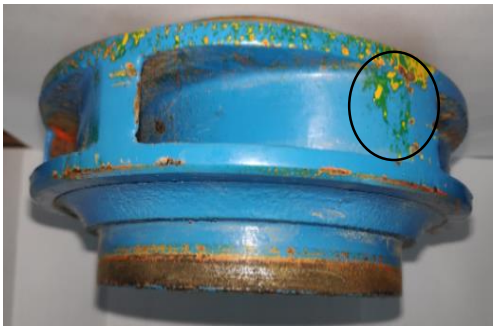

Figure 5.7 Erosion at outlet pressure side for Pump 1

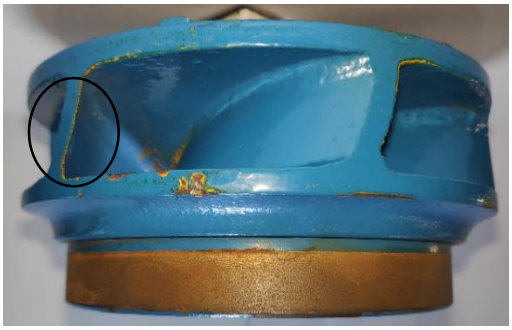

Figure 5.8 Erosions at trailing edge for Pump 2

Figure 5.9 Erosion at Inlet leading edge in Pump 1

Figure 5.10 Erosion near hub at pressure side for Pump 2

This might be due to the erosion model's limitations or the experiment's period, in which case additional regions could be eroded. Figure 5.8 depicts erosion on the trailing edge, which corresponds to CFD findings. The pump mode impeller eroded more areas than the turbine mode impeller, which might be related to the rotating speed of the hydraulic machines and their blade profiles.

The experiment validated the erosion pattern predicted by CFD to some extent. However, certain differences have been observed. Because of the limitations of both methodologies, the results obtained from CFD and the experiment cannot be fully trusted at this time. The experiment illustrates that certain locations of the impeller that are more prone to erosion. Although the experiment was carried out in a relatively simple arrangement, locations that are more prone to erosion were observed. The objective of this study was to evaluate the erosion-prone locations in the hydraulic profile of the impeller blades using computational and experimental methods. The technique utilized in this study is one of the most cost-effective and efficient methods for predicting erosion patterns.

CHAPTER 6 CONCLUSION

In this research the existing locally available 3.7 kW centrifugal pump was tested in both pump mode and turbine mode experimentally. The impeller was also modified in various versions of D1, D2, and D3 of which performance of D1 and D2 was studied experimentally as well as numerically. It has been revealed Nepal imports Nrs. 3 Billion worth of pumps each year. Out of which about 34 % of non-priming centrifugal pumps are used in Nepal for the household to industrial applications with a provision to be used as a turbine for power generation. Numerical analysis of the centrifugal pump reveals that it is comparable to micro-class turbines with maximum efficiency of 94.57%. While experimental analysis shows that the centrifugal pump can be used in turbine mode without any modification with an efficiency of 64.56%. The result has also shown that the BEP shifts to higher values of head and flow in the case of turbine mode from both numerical and experimental results. The numerical and experimental analysis in sediment environment both showed that erosion was maximum in leading-edge pressure areas in pump mode while in turbine mode erosion near hub region at pressure side. So, the erosion-prone areas could be revealed by the acrylic-based paint method.

For performance improvement of centrifugal pump in turbine mode, decreasing the outlet angle improves PAT performance by 3 % by selecting the outlet angle as 10 degrees. Impeller modifications at the leading and trailing edge of the centrifugal pump to match the profile of the turbine is beneficial for the performance of PAT in all loading condition. Trimming the leading edge and changing the trailing profile to elliptical with an axis ratio of 3 enhance efficiency by 3 % at BEP conditions while part load efficiency is even better. Modified Francis Turbine is also another methodology for improving turbine mode performance of PAT in which maximum efficiency of 72.13 % has been obtained in turbine mode.

CHAPTER 7 FUTURE WORKS/RECOMMENDATION

As a future recommendation, there are various things which could be done more. The experiments were carried out in a PLA material impeller which has some porosity in itself. So, the steel material impeller could be an option for testing. Since the pumps were tested in the lab, the actual operation of PAT in field conditions with electrical connections should be focused more. As the qualitative analysis method has only been performed for the performance of the pump in an erosion environment, the weight loss method could be implemented in the future to analyze. Another interesting fact from the experiment was that the two designs D1 and D2 from the experiment which were fabricated from PLA material could operate without any mechanical failure. So, this opens a door for further analysis of PLA material for pump and their fatigue cycle. Since the FSI analysis of PAT is limited the FSI results of MS material and PLA material could be a further topic of research.

REFRENCES

[1] H. M. Shrestha, “Exploitable Potential, Theoretical Potential, Technical Potential, Storage Potential and Impediments to Development of the Potential: The Nepalese Perspective,” *Hydro Nepal J. Water, Energy Environ.*, vol. 19, pp. 1–5, 2016, doi: 10.3126/hn.v19i0.15340.

[2] NMHDA, “Jalshakti Vol. No. 13,” *Jalashakti*, vol. 13, no. 13. NMHDA, Kathmandu, pp. 1–41, 2014.

[3] NEA, “Annual report of Nepal Electricity Authotity, 2020/2021,” Kathmandu, 2021.

[4] S. Panta, M. Lamsal, B. Thapa, and B. S. Thapa, “Prediction of Turbine Needed For Future Hydropower Projects in Nepal,” *Hydro Nepal J. Water, Energy Environ.*, vol. 14, pp. 23–26, 2014, doi: 10.3126/hn.v14i0.11250.

[5] B. Baidar, R. Koirala, H. P. Neopane, M. V. Shrestha, and B. Thapa, “Strategic rehabilitation of the earthquake affected microhydropower plants in Nepal,” *IOP Conf. Ser. Earth Environ. Sci.*, vol. 49, no. 10, 2016, doi: 10.1088/1755-1315/49/10/102003.

[6] A. Ghimire, D. Dahal, A. Kayastha, S. Chitrakar, B. S. Thapa, and H. P. Neopane, “Design of Francis turbine for micro hydropower applications,” *J. Phys. Conf. Ser.*, vol. 1608, no. 1, 2020, doi: 10.1088/1742-6596/1608/1/012019.

[7] B. Chhetry, “Assembly design of Francis turbine from maintenance perspective in context to sediment-laden river projects,” Kathmandu University, 2017.

[8] S. V. Jain and R. N. Patel, “Investigations on pump running in turbine mode: A

review of the state-of-the-art," *Renew. Sustain. Energy Rev.*, vol. 30, pp. 841–868, 2014, doi: 10.1016/j.rser.2013.11.030.

[9] F. G. Chapallaz JM Eichenberg P, "MHPG series," *Manual on pumps used as turbines*, vol. 11, no. ISBN 3-528-02069-5. p. 221, 1992.

[10] D. Dahal, "Design of Francis Turbine and Propose its Manufacturing Procedure in Context of Himalayan region," Kathmandu University, 2019.

[11] N. Pokharel, A. Ghimire, B. S. Thapa, and B. Thapa, "Opportunity for research and manufacturing of pump in Nepal," *J. Phys. Conf. Ser.*, vol. 1608, no. 1, 2020, doi: 10.1088/1742-6596/1608/1/012018.

[12] Jagadish Lal, *Hydraulic Machines*. New Delhi, 2014.

[13] I. J. Karassik, J. P. Messina, P. Cooper, and C. C. Held, *Pump Handbook*, Fourth Edi. New York: McGraw-Hill, 1976.

[14] "Classification of pumps | All Pumps." [Online]. Available: https://allpumps.com.au/classification-of-pumps/. [Accessed: 06-May-2021].

[15] Dale Conwey, "Pump Motor Drives," *www.flowcontrolnetwork.com*. [Online]. Available: https://www.flowcontrolnetwork.com/pumps-motors-drives/article/15553254/qa-pump-cavitation-diagnosis-and-control. [Accessed: 20-Mar-2020].

[16] L. Val S. and R. Robert R., *Centrifugal Pumps Design and Application*, 2nd editio. Houston: Gulf Publishing Company, 1985.

[17] Stepanoff A.J., *Centrifugal and axial flow pumps*, Second. New York: John Wiley & Sons, Inc.

[18] J. F. Gülich, "Corrosion," in *Centrifugal Pumps*, 3rd editio., New York, NY:

Springer, 2014, pp. 956–979.

[19] I. J. Karassik and T. McGuire, *Centrifugal Pumps*, Second Edi. London: Champman & Hall, 1998.

[20] M. Güner and M. M. Özbayer, “Wear and its effects in centrifugal pumps,” *Yuz. Yil Univ. J. Agric. Sci.*, vol. 29, no. 3, pp. 569–582, 2019, doi: 10.29133/yyutbd.518139.

[21] R. H. Greene and D. a. Casada, “Detection of Pump Degradation, NUREG/CR-6089,” Washington,DC, 1995.

[22] Jackson Crater, “Water Pump Cavitation.” [Online]. Available: https://www.absolutewaterpumps.com/blog/water-pump-cavitation/. [Accessed: 11-May-2021].

[23] S. Hernandez, A. S. Nassef, and G. Corrosion, *Trends in Oil and Gas Corrosion Research and Technologies*. Science Direct, 2017.

[24] Thapa, “Sand erosion hydraulic machinery,” NTNU, 2004.

[25] Z. Shen, W. Chu, X. Li, and W. Dong, “Sediment erosion in the impeller of a double-suction centrifugal pump – A case study of the Jingtai Yellow River Irrigation Project, China,” *Wear*, vol. 422–423, no. January, pp. 269–279, 2019, doi: 10.1016/j.wear.2019.01.088.

[26] K. McKee et al., “A review of major centrifugal pump failure modes with application to the water supply and sewerage industries,” *ICOMS Asset Manag. Conf. , Gold Coast, QLD, Aust.*, pp. 1–12, 2011.

[27] M. N. Tamin and M. A. Hamzah, “Fatigue Failure Analysis of a Centrifugal Pump Shaft,” *INTECH*, pp. 1–14, 2017, doi: 10.5772/intechopen.70672.

[28] M. Binama, W. Su, X. Li, F. Li, X. Wei, and S. An, “Investigation on pump as turbine (PAT) technical aspects for micro hydropower schemes : A state-of-the-art review,” *Renew. Sustain. Energy Rev.*, vol. 79, no. February, pp. 148–179, 2017, doi: 10.1016/j.rser.2017.04.071.

[29] A. A. Williams, “Pumps as turbines for low cost micro hydro power,” *Renew. Energy*, vol. 9, no. 1–4, pp. 1227–1234, 2002, doi: 10.1016/0960-1481(96)88498-9.

[30] S. Derakhshan and A. Nourbakhsh, “Experimental study of characteristic curves of centrifugal pumps working as turbines in different specific speeds,” *Exp. Therm. Fluid Sci.*, vol. 32, no. 3, pp. 800–807, 2008, doi: 10.1016/j.expthermflusci.2007.10.004.

[31] S. P. Engeda A and R. M, “Selection of Centrifugal pumps as turbines.,” in *Pump Conference Karlsruhe ’88*, 1988.

[32] J. Steller, A. Adamkowski, Z. Stankiewicz, A. Lojek, J. Rduch, and M. Zarzycki, “Pumps as turbines for hydraulic energy recovery and small hydropower purposes in Poland,” *Hidroenergia*, no. June, pp. 2018–2020, 2008.

[33] Z. Zuo, H. Fan, S. Liu, and Y. Wu, “S-shaped characteristics on the performance curves of pump-turbines in turbine mode - A review,” *Renew. Sustain. Energy Rev.*, vol. 60, pp. 836–851, 2016, doi: 10.1016/j.rser.2015.12.312.

[34] X. Tan, “Design and Performance Analysis of Gas and Liquid Radial Turbines,” Michigan State University, 2016.

[35] H. Nautiyal, Varun, and A. Kumar, “Reverse running pumps analytical, experimental and computational study: A review,” *Renew. Sustain. Energy*

Rev., vol. 14, no. 7, pp. 2059–2067, 2010, doi: 10.1016/j.rser.2010.04.006.

[36] M. Amelio, S. Barbarelli, and D. Schinello, "Review of methods used for selecting Pumps as Turbines (PATs) and predicting their characteristic curves," *Energies*, vol. 13, no. 23, 2021, doi: 10.3390/en13236341.

[37] S. Barbarelli, M. Amelio, and G. Florio, "Using a statistical-numerical procedure for the selection of pumps running as turbines to be applied in water pipelines: Study cases," *J. Sustain. Dev. Energy, Water Environ. Syst.*, vol. 6, no. 2, pp. 323–340, 2018, doi: 10.13044/j.sdewes.d5.0181.

[38] I. M. Hossain, S. M. Ferdous, S. Salehin, A. M. Saleque, and T. Jamal, "Pump as Turbine (PAT) for small scale power generation: A comparative study," in *3rd International Conference on the Developments in Renewable Energy Technology (ICDRET)*, 2014, doi: DOI: 10.1109/ICDRET.2014.6861698.

[39] K. R. Sharma, "Small hydroelectric project-use of centrifugal pumps as turbines," Banglore, 1985.

[40] K. R. Gautam, P. R. Pande, R. Paudel, and A. B. Pradhan, "Nepal: Water Resources Project Preparatory Facility Pre-Feasibility Study Report of Mid-Hill Lift Irrigation Project (Package 6)," Kathmandu, 2016.

[41] World Bank, "PROJECT PERFORMANCE AUDIT REPORT NEPAL BRAIRAWA-LUMBINI GROUNDWATER PROJECT," 1984.

[42] S.Upadhaya, "Water Nepal : A Historical Perspective," 2018.

[43] Kathmandu Upatyaka Khanepani Limited, "Resettlement Plan Nepal: Kathmandu Valley Wastewater Management Project," 2013.

[44] A. Kumar Jha and T. Ratna Bajracharya, "Wastewater Treatment Technologies in Nepal," in *IOE Graduate Conference*, 2014, pp. 76–81.

[45] Goverment of Nepal, “Department of Customs, Nepal - FY 2075/76 (2018/19).” [Online]. Available: https://www.customs.gov.np/en/monthlystatstics.html. [Accessed: 22-Apr-2020].

[46] A. W. B. Gwidon Stachowiak, “Abrasive Wear,” in *Engineering Tribology*, 1993, pp. 550–551.

[47] F. R. Menter, “Two-equation eddy-viscosity turbulence models for engineering applications,” *AIAA J.*, vol. 32, no. 8, pp. 1598–1605, 1994, doi: 10.2514/3.12149.

[48] S. Chitrakar, B. S. Thapa, O. G. Dahlhaug, and H. P. Neopane, “Numerical and experimental study of the leakage flow in guide vanes with different hydrofoils,” *J. Comput. Des. Eng.*, vol. 4, no. 3, pp. 218–230, 2017, doi: 10.1016/j.jcde.2017.02.004.

[49] A. Williams, “Pumps as turbines.” Intermediare Technology Publications Ltd, London, pp. 28–30, 1995.

[50] A. Kayastha, Y. Lee, H. P. Neopane, and B. Thapa, “Numerical study of hydro cyclone separator to reduce sediment erosion potential in Micro / Pico hydro turbines,” *Curr. Res. Hydraul. Turbines VI*, 2016.

[51] H. P. Pandit, “Hydrocyclones: Alternative Devices for Sediment Handling in ROR Projects,” no. November 2007, pp. 22–24, 2007.

[52] H. P. Neopane and S. Sujakhu, “Particle Size Distribution and Mineral Analysis of Sediments in Nepalese Hydropower Plant: a Case Study of Jhimruk Hydropower Plant,” *Kathmandu Univ. J. Sci. Eng. Technol.*, vol. 9, no. I, pp. 29–36, 2013.

[53] M. Rakibuzzaman, H. H. Kim, K. Kim, S. H. Suh, and K. Y. Kim, “Numerical

study of sediment erosion analysis in Francis turbine," *Sustain.*, vol. 11, no. 5, 2019, doi: 10.3390/su11051423.

[54] X. Song *et al.*, "Numerical Simulation Prediction of Erosion Characteristics in a Double-Suction Centrifugal Pump," *Processes*, vol. 9, no. 1483, 2021, doi: https://doi.org/10.3390/pr9091483.

[55] J. Dong, Z. Qian, B. S. Thapa, B. Thapa, and Z. Guo, "Alternative Design of Double-Suction Centrifugal Pump to Reduce the Effects of Silt Erosion," *Energies*, vol. 12, no. 158, 2019, doi: 10.3390/en12010158.

APPENDIX I: Summary of Publications

Paper 1

Title: *Experimental Analysis of a Centrifugal pump in pump mode and turbine mode*

Authors: Nischal Pokharel, Prajwal Sapkota, Amul Ghimire, Biraj Singh Thapa, Bhola Thapa

Status of the paper: Accepted for Publication

Journal: IOP Earth and Environmental Science (IAHR 2022, Trondheim Norway)

Abstract

The national grid of Nepal faces several hurdles during its operation, especially in remote areas of hilly and mountain region. Citizens face blackouts of days to weeks, due disturbances caused in the grid in those regions. Micro hydro can be a very strategic backup for the national grid in those regions. However, due to lack of subsidy, which used to be provided in the past, for development of micro hydro, micro developers are unable to afford the construction cost of the micro hydro. Thus using Pumps that are readily available in the market at a much cheaper price, compared to custom built hydro turbines, as turbines can be a very economical alternative for such cases. But the concept of pump as turbine has not been utilized in Nepalese market. In this study, a centrifugal pump abundantly available in the Nepalese market has been used to evaluate its performance in turbine mode as well as in pump mode. A characteristic performance curve of the pump operated in turbine mode is obtained from the experimental data. The Best efficiency point and the operating regime is also determined based on the results obtained from experiments. The head conversion factor and discharge conversion factor calculated based on the data measured from the experiment, at various operating conditions, are compared to previous works done by other researchers. The performance

obtained from the experimental analysis is comparable to the performance of the turbines installed in the micro hydro power projects. PAT can be a game changer in the micro hydro sector, by providing a very economical and technically viable option of expensive hydro turbines

Paper 2

Title: *Wear in centrifugal pumps with causes, effects and remedies: A Review*

Authors: Nischal Pokharel, Amul Ghimire, Biraj Singh Thapa, Bhola Thapa

Status of the paper: Accepted for publication

Journal: IOP Journal of Physics (IAHR-Asia 2021, Kathmandu University)

Abstract

Pumps are widely used machinery in various applications. Mostly now, a day in importance is seen from household applications to different industrial level. Various types of pumps are available in the market according to their applications and centrifugal pumps are one of most common types among them. In the course of time, pumps faces various problems and repairing is required. Among them wear is one of the most common problem for reduction in pump performance. Cavitation, corrosion, erosion, fatigue are the common wear mechanisms faced by the centrifugal pumps. In order to minimize such problems frequent maintenance strategies are required. Various researchers have purposed different methodologies. Material properties, coatings in design and optimizing hydraulic and mechanical design for such challenges has been now a major topic of research. In this study, the different wear mechanisms and their causes with reference to various research paper is presented. Different effects for such problems is highlighted. Finally, new emerging technology developed by various researchers for minimizing such wear challenges are discussed.

Paper 3

Title: *Numerical and Experimental Study of pump as turbine for sediment affected micro hydropower project in Nepal*

Authors: Nischal Pokharel, Amul Ghimire, Biraj Singh Thapa, Bhola Thapa, Zhongdong Qian, Zhiwei Guo

Status of the paper: Published

Journal: IOP Conf. Series: Earth and Environmental Science 774 (2021) 012062

https://iopscience.iop.org/article/10.1088/1755-1315/774/1/012062

Abstract

Designing and manufacturing site-specific turbines for small hydropower is not economical. Using abundantly available Pump, from the market, as Turbine (PAT) instead of designing a completely different turbine can be much more economical for small-scale hydropower. Lot of research have been going throughout the world on this and has already proven its effectiveness. In Nepalese hydropower, including the ones already developed and the ones that will be developed in the future, Francis turbines are supposedly the suitable turbine of choice. However, designing and manufacturing Francis turbine is a tedious task and the local manufacturers, who are expert in manufacturing Cross-flow turbines; do not have the technology and competence to manufacture the modern Francis turbines. Sediment in Himalayan rivers are the major hurdles of operation as they reduce the lifetime of the turbine by a very large factor, shooting up the maintenance cost of the hydropower. The operational region of Francis turbine and PAT overlaps quite a lot, thus indicating that PAT can be used in many of the hydropower in Nepal. The Chinese and Indian pump manufacturers are already renowned in developing a wide range of pumps and supplying them in Nepal. Despite having such great opportunity, pumps have never been used in turbine mode in Nepalese

hydropower. In addition to that, no research has been done, in Nepal, regarding the effects of sediment on pumps being operated as pump or turbine. This paper describes performance of pump in erosive environment using Computational Fluid Dynamics (CFD). It also compares the results obtained from the CFD analysis of sediment erosion in pump operated in pump mode as well as turbine mode with other researchers work.

Finally, it compares the results obtained from the CFD with the results obtained from the experiment.

Paper 4

Title: *Opportunity for research and manufacturing of pump in Nepal*

Authors: Nischal Pokharel, Amul Ghimire, Biraj Singh Thapa, Bhola Thapa,

Status of the paper: Published

Journal: Journal of Physics: Conference Series 1608 (2020) 012018

https://iopscience.iop.org/article/10.1088/1742-6596/1608/1/012018

Abstract

Pumps are the mechanical device used to increase the pressure energy of fluids. Pumps of different types and size are being used in Nepal, for different applications. Despite the wide spread applications of pumps not much have been done to manufacture pumps in Nepal. This study investigates the opportunity of manufacturing pumps in Nepal. It shows the history of usage of pumps in Nepal and also depicts the problems faced by the pumps used in different projects. It discusses about the current market trend related to the import of pumps from foreign countries and develops an argument to start a new business for manufacturing pumps. Role of research institutes like Turbine Testing Laboratory in design of pumps has been discussed as a future prospect for Nepalese academia and industry.

Paper 5

Title: *An Experimental Investigation of PAT in Direct and Reverse Mode at Turbine Testing Lab*

Authors: Samita Rimal, Sanjay Prasad Shah, **Nischal Pokharel**, Biraj Singh Thapa

Status of the paper: Published

Journal: Journal of Physics: Conference Series 1608 (2020) 012006

https://iopscience.iop.org/article/10.1088/1742-6596/1608/1/012006

Abstract

PAT is typically employed as the electromechanical component, especially in the rural communities of developing countries in order to reduce the initial cost of a power plant. In the context of Nepal, there have been few researches about its feasibility but have given promising outcomes regarding its implementation. As a part of this continuation, this paper deals with the experimentation performed on end suction, KDS-520+ centrifugal pump of 3.5 kW on direct as well as reverse mode to study its performances. The main purpose of this study was to test the characteristic performance of the pump in turbine as well as pump mode to compare the variation in their efficiency in laboratory environment so as to shed light upon the importance of PAT in micro and mini hydropower and to study the prospect of replacing traditional water mills with PAT. The test rig for the operation of pump in turbine mode was developed as a part of the research and characteristic curves have been plotted on different flow rates. The efficiency of the centrifugal pump was found similar to the rated efficiency, 60.85% at the best efficiency point at the head of 17m and discharge of 17lps. In addition, performance of the same pump in turbine mode showed a maximum efficiency of 40.15% at flow of 11.5lps and head 10m which concluded that the centrifugal pump can operate in turbine mode without any modifications.

APPENDIX II: Introduction to CFturbo for CAD modelling of Pump

II.1 Introduction

CFturbo is one of the design software in turbo machinery for design, simulation, and optimization. By using CFturbo, we can create completely new geometries as well as modify existing designs. Also the use of reverse engineering is supported in it. CFturbo guides the user step-by-step through the complete design process in a turbomachine. Firstly a draft design can be generated automatically and in the subsequent design process, the user has control over every detail. The designs are based upon the governing equations and empirical relations provided by various designers and scholars. CFturbo mainly covers the design of pumps, ventilators, compressors, and turbines with their related components. For this study, CFturbo was used to model the existing pump impeller with reverse engineering. When we open the CF turbo we can see as user interface shown in Figure 1.

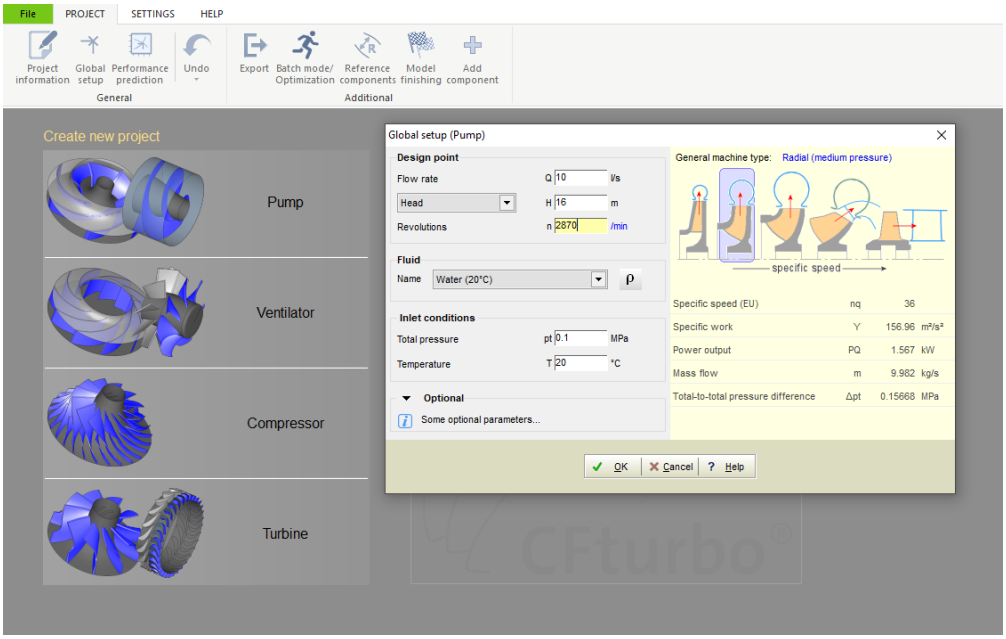

Figure 1User interface in CFturbo

We have mainly three input parameters for its design. i.e Q, H, and n which are known from the existing pump model used in this study. Similarly, the value of temperature and pressure are kept normal in the atmosphere. After the input parameter was given, the CFturbo indicated the general machine type based on the specific speed.

After this, it is directed into the setup interface as shown and the impeller type should be selected according to a specific speed and it will be directed to the main dimension interface.

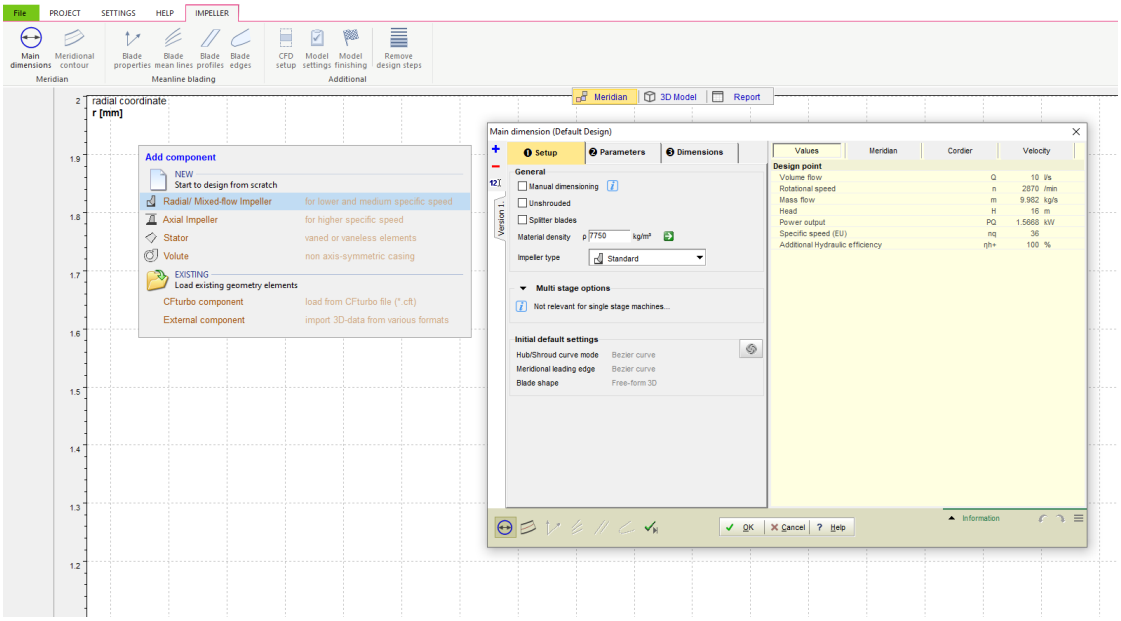

Figure 2 Impeller selection option

In the main dimension parameters, the input parameters are asked. This is the main tab in order to determine the size of the impeller. The software mainly seeks the three values of the impeller dimension. Diameter of the impeller, suction diameter, outlet width, and also the shaft diameter.

For each calculation various options are available. For suction diameter calculation ds different options are available including Rel. inlet flow angle, Intake number, Min. rel velocity, Diameter ratio, and Minimal NPSHR.

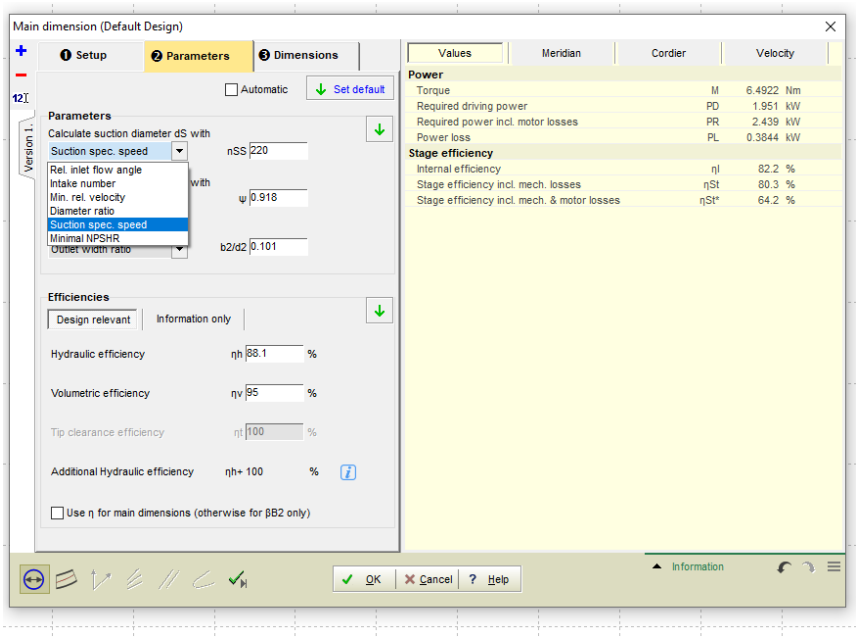

Figure 3 Constant for basic dimension

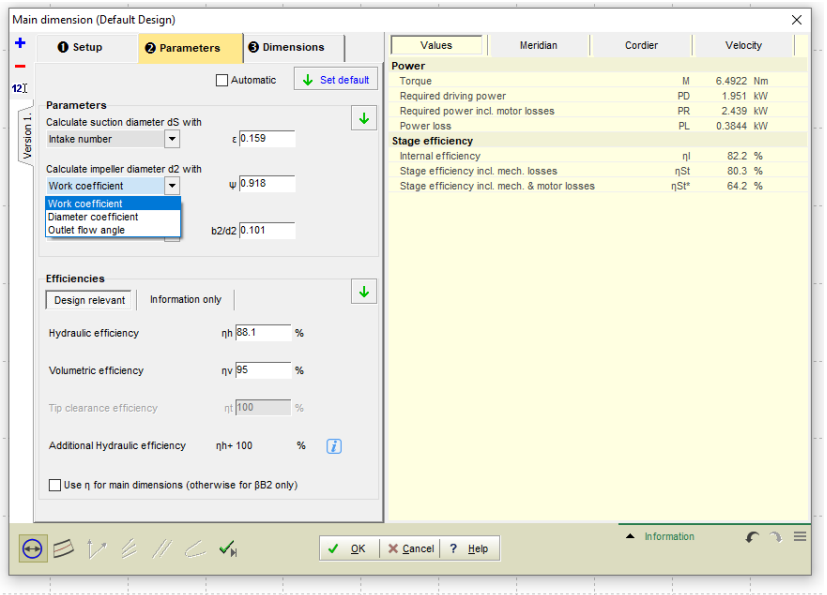

Figure 4 Design Constant for basic dimension

Similarly for impeller diameter also, different design constants are available i.e. work coefficient, Diameter coefficient, and Outlet flow angle.

Lastly, for the outlet width calculation, three options are available i.e outlet width ratio, Merid. Deceleration and outlet number.

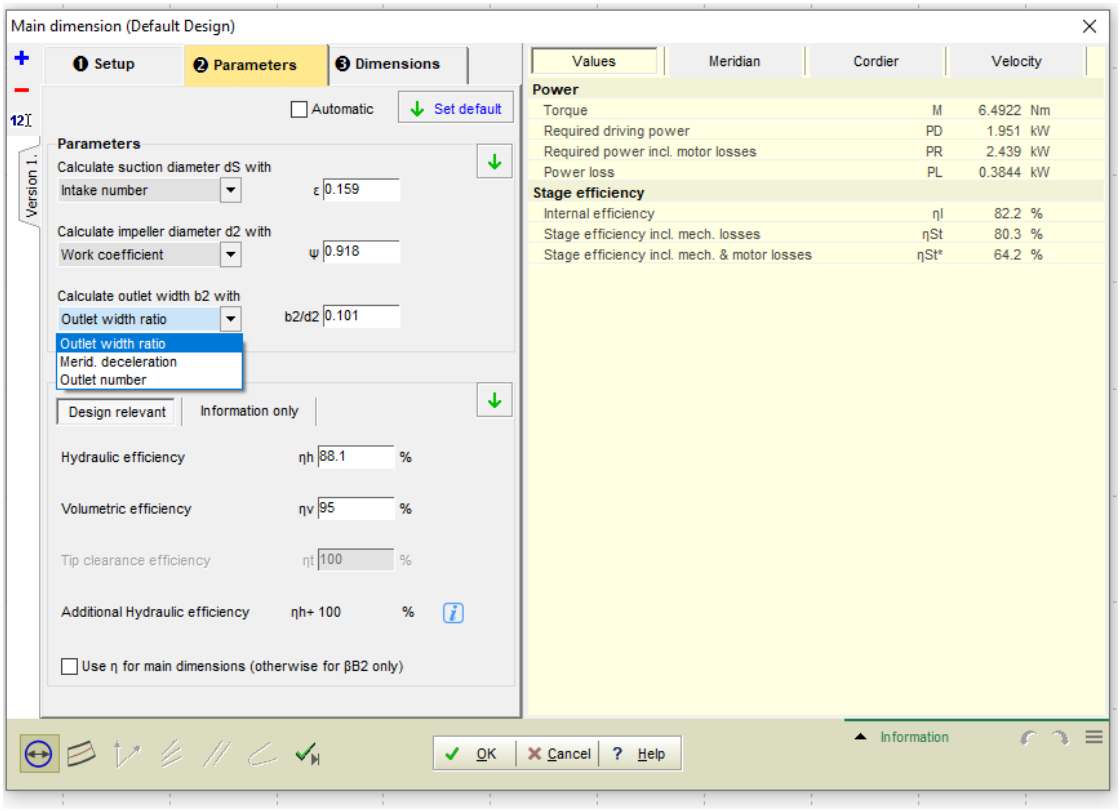

Figure 5 Constant for basic dimension

The value of such a design constant is based upon the various theoretical empirical relations which are given in the CFturbo manual.

For suction diameter ds calculation, the following coefficients are available.

Intake coefficient ε	▪ Ratio between meridional inflow velocity and specific energy $\varepsilon = c_0/\sqrt{2Y}$ ▪ 0.05…0.4 (rising with nq) ▪ (k_{m1} at Stepanoff)
Inflow angle β_{0a}	▪ high → smaller dimensions, lower friction losses ▪ < 20° → prevent the risk of cavitation ▪ > 15° → with regard to efficiency ▪ 12°…17° → recommended for good suction capability
Minimal relative velocity w	▪ small friction and shock losses ▪ only if no cavitation risk ! ▪ f_{dS}=1.15…1.05 standard impeller, nq=15…40 ▪ f_{dS}=1.25…1.15 suction impeller
suction specific speed n_{SS}	$n_{SS} = n\left[\text{min}^{-1}\right]\frac{\sqrt{Q\left[m^3/s\right]}}{\left(NPSH_R\,[m]\right)^{3/4}}$ (European definition for illustration) Standard suction impeller u_1<50 m/s 160…220 Suction impeller, axial inflow u_1<35 m/s 220…280 Suction impeller, cont. shaft u_1<50 m/s 180…240 High pressure pump u_1>50 m/s 160…190 Standard inducer u_1>35 m/s 400…700 Rocket inducer >>1000
Min. NPSH	$NPSH_R = \lambda_c \frac{c_{m1}^2}{2g} + \lambda_w \frac{w_1^2}{2g}$ ▪ λ_c suction pressure coefficient for absolute velocity c (inflow acceleration and losses): 1.1 for axial inflow; 1.2…1.35 for radial inflow casing ▪ λ_w suction pressure coefficient for relative velocity w (pressure drop at leading edge): 0.10…0.30 for standard impeller; 0.03…0.06 for inducer

Work coefficient Ψ (= pressure and head coefficient)	▪ dimensionless expression for the specific energy: $\psi = Y/\left(u_2^2/2\right)$ and $\psi = Y_{eff}/\left(u_2^2/2\right)$ 0.7 ...1.3 centrifugal impeller 0.25...0.7 mixed-flow impeller 0.1 ...0.4 axial impeller ▪ high → small d_2, flat characteristic curve low → high d_2, steep characteristic curve
Specific diameter δ	▪ according to Cordier diagram (see Dimensions 263)
Outflow angle β_3	▪ 6°...13°: recommended for stable performance curve (with nq rising)

For outlet width calculation b2, the following option is available.

Outlet width ratio b_2/d_2	▪ 0.04...0.30 (rising with nq)
for pumps: Mer. deceleration c_{m3}/c_{mS}	▪ 0.60...0.95 (rising with nq)
for pumps:	▪ Ratio between meridional outlet velocity and specific energy
Outlet coefficient ε_2	▪ 0.08...0.26 (rising with nq) ▪ (k_{m2} at Stepanoff)
for fans: Shroud angle ε_{Shr}	$\varepsilon_{Shr} = \arctan\left(2\frac{b_1 - b_2}{d_2 - d_1}\right) = 0° \ldots 20°$

The value of those constants is based on theoretical calculations. As an example

The impeller design in terms of intake coefficient is the km1 design constant explained by stepanoff as shown in Figure 6.

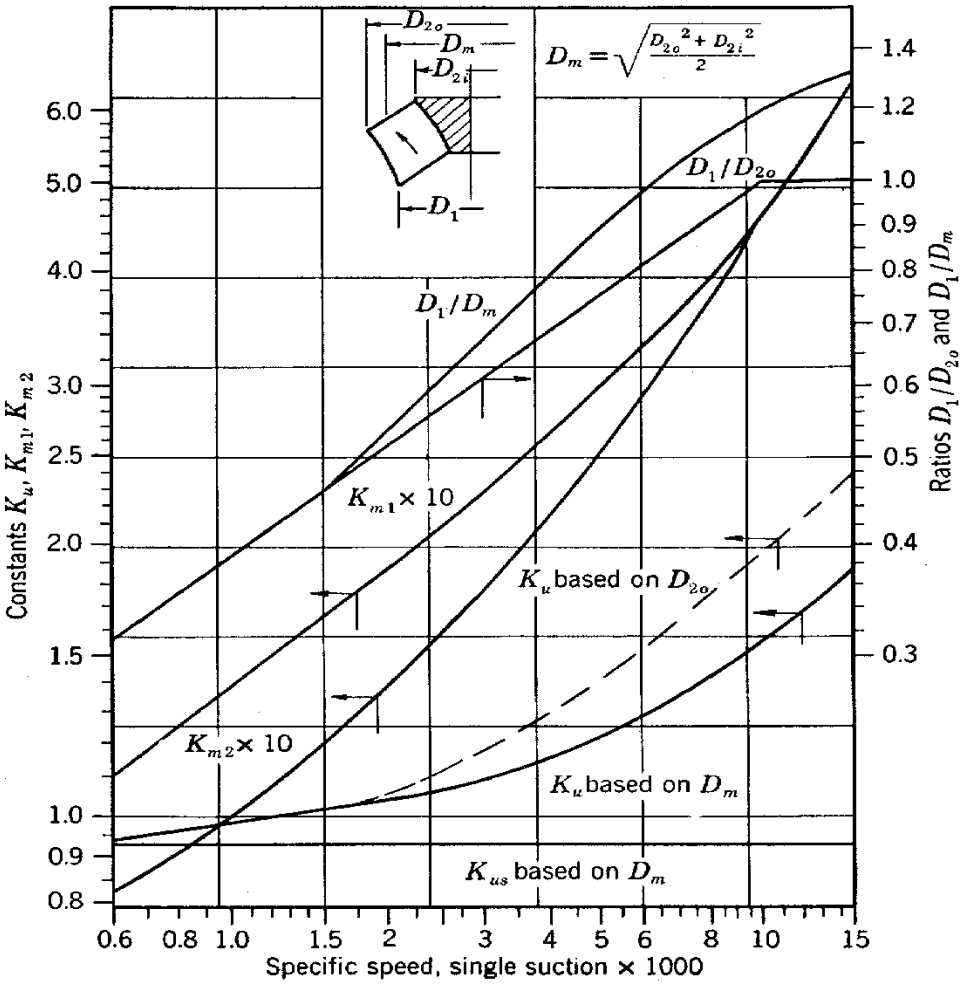

Figure 6 Stepanoff Constant for Diameter Calculation

Stepanoff defines mainly three constants for determining suction diameter, impeller diameter, and width.

After properly defining the dh, ds, d2, and b1 we enter into the meridional section of CFturbo.

Since the reverse engineering approach was designed for impeller modeling. The value of different dimensions was taken from measurements of the original impeller as shown in Table 1 below.

Table 1: Basic Dimension of the impeller from Reverse Engineering

S.N.	**Parameter**	**Unit**
1.	Impeller diameter	116 mm
2.	Suction diameter	85 mm
3.	Hub diameter	38 mm
4.	Outlet width	19 mm
5.	Shaft diameter	20 mm

After the insertion of the original dimension as above, we get the meridional view of the impeller as below:

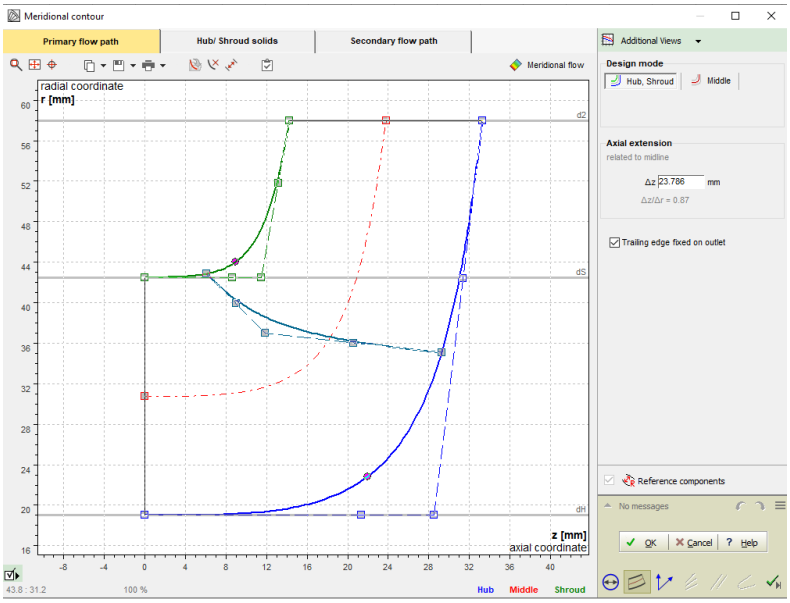

Figure 7 Meridonial view of the impeller

Again different measurements were taken from different location for the impeller as the most developed profile from the reverse engineering is as below.

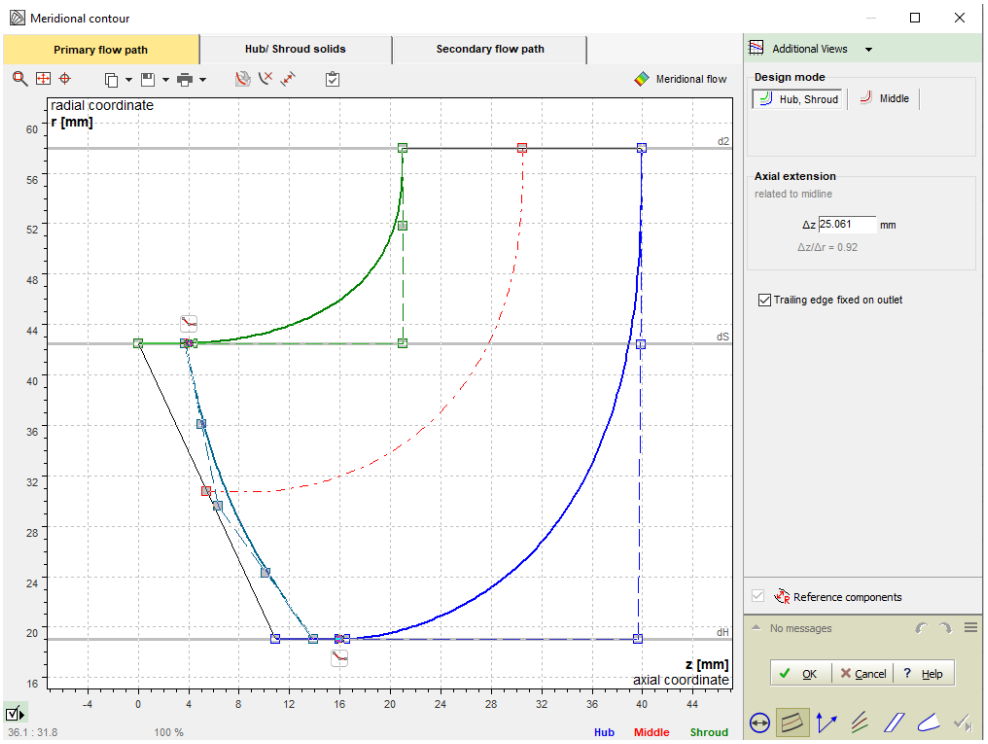

Figure 8 Blade area in meridional view

For the complete design of the impeller, the meridional view is not sufficient to develop the complete view of the impeller. The radial view of the blade with be more important. The radial view is government by the vane angle β and its distribution from inlet to outlet. Since the pump manufacturer has not provided such information. The value of the beta should be estimated and optimized. In CFturbo we have such an option for it. Just after the meridional view, we get we can fix the value of β_1 and β_2. The value of β_1 and β_2 can be taken following different works of literature. For this case, those values are put as suggested by stepanoff as shown in Figure 9.

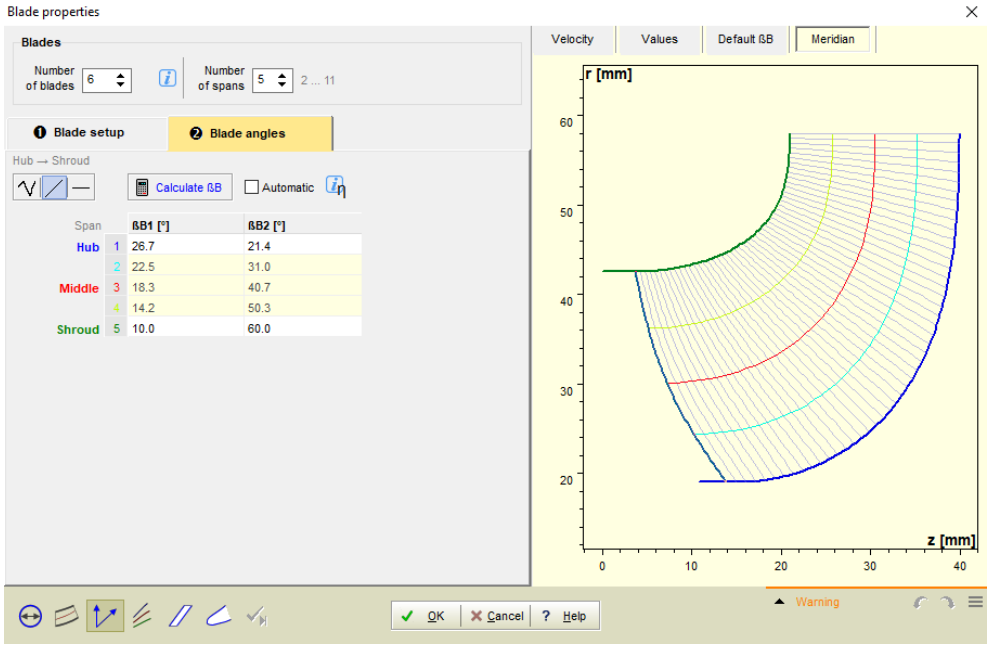

Figure 9 Beta angle distribution at inlet and outlet

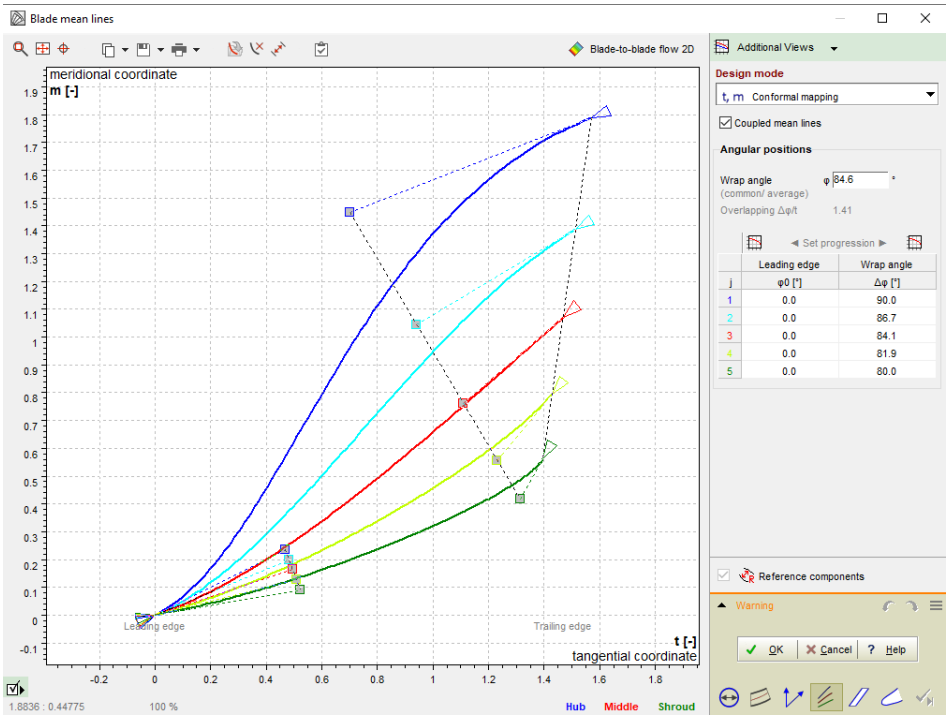

Figure 10 Blade angle progression along the blade length

After defining the blade angles. Another factor for the impeller is the blade mean lines. The blade means line shows the information about the radial/tangential coordinate of the blade with respect to the meridional coordinate from the leading edge to the trailing edge. Similarly, it also asks for the wrap angle which reflects how much area the blade covers from the leading edge to the trailing edge. After closely measuring the impeller the approximate wrap angle was found as 85 degrees.

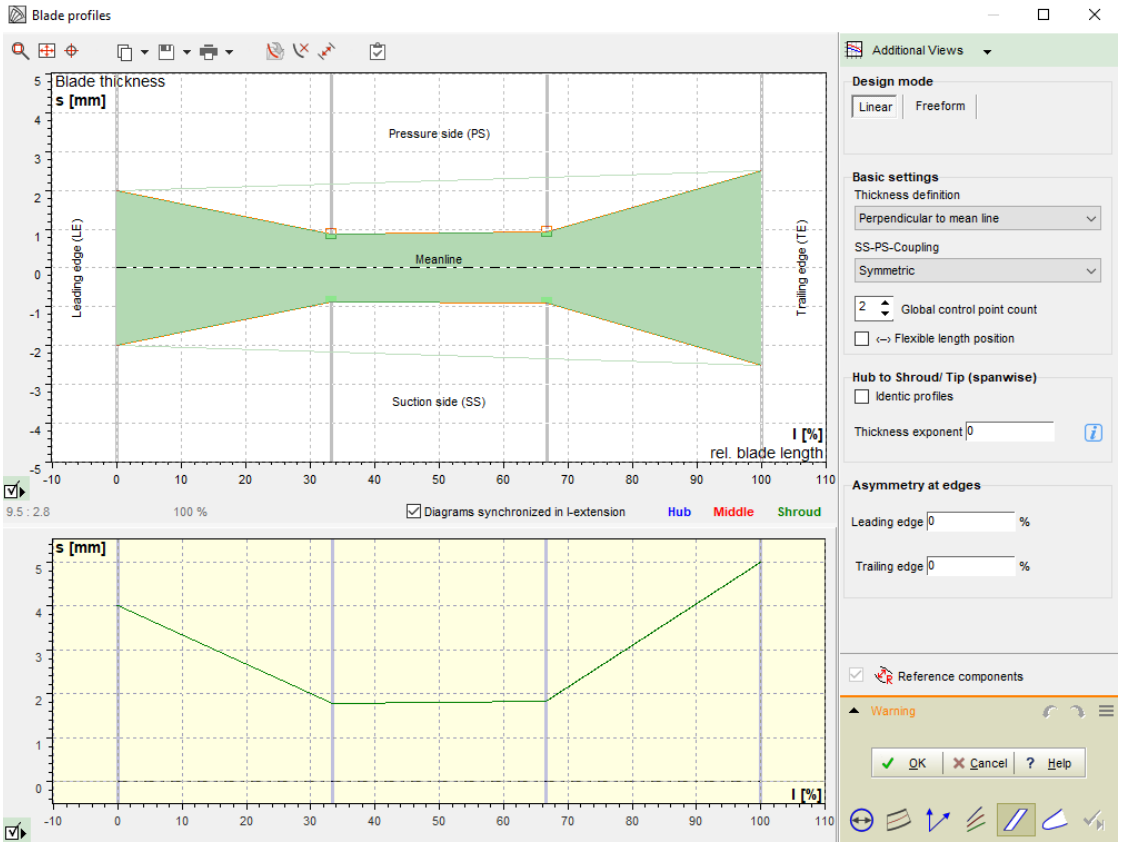

Figure 11 Blade profiles

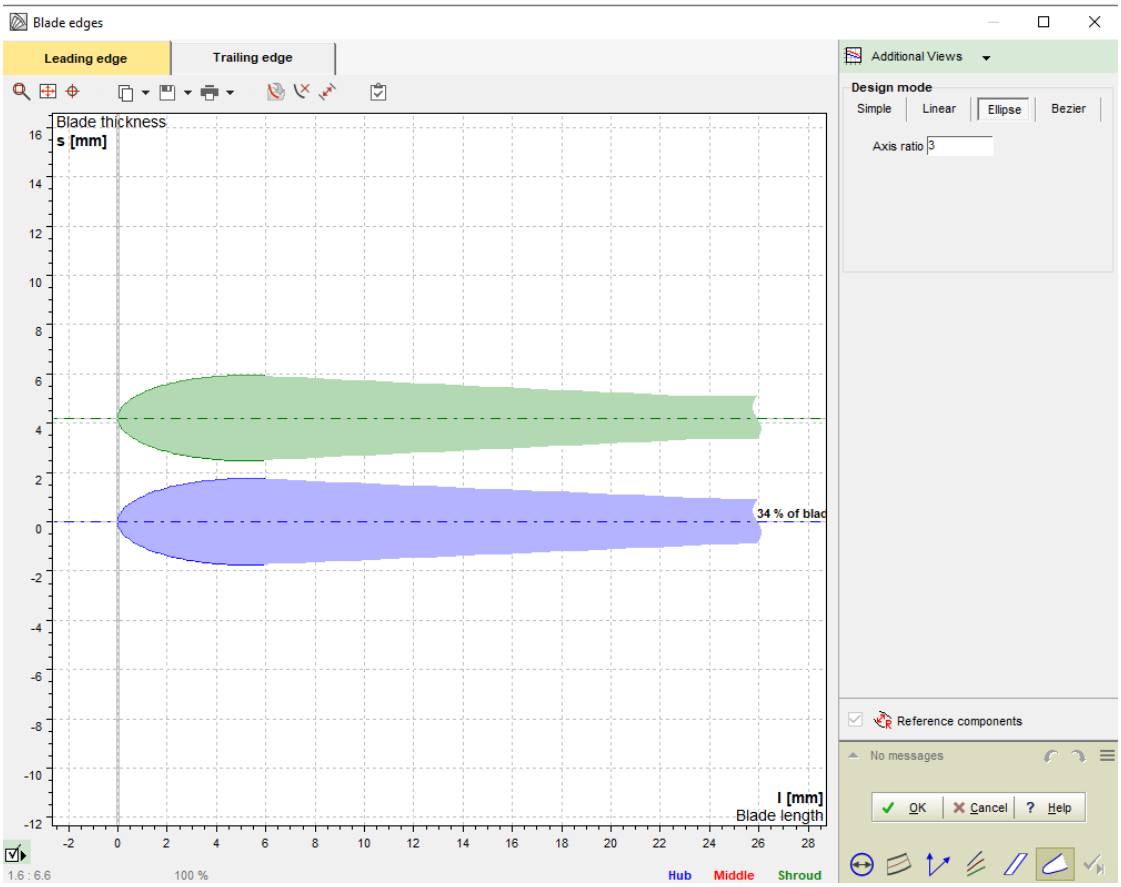

Figure 12 Defining blade profile at leading and trailing edge

In this way, we get the complete hydraulic design of the centrifugal pump in CFturbo.